

PRODUCTION OF BORON NITRIDE NANOTUBES AND THEIR USES  
IN POLYMER COMPOSITES

A THESIS SUBMITTED TO  
THE GRADUATE SCHOOL OF NATURAL AND APPLIED SCIENCES  
OF  
MIDDLE EAST TECHNICAL UNIVERSITY

BY

CAN DEMİR

IN PARTIAL FULFILLMENT OF THE REQUIREMENTS  
FOR  
THE DEGREE OF MASTER OF SCIENCE  
IN  
CHEMICAL ENGINEERING

NOVEMBER 2010

Approval of the thesis

**PRODUCTION OF BORON NITRIDE NANOTUBES AND THEIR USES IN  
POLYMER COMPOSITES**

submitted by **CAN DEMİR** in partial fulfillment of the requirements for the degree of  
**Master of Science in Chemical Engineering Department, Middle East  
Technical University** by,

Prof. Dr. Canan Özgen  
Dean, Graduate School of **Natural and Applied Sciences**

\_\_\_\_\_

Prof. Dr. Gürkan Karakaş  
Head of Department, **Chemical Engineering**

\_\_\_\_\_

Assoc. Prof. Dr. Naime Aslı Sezgi  
Supervisor, **Chemical Engineering Dept., METU**

\_\_\_\_\_

Prof. Dr. Göknur Bayram  
Co-Supervisor, **Chemical Engineering Dept., METU**

\_\_\_\_\_

**Examining Committee Members:**

Prof. Dr. H. Önder Özbelge  
Chemical Engineering Dept., METU

\_\_\_\_\_

Assoc. Prof. Dr. Naime Aslı Sezgi  
Chemical Engineering Dept., METU

\_\_\_\_\_

Prof. Dr. Göknur Bayram  
Chemical Engineering Dept., METU

\_\_\_\_\_

Prof. Dr. Ülkü Yilmazer  
Chemical Engineering Dept., METU

\_\_\_\_\_

Assoc. Prof. Dr. Ayşen Yılmaz  
Chemistry Dept., METU

\_\_\_\_\_

**Date:**

24.11.2010

\_\_\_\_\_

**I hereby declare that all information in this document has been obtained and presented in accordance with academic rules and ethical conduct. I also declare that, as required by these rules and conduct, I have fully cited and referenced all material and results that are not original to this work.**

Name, Last name: Can DEMİR

Signature:

## **ABSTRACT**

### **PRODUCTION OF BORON NITRIDE NANOTUBES AND THEIR USES IN POLYMER COMPOSITES**

Demir, Can

M.Sc. Department of Chemical Engineering

Supervisor: Assoc. Prof. Dr. Naime Aslı Sezgi

Co-supervisor: Prof. Dr. Göknur Bayram

November 2010, 125 Pages

Boron nitride nanotubes (BNNTs), firstly synthesized in 1995, are structural analogues of carbon nanotubes (CNTs) with alternating boron and nitrogen atoms instead of carbon atoms. Besides their structure, mechanical and thermal properties of BNNTs are very similar to the remarkable properties of CNTs. However, BNNTs have higher resistance to oxidation than CNTs. Also, BNNTs are electrically isolating. Therefore, they are envisioned as suitable fillers for the fabrication of mechanically and thermally enhanced polymeric composites, while preserving the electrical isolation of the polymer matrix.

In this study, polypropylene (PP) – boron nitride nanotube (BNNT) composites were prepared using a twin-screw extruder. Mechanical and thermal properties of PP–BNNT composites were investigated as a function of nanotube loading. The nanotubes used in the composites were synthesized from the reaction of ammonia gas with a powder mixture of elemental boron and iron oxide. X-ray diffraction (XRD) analysis revealed the predominant hexagonal boron nitride in the synthesized product. Multi-wall nanotubes with outer diameters ranging from 40 to 130 nm were observed with SEM and TEM analyses.

Tensile testing of PP–BNNT composites revealed slight increases in the Young’s modulus and yield strength of neat PP with 0.5 and 1 wt% of the as-synthesized BNNT additions. On the other hand, due to the agglomeration of BNNTs, elongation at break and tensile strength values of composites decreased with increasing nanotube content. In the case of using 0.5 wt% loading of purified and then surface modified BNNTs, slight improvement in all mechanical properties of neat PP was achieved. Differential scanning calorimetry (DSC) analysis revealed a noticeable increase in the crystallization temperature of BNNT–added composites. Coefficient of linear thermal expansion (CLTE) of polymeric composites were studied and no significant change in the CLTE of neat PP was observed with the addition of BNNTs. Results of thermal gravimetric analysis (TGA) indicated improvements in the thermal stability of neat PP with BNNT additions.

**Key words:** Polypropylene, Boron Nitride Nanotubes, Extrusion, Polymeric Nanocomposites.

## ÖZ

# BOR NİTRÜR NANOTÜPLERİN ÜRETİLMESİ VE POLİMER KOMPOZİTLERDE KULLANIMI

Demir, Can.

Yüksek Lisans, Kimya Mühendisliği

Tez Yöneticisi: Doç. Dr. Naime Aslı Sezgi

Ortak Tez Yöneticisi: Prof. Dr. Göknur Bayram

Kasım 2010, 125 Sayfa

İlk kez 1995 yılında sentezlenen bor nitrür nanotüpler (BNNT), yapılarında karbon atomları yerine eşit sayıda bor ve azot atomları ile karbon nanotüplerin yapısal benzerleridir. Yapılarının yanında, bor nitrür nanotüplerin mekanik ve termal özellikleri de karbon nanotüplerin büyük ilgi çeken özelliklerine oldukça benzerdir. Fakat karbon nanotüplerden farklı olarak oksidasyona karşı daha fazla dayanıklılığa sahiptirler. Ayrıca elektriksel olarak yalıtıcıdır. Bu özellikleriyle bor nitrür nanotüpler, mekanik ve termal özellikleri geliştirilmiş, aynı zamanda elektriksel yalıtıcılığı korunmuş polimer kompozitlerin hazırlanması için uygun katkı maddeleri olarak öngörülmektedirler.

Bu çalışmada, çift vidalı bir ekstruder kullanılarak polipropilen(PP) – bor nitrür nanotüp(BNNT) kompozitleri hazırlanmıştır. Hazırlanan PP–BNNT kompozitlerin mekanik ve termal özellikleri bor nitrür nanotüp katkısına bağlı olarak araştırılmıştır. Kompozitlerde kullanılan bor nitrür nanotüpler amonyak gazının bor ve demir oksit toz karışımıyla tepkimeye sokulmasıyla elde edilmiştir. X-ışını kırınım ölçümü (XRD) analizi üretilen ürünün büyük oranda hekzagonal bor nitrür'den oluştuğunu

göstermiştir. SEM ve TEM görüntüleri ile ürünün 40 ila 130 nm arasında değişen dış çaplara sahip çok duvarlı nanotüpler içerdiği gözlenmiştir.

PP–BNNT kompozitlerinin gerilme testleri, ağırlıkça %0,5 ve %1 oranında BNNT katkısının saf PP'nin Young modülü ve akma dayanımını az miktarda arttırdığını göstermiştir. Diğer taraftan, nanotüplerin polimer içinde kümeleşmelerinden dolayı kompozitlerin kopmada uzama ve çekme dayanımı değerleri nanotüp katkısının artmasıyla azalmıştır. Saflaştırma ve yüzey modifikasyonu işlemlerinden geçirilen nanotüplerin ağırlıkça %0,5 oranında kullanılmasıyla saf PP'nin tüm mekanik özelliklerinde az bir gelişim sağlanmıştır. Diferansiyel taramalı kalorimetre (DSC) analizleri, nanotüp katkılı kompozitlerin kristallenme sıcaklıklarında yükselme olduğunu ortaya çıkarmıştır. Kompozitlerin doğrusal ısıl genişleme katsayıları (DIGK) çalışılmıştır ve saf PP'nin DIGK değerinde BNNT eklenmesiyle önemli bir değişiklik gözlenmemiştir. Termal gravimetrik analiz (TGA) sonuçları BNNT katkısının saf PP'nin ısıl dayanımını geliştirdiğini göstermiştir.

**Anahtar Kelimeler:** Polipropilen, Bor Nitür Nanotüpler, Ekstrüzyon, Polimer Nanokompozitler.

***To my family***



## ACKNOWLEDGEMENTS

Firstly, I would like to express my gratitude to my supervisor, Assoc. Prof. Dr. Naime Aslı Sezgi, for her guidance, understanding, criticism and encouragement in the process of making this thesis. I also express my thanks and appreciations to my co-supervisor Prof. Dr. Göknur Bayram for her generous support and guidance at all levels of my thesis study.

I would like to thank Didem Özmen for kindly introducing me the experimental system in the first days of my graduate studies. I sincerely thank my lab friends Berk Baltacı, Nisa Ilgaz, Buğçe Aydemir, Dr. Zeynep Obalı for their valuable help and friendship. I would also like to open parenthesis for Dr. Sertan Yeşil who shared his time and experience with me whenever I needed, and İrem Şengör for her invaluable support.

Thanks to METU Central Laboratory for microscopy and thermal analyses, Necmi Avcı from Department of Metallurgical and Materials Engineering for XRD analyses; Mihrican Açıkgöz from Department of Chemical Engineering for TGA analyses, and Prof. Dr. Suna Balcı from Gazi University for FTIR analyses.

I want to thank my sister Beyza Göktürk and her dear husband Erek Göktürk for their everlasting support and guidance. Finally I wish to thank my parents, Halit and Nursel Demir who made all these possible for me.

# TABLE OF CONTENTS

ABSTRACT.....	iv
ÖZ.....	vi
ACKNOWLEDGEMENTS.....	ix
TABLE OF CONTENTS.....	x
LIST OF FIGURES.....	xiv
LIST OF TABLES.....	xviii
NOMENCLATURE.....	xix
CHAPTERS	
1 INTRODUCTION .....	1
2 NANOTUBES .....	4
2.1 Classification of Nanotubes .....	5
2.2 Carbon Nanotubes .....	6
2.3 Boron Nitride Nanotubes .....	8
2.3.1 Properties of Boron Nitride Nanotubes.....	8
2.3.2 Applications of Boron Nitride Nanotubes.....	9
2.3.3 Synthesis Methods of Boron Nitride Nanotubes.....	10
2.3.3.1 Arc-discharge Method.....	10
2.3.3.2 Laser Ablation Method .....	11
2.3.3.3 Ball Milling and Annealing Method .....	11
2.3.3.4 Chemical Vapor Deposition (CVD) Method .....	11
3 POLYMERIC NANOCOMPOSITES .....	13
3.1 Composite Materials.....	13
3.1.1 Classification of Composites .....	13
3.1.2 Polymer Matrix Composites .....	14
3.2 Polymeric Nanocomposites .....	14
3.3 Fabrication of Polymer – Nanotube Composites.....	16
3.3.1 Solution Dispersion Method .....	17
3.3.2 In-Situ Polymerization .....	18
3.3.3 Extrusion.....	18

3.3.3.1	Function of Extruder Screw.....	19
3.3.3.2	Twin-Screw Extrusion.....	20
3.3.4	Melt Injection .....	22
3.4	Polypropylene .....	22
3.4.1	Structure of Polypropylene .....	23
3.4.2	Properties of Polypropylene .....	24
3.4.3	Applications of Polypropylene.....	25
3.5	Characterizations of the Materials .....	25
3.5.1	X-Ray Diffraction (XRD) .....	25
3.5.2	Fourier Transform Infrared (FTIR) Spectroscopy .....	26
3.5.3	Multi-Point BET Surface Analysis .....	27
3.5.4	Scanning Electron Microscopy (SEM) .....	27
3.5.5	Transmission Electron Microscopy (TEM) .....	28
3.5.6	Mechanical Characterization .....	29
3.5.6.1	Tensile Test.....	29
3.5.7	Thermal Characterization .....	32
3.5.7.1	Differential Scanning Calorimetry (DSC) .....	32
3.5.7.2	Thermal Gravimetric Analysis (TGA) .....	33
3.5.7.3	Thermal Mechanical Analysis (TMA) .....	33
4	LITERATURE SURVEY.....	34
4.1	Production of Boron Nitride Nanotubes .....	35
4.2	Polypropylene – Carbon Nanotube Composites .....	36
4.3	Polymer – Boron Nitride Nanotube Composites .....	37
4.4	Objectives of the Study.....	38
5	EXPERIMENTAL .....	40
5.1	Production of Boron Nitride Nanotubes.....	42
5.1.1	Experimental Set-Up .....	42
5.1.2	Experimental Procedure .....	43
5.1.2.1	BNNT Synthesis Parameters.....	44
5.2	Purification and Modification of BNNTs.....	45
5.2.1	Purification of BNNTs .....	45
5.2.2	Modification of BNNTs.....	46
5.3	Characterizations of BNNTs.....	46
5.3.1	X-Ray Diffraction (XRD).....	46

5.3.2	Fourier Transform Infrared (FTIR) Spectroscopy.....	47
5.3.3	Multi-point BET Surface Surface Analysis.....	47
5.3.4	Scanning Electron Microscopy (SEM).....	47
5.3.5	Transmission Electron Microscopy (TEM).....	47
5.4	Fabrication of Polypropylene – BNNT Composites.....	48
5.4.1	Materials.....	48
5.4.1.1	Polymer Matrix.....	48
5.4.1.2	Antioxidant Agent.....	48
5.4.2	Extrusion of PP– BNNT Composites .....	49
5.4.2.1	Experimental Set–Up.....	49
5.4.2.2	Experimental Procedure.....	50
5.4.3	Injection Molding.....	53
5.4.3.1	Experimental Set–Up.....	53
5.4.3.2	Experimental Procedure.....	54
5.5	Characterizations of PP – BNNT Composites.....	54
5.5.1	Mechanical Characterization (Tensile Testing).....	54
5.5.2	Thermal Characterizations.....	55
5.5.2.1	Differential Scanning Calorimetry (DSC).....	55
5.5.2.2	Thermal Gravimetric Analysis (TGA) .....	55
5.5.2.3	Thermal Mechanical Analysis (TMA) .....	56
6	RESULTS AND DISCUSSION .....	57
6.1	Production of BNNTs.....	57
6.1.1	Effect of Ammonia Flow Rate on BNNT Production.....	57
6.2	Characterizations of BNNTs .....	61
6.2.1	X-Ray Diffraction (XRD) Analysis .....	61
6.2.2	Fourier Transform Infrared (FTIR) Spectroscopy Analysis.....	62
6.2.3	Multi-Point BET Surface Analysis .....	63
6.2.4	Scanning Electron Microscopy Analysis.....	66
6.2.5	Transmission Electron Microscopy Analysis.....	67
6.3	Characterizations of PP – BNNT Composites.....	70
6.3.1	Mechanical Characterization (Tensile Testing).....	70
6.3.1.1	First Group Composites .....	71
6.3.1.2	Second Group Composites.....	73
6.3.1.3	Third Group Composites.....	75

6.3.2	Differential Scanning Calorimetry (DSC)	79
6.3.3	Thermal Gravimetric Analysis (TGA)	80
6.3.3.1	First Group Composites	81
6.3.3.2	Second Group Composites	82
6.3.3.3	Third Group Composites	83
6.3.4	Thermal Mechanical Analysis (TMA)	84
7	CONCLUSIONS	88
	REFERENCES	90
	APPENDICES	97
A.	XRD DATA	97
B.	FTIR SPECTRA OF BORON AND IRON OXIDE	101
C.	BET METHOD FOR SURFACE AREA DETERMINATION	103
D.	TENSILE TEST RESULTS OF ALL SAMPLES	105
E.	REPRESENTATIVE STRESS-STRAIN CURVES	106
F.	DETERMINATION OF PERCENT CRYSTALLINITY ( $X_c$ )	109
G.	DSC PLOTS OF ALL SAMPLES	110
H.	TGA CURVE OF THE AS-SYNTHESIZED BNNTs	118
I.	TMA CURVES OF SECOND AND THIRD GROUP COMPOSITES	119

## LIST OF FIGURES

### FIGURES

Figure 2.1	Computer made illustrations: (a) Multi-wall nanotube (MWNT) (b) Single-wall nanotube.....	5
Figure 2.2	Structural types of nanotubes.....	6
Figure 2.3	Atomic model of a single-wall CNT.....	7
Figure 2.4	Molecular model of a single-wall BNNT.....	8
Figure 2.5	Experimental set-up for CVD method.....	12
Figure 3.1	Typical procedure for preparing polymer – nanotube composites using solution dispersion method.....	17
Figure 3.2	Schematic representation of a single screw extruder.....	19
Figure 3.3	Sections of an extruder screw.....	20
Figure 3.4	Types of twin screw extruders.....	21
Figure 3.5	Motion of material in co-rotating, non-intermeshing twin-screw extrusion.....	21
Figure 3.6	Steps of injection molding process.....	22
Figure 3.7	Synthesis of polypropylene.....	23
Figure 3.8	Stereo chemical structures of polypropylene.....	24
Figure 3.9	Diffraction of X-ray beam from a crystalline material.....	26
Figure 3.10	Schematic illustration of a TEM apparatus.....	28
Figure 3.11	Tensile test apparatus.....	29
Figure 3.12	Stress–strain curves: (a) Tensile strength at fracture (b) Tensile strength at yield.....	31
Figure 3.13	Different stress–strain behaviors of materials.....	31
Figure 3.14	A typical DSC plot.....	32
Figure 4.1	Number of publications on the sheet and nanotube structures of carbon and boron nitride by years.....	35
Figure 5.1	Experimental work of the study.....	41
Figure 5.2	Lay–out of the BNNT production system.....	42
Figure 5.3	Temperature–time profile of BNNT synthesis.....	44

Figure 5.4	Thermoprism TSE 16 TC model co-rotating twin-screw extruder.....	50
Figure 5.5	DSM Xplore laboratory scale (10 cc) injection molding machine.....	53
Figure 6.1	Effect of ammonia inlet flow rate on the amount of synthesized product .....	58
Figure 6.2	Photograph of the product synthesized under optimum conditions.....	60
Figure 6.3	Typical XRD pattern of the as-synthesized BNNTs.....	61
Figure 6.4	Typical FTIR Spectrum of the as-synthesized BNNTs.....	63
Figure 6.5	Adsorption/desorption isotherms of the as-synthesized BNNTs.....	64
Figure 6.6	Pore size distribution of the as-synthesized BNNTs.....	65
Figure 6.7	SEM images of the as-synthesized BNNTs (a) 24,000x magnification (b) 50,000x magnification.....	66
Figure 6.8	SEM images of the as-synthesized BNNTs (a) 50,000x Magnification (b) 100,000x magnification.....	67
Figure 6.9	TEM image of a bamboo-like multi-wall BNNT.....	68
Figure 6.10	TEM image of a hollow cylinder multi-wall BNNT.....	69
Figure 6.11	TEM image of a bamboo-like multi-wall BNNT that is broken from ends.....	69
Figure 6.12	Six replicates of tensile test specimens at different BNNT loadings.....	71
Figure 6.13	Tensile properties of first group composites.....	72
Figure 6.14	Tensile properties of second group composites.....	74
Figure 6.15	Young's modulus of third group composites.....	75
Figure 6.16	Yield strength of third group composites.....	76
Figure 6.17	Elongation at break of third group composites.....	77
Figure 6.18	Tensile strength of third group composites.....	78
Figure 6.19	TGA plots of first group composites.....	81
Figure 6.20	TGA plots of second group composites.....	82
Figure 6.21	TGA plots of third group composites.....	84
Figure 6.22	CLTE of second group composites.....	85

Figure 6.23	CLTE of composites with respect to the as-synthesized BNNT loadings.....	86
Figure 6.24	CLTE of composites with respect to 0.5 wt% of the as-synthesized, purified and purified – surface modified BNNT additions.....	87
Figure B.1	FTIR spectra of boron.....	101
Figure B.2	FTIR spectra of iron oxide (Fe <sub>2</sub> O <sub>3</sub> ).....	102
Figure E.1	Representative stress-strain curve for [PP2].....	106
Figure E.2	Representative stress-strain curve for [PP2+0.5B].....	107
Figure E.3	Representative stress-strain curve for [PP2+1B].....	107
Figure E.4	Representative stress-strain curve for [PP2+3B].....	108
Figure E.5	Representative stress-strain curve for [PP2+6B].....	108
Figure G.1	DSC plot of [PP1].....	110
Figure G.2	DSC plot of [PP1+1A].....	111
Figure G.3	DSC plot of [PP1+1A+1B].....	111
Figure G.4	DSC plot of [PP2] (1 <sup>st</sup> analysis).....	112
Figure G.5	DSC plot of [PP2] (2 <sup>nd</sup> analysis) .....	112
Figure G.6	DSC plot of [PP2] (3 <sup>rd</sup> analysis).....	113
Figure G.7	DSC plot of [PP2+1A].....	113
Figure G.8	DSC plot of [PP2+1A+1B].....	114
Figure G.9	DSC plot of [PP2+1A+3B].....	114
Figure G.10	DSC plot of [PP2+0.5B].....	115
Figure G.11	DSC plot of [PP2+1B].....	115
Figure G.12	DSC plot of [PP2+3B].....	116
Figure G.13	DSC plot of [PP2+6B].....	116
Figure G.14	DSC plot of [PP2+0.5PB].....	117
Figure G.15	DSC plot of [PP2+0.5MB].....	117
Figure H.1	TGA curve of the as-synthesized BNNTs.....	118
Figure I.1	TMA curve of [PP2] (1 <sup>st</sup> analysis).....	119
Figure I.2	TMA curve of [PP2] (2 <sup>nd</sup> analysis) .....	120
Figure I.3	TMA curve of [PP2] (3 <sup>rd</sup> analysis).....	120
Figure I.4	TMA curve of [PP2+1A].....	121
Figure I.5	TMA curve of [PP2+1A+1B].....	121
Figure I.6	TMA curve of [PP2+1A+3B].....	122



Figure I.7	TMA curve of [PP2+0.5B].....	122
Figure I.8	TMA curve of [PP2+1B].....	123
Figure I.9	TMA curve of [PP2+3B].....	123
Figure I.10	TMA curve of [PP2+6B].....	124
Figure I.11	TMA curve of [PP2+0.5PB].....	124
Figure I.12	TMA curve of [PP2+0.5MB].....	125

## LIST OF TABLES

### TABLES

Table 2.1	Properties of CNTs and BNNTs .....	9
Table 5.1	Tested parameters in BNNT production optimization runs.....	45
Table 5.2	Properties of EH-241 and MH-418 polypropylene.....	48
Table 5.3	Properties of ®IRGANOX 1010 antioxidant .....	49
Table 5.4	Properties of the twin-screw extruder used in this study.....	50
Table 5.5	Compositions of all extruded materials and their extrusion parameters.....	52
Table 5.6	Dimensions of the injection molded tensile test specimen.....	54
Table 6.1	Color of synthesized material with respect to ammonia inlet flow rate.....	59
Table 6.2	Optimum synthesis conditions for BNNT production.....	59
Table 6.3	Thermal properties of PP–BNNT composites.....	79
Table A.1	XRD data of hexagonal BN .....	97
Table A.2	XRD data of rhombohedral BN.....	98
Table A.3	XRD data of cubic iron ( $\alpha$ -Fe) .....	99
Table A.4	XRD data of iron oxide ( $\text{Fe}_2\text{O}_3$ ) .....	99
Table A.5	XRD data of the as-synthesized BNNTs .....	100
Table D.1	Tensile properties of all samples.....	105

## NOMENCLATURE

$A_0$	Initial cross-sectional area of the tensile test specimen, $m^2$
$D$	Interlayer spacing, $\text{\AA}$
$E$	Young's Modulus, MPa
$F$	Instantaneous load, N
$L_i$	Instantaneous gauge length of tensile specimen, mm
$L_0$	Initial gauge length of tensile specimen, mm
$M$	Molarity, (mol/L)
$M_w$	Molecular Weight (g/mol)
$N_0$	Avogadro's number, $6.02 \times 10^{23}$ molecules/mol
$N$	Order of diffraction peak
$P$	Equilibrium pressure, bar
$P_0$	Saturation vapor pressure of the adsorbate, bar
$T_c$	Crystallization Temperature, $^{\circ}\text{C}$
$T_g$	Glass Transition Temperature, $^{\circ}\text{C}$
$T_m$	Melting Temperature, $^{\circ}\text{C}$
$S_g$	Total surface area, $m^2$
$X_c$	Percent Crystallinity, %
$W_i$	Initial width of TMA specimen, mm
$V_m$	Volume adsorbed for monolayer coverage, $m^3$
$V$	Volume adsorbed, $m^3$

### ***Greek Letters***

$A$	Value for the area covered by one adsorbed molecule, $\text{\AA}$
$\sigma$	Engineering stress, MPa
$\varepsilon$	Engineering strain
$\theta$	Scattering angle, $^{\circ}$
$\lambda$	Wavelength, nm
$\rho$	Density, $\text{g/cm}^3$

## ***Abbreviations***

ASTM	American Society for Testing and Materials
BDDT	Brauner, Deming, Deming, Teller
BET	Brunauer, Emmett and Teller
BJH	Barrett, Joyner and Halenda
BN	Boron Nitride
BNNT	Boron Nitride Nanotube
CLTE	Coefficient of Linear Thermal Expansion
CNT	Carbon Nanotube
CVD	Chemical Vapor Deposition
DSC	Differential Scanning Calorimetry
FTIR	Fourier Transform Infrared
MWNT	Multi-wall Nanotube
PEG	Polyethylene Glycol
PMMA	Poly(methyl methacrylate)
PP	Polypropylene
PP-g-MA	Polypropylene-graft-maleic anhydride
SEM	Scanning Electron Microscopy
SWNT	Single-wall Nanotube
TEM	Transmission Electron Microscopy
TGA	Thermal Gravimetric Analysis
TMA	Thermal Mechanical Analysis
XRD	X-Ray Diffraction

# CHAPTER 1

## INTRODUCTION

Polymers are abundantly used materials owing to their ease of processing, light weight and high toughness. On the other hand, polymers have lower stiffness and strength compared to ceramics and metals. In an attempt to improve their mechanical, thermal or electrical properties, polymers are often reinforced by incorporating fillers into their matrix. Those fillers can be in the form of fibers, platelets, whiskers or particles [Jordan et al., 2005]. Reinforcing polymers with fillers to obtain composites with novel properties has been an active branch of materials science in the last decades.

Real interest to polymer based composite materials as an industrial commodity started in 1960's. Since then, polymeric composites have turned out to be commonly used engineering materials and manufactured in large quantities in order to be used in countless applications in sectors such as automotive, electronics, construction, household goods and etc. [Mazumdar, 2002].

Nanocomposite technology is a new field of composite science. In nanocomposites, at least one dimension of the fillers is in the order of nanometer. Therefore, these types of fillers are usually referred to as nanofillers.

Manufacturing of industrially viable nanocomposites started in 1980's with the development of polymer – nanostructured clay composites by researchers from Toyota Central Research and Development [Kawasumi, 2004]. Today, nanocomposite technology is applicable to almost all types of polymers from thermosets to thermoplastics. Many types of nanocomposites are being studied today parallel to the developments in nanotechnology. Nanotechnology gave rise to the development of high potential nanoscale fillers such as nanostructured silicas,

ceramics or nanotubes [Bhattacharya, Gupta & Kamal, 2008]. Carbon nanotubes (CNTs) have been one of the most influential type of nanotubes so far, with a lot of potential uses in materials science.

Carbon nanotubes are tubular forms of graphite sheets that have dimensions in nanometer scale. The discovery of carbon nanotubes by Iijima [1991] has influenced materials science in many ways. Unusually high mechanical and thermal properties of carbon nanotubes drew worldwide attention, and studies have been intensified in order to convey the high potentials of carbon nanotubes into practical applications, including their utilization as nanofillers to enhance or alter the properties of polymers.

The fabrication of stronger polymer composites by CNT usage has been successful in many ways. However, there are still obstacles that avoid the commercialization of these types of nanocomposites such as the production cost of nanotubes, which is still quite high. Another type of nanotubes that have been subject of polymer–nanotube studies in the last years is boron nitride nanotubes (BNNTs).

Boron nitride nanotubes, firstly synthesized in 1995, are structural analogues of carbon nanotubes with boron and nitrogen atoms instead of carbon atoms [Chopra et al., 1995]. Besides their structure, mechanical and thermal properties of BNNTs are very similar to CNTs. However, BNNTs have better resistance to thermal oxidation than CNTs. Also, BNNTs are electrically isolating materials with uniform electronic properties independent of their size and chirality [Chen et al., 2004]. Therefore, they are evaluated as suitable fillers for the fabrication of mechanically and thermally enhanced polymer composites, while preserving the electrical isolation of the polymer matrix [Zhi et al., 2008]. Over the last decade, a significant effort has been made to synthesize high–yield BNNTs because of their exceptional properties. However, the as-synthesized BNNTs almost always contain undesired impurities and tremendous effort is needed to isolate the nanotubes from the as-synthesized product, which is the case for the CNTs as well.

The studies on the polymeric composites of BNNTs have been flourished only over the last years. The effects of highly pure BNNT addition in polymer matrixes such

as polyaniline (PANI) [Zhi et al., 2005], polyvinyl formal (PVF) [Terao et al., 2009], poly(methyl methacrylate) (PMMA) [Zhi et al., 2008], polystyrene (PS) [Zhi et al., 2006], poly(vinyl butyral) (PVB) and poly(ethylene vinyl alcohol) (PEVA) [Zhi et al., 2009] have been studied. Those studies have documented the improving effect of BNNTs on several mechanical and thermal properties of polymers such as Young's modulus, strength, resistance to oxidation and thermal conductivity. However, the polymer – BNNT composites that have been studied to date were prepared as thin films via solution–mixing and evaporation techniques, which cover the dissolution of polymer and nanotubes in a solution in which both components are miscible. This kind of a composite preparing approach is advantageous for research purposes, however it is not industrially viable [McNally et al., 2005]. Industrially, routine way of manufacturing polymeric commodities is the extrusion process. Extrusion process involves the physical mixing of molten polymer with filler particles in order to disperse the fillers throughout the polymer matrix.

In this study, BNNTs were synthesized from the reaction of ammonia gas with a powder mixture of boron and iron oxide. The synthesized material was characterized using XRD, FTIR, multi-point BET, SEM and TEM analyses. Polypropylene(PP) – BNNT nanocomposites with different concentrations of BNNTs were fabricated using extrusion process. Finally, the effect of BNNT concentration on the thermal and mechanical properties of polypropylene based composites was investigated. Purification and surface modification of the synthesized BNNTs were also carried out and the impacts of these treatments on the polymeric composites were studied with respect to the as-synthesized BNNT usage.

## CHAPTER 2

### NANOTUBES

Nanotechnology term was first introduced by Eric Drexler in mid 1980's. Nanotechnology is defined by American Ceramic Society as: "the creation, processing, characterization, and utilization of materials, devices, and systems with dimensions on the order of 0.1 – 200 nanometers ( $10^{-9}$  meter)". These kinds of extremely small size materials or devices can exhibit much different properties from their conventional macro size counterparts.

Today, nanoparticle studies are ongoing as a branch of nanotechnology. The nanoparticles are defined as "Materials that have dimensions at the scale of nanometers, which typically develop novel properties, at length scale of under 100 nm". Owing to their novel thermal, mechanical, optical, electrical properties or functions, nanoparticles have attracted worldwide attention in the last decades and studies have been focused in order to realize practical applications of these novel materials. Nanotubes have been one of the most regarded and studied type of nanoparticles so far.

Nanotubes are cylindrical forms of specific atoms' sheet. Their diameter can vary from few nanometers to 200 nanometers. Their length varies in a broad range. Nanotubes can be produced from a variety of materials. They arouse great interest with their distinguished mechanical, thermal, optical, electrical, and structural properties that vary depending on their type. The first discovered nanotube structure was carbon nanotube [Iijima, 1991].



## 2.1 Classification of Nanotubes

A widely used classification of nanotubes is made according to the number of concentric cylindrical atom sheets that the nanotube has. If a nanotube is made up of a single tube, it is called a single-wall nanotube (SWNT). If a nanotube is made up of more than one concentric cylindrical wall, it is called a multi-wall nanotube (MWNT). Illustration of the single-wall and multi-wall nanotubes can be seen in Figure 2.1.

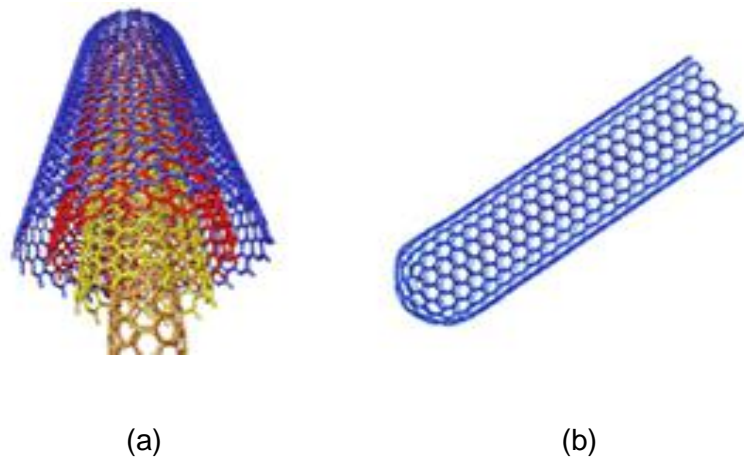


**Figure 2.1** Computer made illustrations: (a) Multi-wall nanotube (MWNT)  
(b) Single-wall nanotube (SWNT)\*.

Another classification of nanotubes is made according to the direction in which the atom sheets are rolled in the construction of nanotubes. A nanotube can be zig-zag, armchair or chiral according to the symmetry axis on which the atom sheet is rolled (Figure 2.2). These structural patterns of nanotubes also govern their mechanical, thermal and electrical properties [Wilson et al., 2002].

\*Retrieved from <http://neurophilosophy.wordpress.com/2006/08/31/carbon-nanotubes-stimulate-single-retinal-neurons/>, last access: 11.10.2010

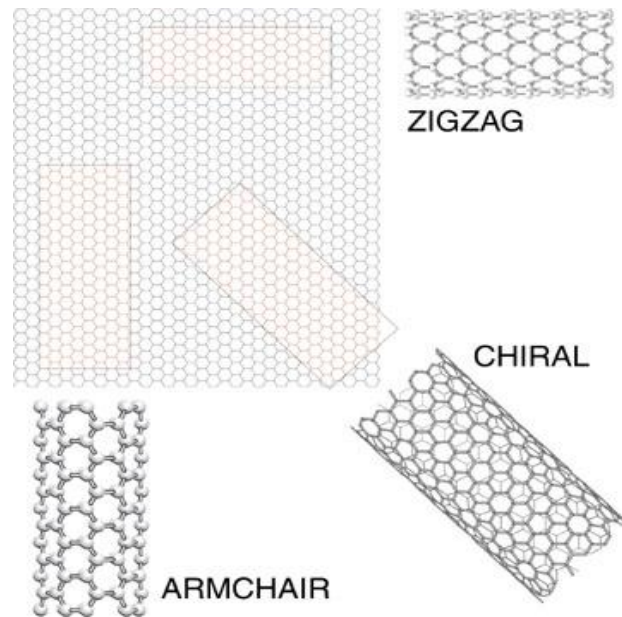


**Figure 2.2** Structural types of nanotubes\*.

## 2.2 Carbon Nanotubes

Carbon nanotubes, which are the most common types of nanotubes, were discovered by Iijima [1991] as a by-product of fullerene (ball of carbon atoms) synthesis. They are cylindrical forms of honeycomb carbon atom sheets, which are called graphite sheets. Figure 2.3 shows the tubular arrangement of a graphite sheet to form a single-wall carbon nanotube. Each black dot on Figure 2.3 represents a single carbon atom.

Since their discovery, carbon nanotubes have turned out to be one of the most intensively studied materials due to their mechanical, thermal, optical, and electronic properties. However, properties of carbon nanotubes can vary with respect to their structure, size or chirality.

\* Retrieved from <http://www.seas.upenn.edu/mse/images/nanotube1.jpg>, last access: 04.10.2010

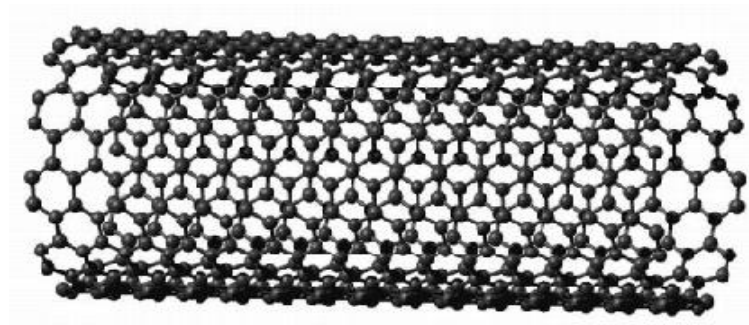


**Figure 2.3** Atomic model of a single-wall CNT [Owen, 2010].

The strength of carbon-carbon bonds is the source of outstanding mechanical properties of carbon nanotubes. Young's modulus and tensile strength values of CNTs change in the interval of 0.27 – 4.15 TPa and 10 – 150 GPa, respectively [Milev & Kannangara, 2005]. However, CNTs have tendency to buckle when a torsion, compression or bending is applied [Milev & Kannangara, 2005]. This is a natural outcome of their hollow cylindrical shape.

CNTs typically have outstandingly high coefficient of thermal conductivity that can approach up to a value of 3000 W/m.K, which is higher than all known substances including Diamond [Yang et al., 2002]. Their high thermal conductivity makes them suitable candidates to be used as thermal conductivity enhancers in composite materials. However, CNTs oxidize in air at 400 °C and burn completely at 700 °C when sufficient oxygen is supplied, thus limiting their applications at very high temperatures [Rinzler et al., 1998]. It is reported that the linear thermal expansion coefficient of CNTs is negative at low and room temperatures, and quite low at higher temperatures [Jiang et al., 200], which constitutes an advantage as they exhibit mechanical stability under increased temperatures.

The electronic properties of carbon nanotubes are not uniform and highly depend on the size and chirality of nanotubes. They can be either metallic or semi-conducting [Rinzler et al., 1998]. It is predicted that metallic nanotubes can carry an electrical current density which is approximately 1,000 times greater than metals such as copper [Hong & Myung, 2004].

## 2.3 Boron Nitride Nanotubes

Having outstanding thermal, mechanical and electronic properties, nanotubes have attracted significant attention over the last decades with the invention of CNTs. BNNTs are structural analogues of CNTs where carbon atoms are substituted by alternating boron and nitrogen atoms. In other words, BNNTs are formed by rolling of boron nitride (BN) atom sheets. Figure 2.4 shows the molecular model of a single-wall BNNT.

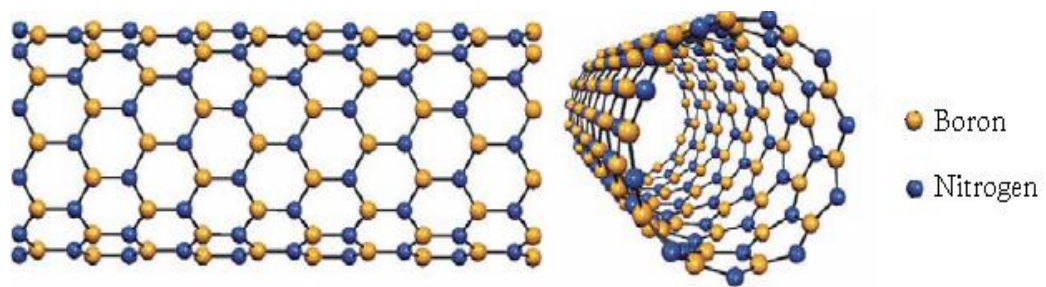


**Figure 2.4** Molecular model of a single-wall BNNT [Terrones et al, 2007].

### 2.3.1 Properties of Boron Nitride Nanotubes

Besides their structure, mechanical properties of BNNTs are very similar to CNTs. BNNTs have extremely high Young's modulus just as carbon nanotubes, which is estimated to be around 1.22 TPa [Chopra & Zettl, 1998].

Coefficient of thermal expansion of BNNTs is estimated to be quite low just as carbon nanotubes. Ishigami et al. [2003] measured the thermal conductivity of BNNTs as 600 W/m.K. Thermal gravimetric analysis (TGA) showed that the oxidation of BNNTs starts approximately at 800 °C, which is much higher than the oxidation temperature of CNTs, which is about 400 °C [Chen et al., 2004]. High oxidation resistance of BNNTs allows their applications in high temperature environments [Chen et al., 2004].

The electronic properties of BNNTs are also different from CNTs. BNNTs have a constant and wide band-gap of 5.5 eV. Therefore, they are electrically isolating independent of their size or chirality's. The electronic properties of BNNTs make them suitable nanofillers for the production of isolating polymeric materials [Zhi et al., 2008]. In Table 2.1, properties of BNNTs and CNTs are summarized.

**Table 2.1** Properties of CNTs and BNNTs.

Property	CNTs	BNNTs
Young's Modulus	1.8 TPa <sup>(a)</sup>	1.22 TPa <sup>(b)</sup>
Thermal Conductivity	~ 3000 W / m.K <sup>(c)</sup>	~ 600 W / m.K <sup>(d)</sup>
Oxidation Resistance <sup>(e)</sup>	400 °C in air	800 °C in air
Electrical Conductivity <sup>(e)</sup>	Metallic or semi-conducting	Isolating

(a) [Treacy, Ebbesen & Gibson, 1996] (b) [Chopra & Zettl, 1998] (c) [Yang et al., 2002] (d) [Ishigami et al., 2003] (e) [Chen et al., 2004]

### 2.3.2 Applications of Boron Nitride Nanotubes

Having very similar properties with CNTs, BNNTs also have wide opportunities for practical usages. Contrary to CNTs, BNNTs are also suitable for high temperature applications owing to their high oxidation resistance [Chen et al., 2004]. Besides, having uniform electronic properties and being electrically isolating, they are suitable candidates to be used as reinforcing nanofillers to fabricate isolating composite materials [Zhi et al., 2008]. In addition, they can be doped with other materials to prepare semiconductors, which can be used in high-powered electronics [Ishigami et al., 2003].

The synthesis of BNNTs is extremely difficult. Therefore, they can only be produced in gram quantities. Today, their applications are at research level. However, owing to their unusual mechanical, thermal and electronic properties, they have great potential for near future use. The improving ability to synthesize pure BNNTs in large quantities might create countless application opportunities just as carbon nanotubes. There are projections that BNNTs can be used in the near future in areas such as: mechanical and thermal reinforcement of composites, development of novel purpose materials, components for batteries, capacitors, fuel cells, transistors, sensors, electronic circuits etc. [Ishigami et al., 2003].

### **2.3.3 Synthesis Methods of Boron Nitride Nanotubes**

Over the last decade, a significant effort has been made to synthesize high-yield BNNTs because of their exceptional properties. There are several methods used for synthesizing boron nitride nanotubes. Mainly used methods are: arc-discharge, laser ablation, ball milling and chemical vapor deposition [Terrones, 2007].

#### **2.3.3.1 Arc-Discharge Method**

After the discovery of CNTs, scientists predicted that the structural analog of CNTs formed by boron and nitrogen atoms could be synthesized. Chopra et al. [1995] achieved to produce this theoretical material in laboratory using an arc-discharge method, which was the first method that was used to synthesize carbon nanotubes as well.

Arc-discharge method involves an anode and a cathode electrode between which an electrical voltage is applied in order to obtain electrical arcs. The electrical arcs are subjected onto a target material, which is placed on the cathode electrode. Ammonia is fed into the vacuum chamber as the reaction gas. Arc discharge between the electrodes supplies the necessary conditions for nanotube formation. Nanotubes, as well as other nanostructures deposit on the cathode electrode and on the inner walls of the chamber [Özmen, 2008].

### **2.3.3.2 Laser Ablation Method**

Laser ablation method encompasses the laser-assisted heating of a target material that performs as substrate for the nanotube synthesis. Synthesis of single and multi wall BNNTs were reported via laser ablation of cubic boron nitride specimen under high-pressured N<sub>2</sub> atmosphere. In addition, synthesis of BNNTs was achieved with laser ablation using a mixture of boron nitride powder with nanostructured Co and Ni particles. However, this technique has drawbacks such as incorporating high amounts of non-tubular structures of boron nitride in the as-synthesized product and lacking a satisfying yield of nanotubes [Terrones, 2007].

### **2.3.3.3 Ball Milling and Annealing Method**

An alternative technique for producing BNNTs involves the ball milling of elemental boron under an ammonia atmosphere, followed by thermal annealing at 1000 - 1200 °C under nitrogen gas flow. High yields of BNNTs with low cost can be produced by this method. In this method, high-energy ball milling is implemented to observe chemical reactions and structural changes in the boron powder [Chen et al., 1999]. The ball milling is usually performed for several days. After the ball-milling, heat treatment is applied and boron nitride nanostructures are formed from the initial powder. The Fe contamination from the milling balls are thought to have catalytic effect on the formation of BNNTs [Chen et al., 1999].

### **2.3.3.4 Chemical Vapor Deposition (CVD) Method**

In this method, a boron source gas and a nitrogen source gas are reacted in elevated temperatures in order to yield a solid deposit containing BNNTs. One of the reaction gases can be acquired by the heating of a solid precursor material. A substrate is used on the surface of which the solid product layer forms. Figure 2.5 demonstrates a typical set-up for the production of nanotubes by chemical vapor deposition technique.

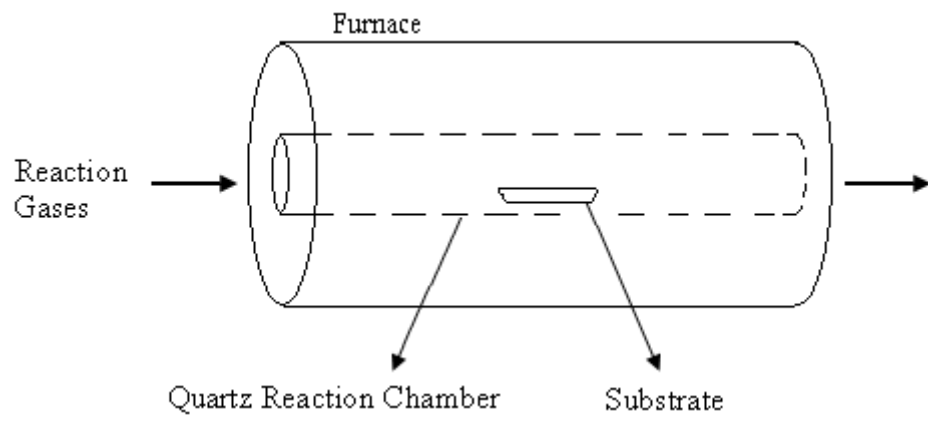


**Figure 2.5** Experimental set-up for CVD method.



## **CHAPTER 3**

### **POLYMERIC NANOCOMPOSITES**

#### **3.1 Composite Materials**

Composites are materials, which are formed by combining two or more constituents. Like in alloys, different substances can be mixed with each other on a molecular level, but that does not necessarily mean the composite material exhibits the separate properties of its ingredients on macro scale. In contrary, the resulting material might come out as a new kind, displaying different properties from its constituents [Kaw, 1997].

The charm of composite materials is due to their ability that, if prepared in a well-planned manner, they tend to display the best properties of their constituents or even display some new desirable properties that neither of its constituents exhibit. Some of the properties that can be improved by forming a composite material are: strength, stiffness, corrosion resistance, attractiveness, fatigue life, temperature dependent behavior and thermal insulation or thermal conductivity [Jones, 1999].

##### **3.1.1 Classification of Composites**

Two different approaches are used for the classification of composites. First approach is according to the physical structure of the filler, such as fibrous or laminate. Second approach is according to the type of the host material (matrix), which is the abundant phase of a composite. The latter system is used more commonly.

According to the classification with respect to the host material, the composites are observed under three main classes: metal, ceramic and polymer matrix composites [Kopeliovich, 2010]. This study is about the polymer matrix composites (PMC).

### **3.1.2 Polymer Matrix Composites**

A polymer is a large molecule composed of repeating structural units (monomers) made up of carbon, hydrogen and other nonmetallic elements. Two main classes of polymers are thermosetting and thermoplastics. Both types of polymers are used in composite making. Thermoplastic polymers are polymers that melt upon heating and in a reversible fashion, get back to a solid state when cooled. Thermosetting polymers are polymers that irreversibly get rigid upon subjecting to certain conditions such as heating, cooling or irradiating [Ebewele, 2000]. PMCs are materials, which compose of a polymer matrix combined with a reinforcing dispersed phase, which is also referred to as filler. PMCs are very popular due to their low cost and simple fabrication methods.

Use of neat polymers for structural purposes is limited by the low mechanical properties of polymers. PMCs offer improvements with respect to neat polymers in properties such as tensile strength, stiffness, corrosion resistance, temperature resistance, thermal conductivity, coefficient of thermal expansion and flammability. Properties of PMCs are determined by factors such as properties of the filler, orientation of the filler in the polymer matrix, concentration of the filler in polymer matrix and properties of the host polymer matrix [Kopeliovich, 2010].

### **3.2 Polymeric Nanocomposites**

Nanotechnology has revolutionized the materials science in 21<sup>st</sup> century by unraveling the novel properties of nanoparticles. It was observed that the properties of these novel nanostructured materials were exhibiting much more enhanced properties than the conventional materials. Accordingly, much more attention was focused on the nanostructured materials to be used as fillers in composites over the last decades.

Nanocomposites are composites that have nanostructured materials in their structure in order to reflect the unique properties of nanostructured materials in the resulting composite material. Just like composites, nanocomposites consist of a matrix phase (host) and a reinforcing phase (filler). The matrix can either be ceramic, metal, or polymer. Filler particles have dimensions in the order of nanometers. For this reason, the fillers used in the fabrication of nanocomposites are also referred to as nanofillers [Bhattacharya et al., 2008].

Polymeric nanocomposites are composites in which nanofillers are added and dispersed inside a polymer matrix for reinforcement purposes, or for providing new characteristics. The polymer matrix can be either thermoplastic or thermosetting. Nanofillers can be chosen from a variety of fillers according to the properties requested in the final composite.

Commonly used nanofillers in polymer matrixes are natural and synthetic clays, nanostructured silicas, ceramics, calcium carbonates, and with their increasing popularity, nanotubes. These fillers are still in research & development stage but have large potentials for near future use as they are proven to enhance the properties of neat polymers to a remarkable extent. The industrially feasible applications of these novel materials are underway [Bhattacharya et al., 2008].

As listed by Collister [2001], some of the property improvements that can be achieved by incorporating nanofillers into polymer matrixes are:

- Efficient reinforcement with minimal loss in ductility and impact strength.
- Thermal endurance.
- Flame retardance, improved liquid and gas barrier properties.
- Reduced shrinkage and residual loss.
- Altered electrical, electronic and optical properties.

One of the most studied type of polymeric nanocomposites are polymer–nanotube composites. With their outstanding mechanical, thermal, chemical and electronic properties, nanotubes are promising fillers for the reinforcement of polymeric materials. However, several obstacles limit the effective usage of polymer–nanotube composites in industry today. These obstacles are mainly due to the

difficulty in producing high amounts of pure nanotubes with low cost and in dispersing the nanotubes inside the polymer matrix in a manner that the properties of nanotubes are effectively reflected on the resulting composite [Zhi et al., 2006]. Today, the studies on polymer–nanotube composites are mainly focused on these two main problems.

### **3.3 Fabrication of Polymer – Nanotube Composites**

The process of preparing a polymer–nanotube composite involves the mixing of polymer and nanotubes in a manner that nanotubes are dispersed homogeneously throughout the polymer matrix. The success of a polymer–nanotube composite lies in the degree of cooperation of individual nanotubes within the polymer matrix, which is directly proportional to the total surface area between the nanotubes and the polymer. More contact area between the nanotubes and the polymer matrix means more pronounced exhibition of extraordinary mechanical, thermal and electronic properties of nanotubes in the resulting composite [Zhi et al., 2008]. Today, mainly three methods are used to fabricate polymer–nanotube composites: solution dispersion, in-situ polymerization and extrusion.

Solution dispersion method encompasses the dispersion of nanotubes inside a polymer matrix by using a solution medium and it is employed mostly for research purposes. In-situ polymerization is a method for preparing polymer–nanotube composites in which the allocation of nanotubes in the polymer matrix is achieved during the course of polymerization, which is the process of obtaining the polymer from its monomer blocks. Extrusion process (also referred to as melt blending) involves the physical blending of molten polymer with other possible additives. It is a widely used route in industry for the processing of polymers. Extrusion process is generally coupled with melt injection process in order to give specific shapes to polymeric commodities.

### 3.3.1 Solution Dispersion Method

In order to maintain an advanced dispersion of fillers inside the polymer matrix, researchers often apply the solution dispersion method for fabricating polymer composite specimens. This route is also referred to as solution intercalation or solution mixing method. Figure 3.1 demonstrates the steps of solution dispersion method to fabricate a polymer–nanotube composite.

In this method, first nanotubes, then the polymer are dispersed in a solvent. The solvent is sonicated in order to disengage the agglomerated nanotubes and allocate them throughout the solution. The sonicated solution is cast on a glass plate or silicon wafer and allowed to evaporate. After the evaporation, composite film precipitates on the surface of the plate. Precipitate is peeled off and hot pressed in order to give a specific shape (Figure 3.1). This method provides nicely dispersed polymer–nanotube composites.

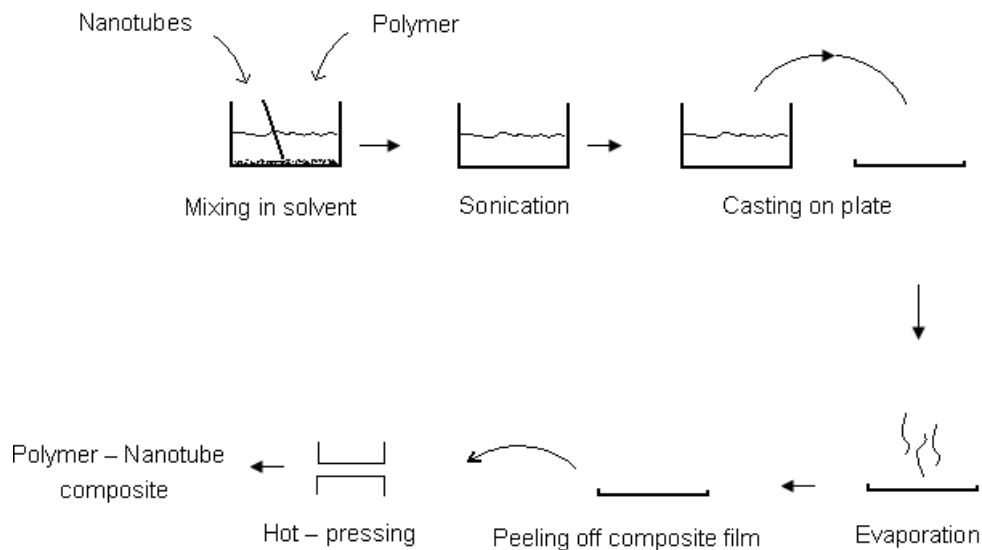


**Figure 3.1** Typical procedure for preparing polymer–nanotube composites using solution dispersion method.

### **3.3.2 In-Situ Polymerization**

In-situ polymerization is a widely used technique to prepare polymer–nanotube composites. In this technique, the nanotubes are positioned inside a fluidic medium of monomers and polymerization catalysts. The polymerization of the monomers is performed and the polymer composite is obtained with nanotubes allocated inside the matrix.

### **3.3.3 Extrusion**

Extrusion is the widespread technique being used to process polymers for producing final products from raw polymers. Fabrication of polymer–nanotube composites by extrusion process encompasses the dispersion of nanotubes inside the polymer matrix by simply blending the polymer melt together with nanotubes and other possible additives. In practice, this is carried out by passing a polymer–nanotube mixture through an extruder. Figure 3.2 shows the schematic representation of a typical single-screw extruder.

A typical extruder has a horizontally placed barrel, the temperature profile inside which is controllable. Inside the barrel, there is a single or double screw. The rotating motion of the screws creates a mixing regime inside the barrel. The shear forces created by the motion of screws blend the polymer melt, causing the additives to be dispersed in the polymer matrix [Crawford, 1998]. The rotating speed of the screws, hence the speed of mixing is adjustable. The extruded polymer exits the barrel from the die, which is the ending section of the barrel.

This process is an easy way to produce well-dispersed polymer–nanotube composites. However, in high loadings of nanotubes, polymer melt gets much more viscous with the effect of nanotubes and the rotation of the screws becomes insufficient to disperse the nanotubes [Mark, 2007].

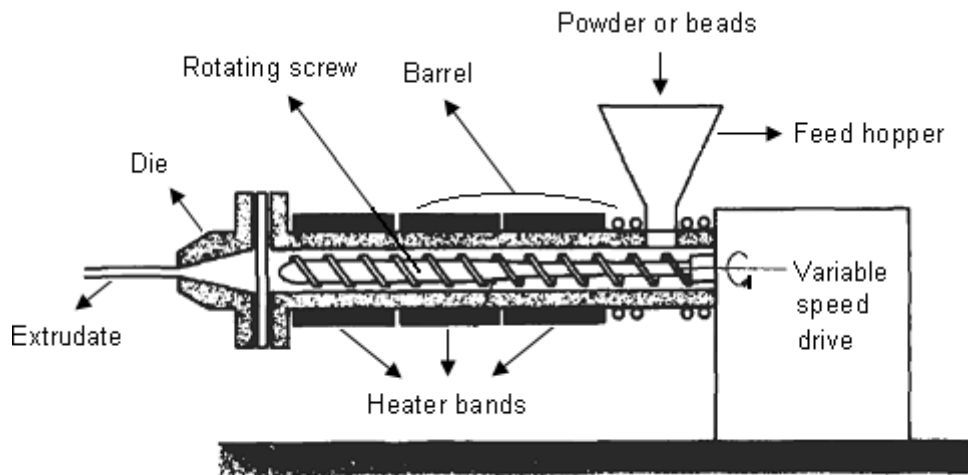


**Figure 3.2** Schematic representation of a single screw extruder [Crawford, 1998].

### 3.3.3.1 Function of Extruder Screw

The screw inside the barrel is the most crucial part of an extruder since it governs the mixing regime of the molten material along the barrel. The screw is designed specially for maintaining a better mixing inside the barrel. For that purpose, it is divided into sections and each section is designed differently to conduct a specific function [Crawford, 1998]. Figure 3.3 shows the sections of an extruder screw.

The extrusion process starts with the feeding of raw polymeric materials from the feed hopper or feeding hole. Upon feeding, the solid material is grabbed and transferred into a solid bed section by the motion of first section of the screw, which is also called the feed section (Figure 3.3).

After the feed section, the polymeric material enters the compression section of the screws, where the polymer is melt mixed and pressurized by the rotating motion of screws. The screws located in this area are designed to compress the molten polymer and create shear forces inside the molten material for an efficient mixing.

The screws at the compression section have a lower screw depth than the feed section in order to impose a pressure to the polymer melt (Figure 3.3). This

squeezing regime compresses the air bubbles formed in the polymer melt and sends them back to the feeding section, avoiding their creep into the final section.

Extruded material is withdrawn from the die by forward pressure created by the metering section of the screw (Figure 3.3), which has a constant screw depth. The metering section also has the lowest screw depth along the whole screw [Kroschwitz & Mark, 2003].

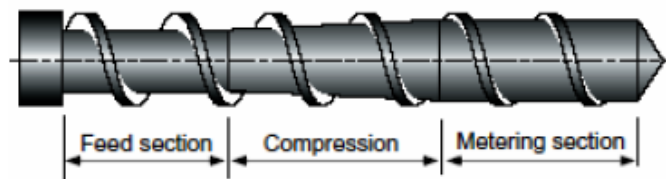


**Figure 3.3** Sections of an extruder screw [Crawford, 1998]

### 3.3.3.2 Twin-Screw Extrusion

Twin-screw extruders are extruders that have two co-operating screws in their heated barrels. By the usage of double screw, operation parameters of extrusion such as output rates, mixing efficiency or heat generation (by the shear forces created by the screws) are aimed to be improved [Crawford, 1998]. Different types of twin-screw extruders are possible according to the rotation direction and the arrangement of the double screw inside the barrel. These types are illustrated in Figure 3.4.



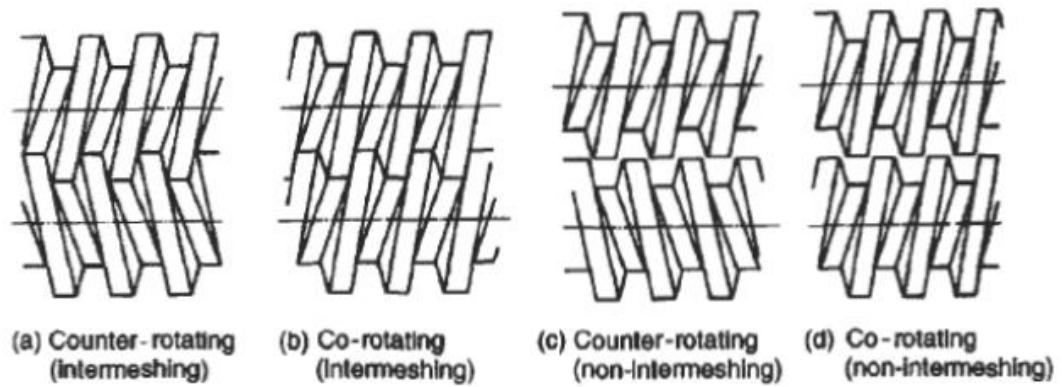


**Figure 3.4** Types of twin-screw extruders [Crawford, 1998].

As seen in Figure 3.4, several arrangements are possible for twin-screw extrusion. Intermeshing or non-intermeshing arrangements of screws determine the flow regime of molten material inside the extruder barrel. In non-intermeshing twin-screw extrusion, there is a clearance between the screws, so that the molten material can follow a path between the screws. In counter rotating motion, the molten material is squeezed between the screws. In co-rotating motion, the molten material is transferred from one screw to another, following a figure-of-eight pattern as shown in Figure 3.5.

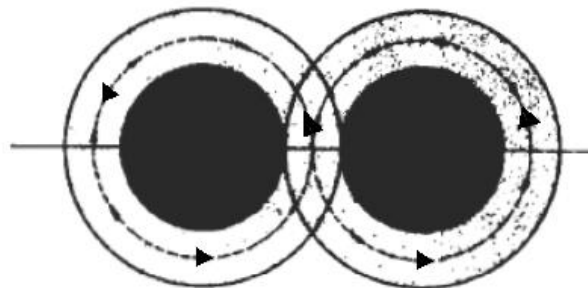


**Figure 3.5** Motion of material in co-rotating, non-intermeshing twin-screw extrusion [Crawford, 1998].

### 3.3.4 Melt Injection

Melt injection is a simple and frequently used process to manufacture polymeric materials of desired shapes. Figure 3.6 summarizes the steps of melt injection process.

The melt injection process is practically carried out by a melt injection machine, in which the polymeric material is melted under a controlled temperature medium. Then, the molten polymer is injected into a cold mold. The polymer solidifies inside the mold, which functions as a template of desired shape. Finally, the solidified polymer is ejected from the mold as a usable final product. According to the type of polymer to be injected, process variables of the melt injection can be adjusted [Middleman, 1997].

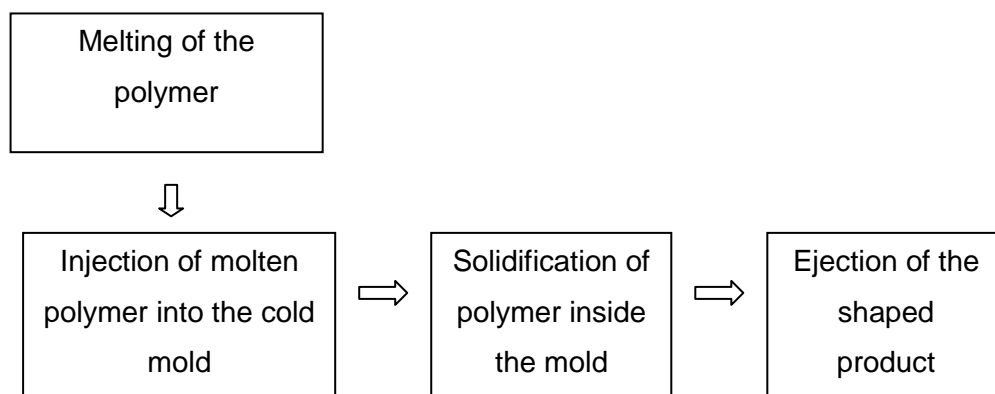


**Figure 3.6** Steps of injection molding process.

### 3.4 Polypropylene

Polypropylene (PP) was used as the polymer matrix in this study. PP is a thermoplastic polyolefin produced by the polymerization of propylene molecule, which is a gaseous by-product of petroleum refining [Tripathi, 2002]. Polypropylene

was first synthesized by the polymerization of propylene monomers by G. Natta in 1954.

### 3.4.1 Structure of Polypropylene

Polypropylene (PP) is a vinyl polymer, which has methyl groups attached on every second carbon in its carbon chain (Figure 3.7). Each macromolecule of polypropylene might contain up to 20,000 propylene units [Tripathi, 2002].

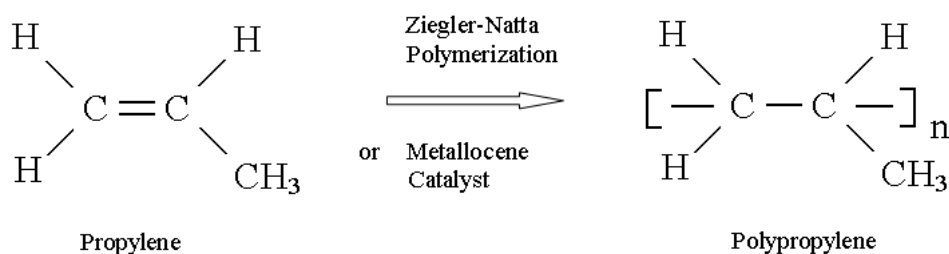


**Figure 3.7** Synthesis of polypropylene.

Several isomeric structures of polypropylene are possible according to the arrangement of methyl groups that are attached to the carbon chain (Figure 3.8). The degree of proximity of methyl groups bounded to the carbon chain determines the tacticity of a polypropylene. If all methyl groups are arranged adjacently on the same side of the carbon chain, the polypropylene is referred to as isotactic. If methyl groups are arranged randomly alongside the chain, the polypropylene is atactic. If the methyl groups are alternating on the adjacent sides of carbon chain, the polypropylene is syndiotactic [Tripathi, 2002]. Isotactic, atactic and syndiotactic configurations of polypropylene are illustrated in Figure 3.8.

The tacticity of carbon rings of a polypropylene determines the physical properties on macro level. Isotactic polypropylene is the most commercialized type of polypropylene with low specific weight, high toughness and medium flexibility.

Syndiotactic polypropylene has less crystalline structure than the isotactic polypropylene. Therefore, it is softer and more flexible than the isotactic polypropylene. The carbon chains of atactic polypropylene lack of molecular integrity. Therefore, it is a soft, transparent, viscous fluid and used only as a softener for other polymers [Seymour & Carraher, 1984].

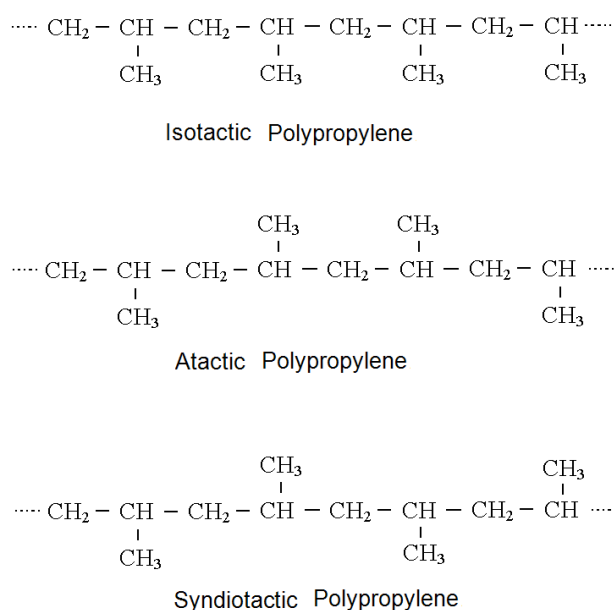


**Figure 3.8** Stereo chemical structures of polypropylene.

### 3.4.2 Properties of Polypropylene

Polypropylene is an abundantly used polymer owing to its ease of production and processing. It has many advantageous properties while having a low production cost. In 2007, global sales of PP have reached to a volume of 45.1 million tons, which corresponds to a turnover of about 65 billion US \$ [Ceresena, 2007].

Polypropylene has very desirable physical, thermal and mechanical properties for room temperature uses. Properties of polypropylene such as low density, high impact and fatigue resistance, toughness, flexibility, resistance to heat, high

melting point (160–170 °C for commercial isotactic PP), regular melting rheology and ease of processing make polypropylene a preferable material to be used in the manufacturing of many consumer products [Tripathi, 2002].

### **3.4.3 Applications of Polypropylene**

Commercial isotactic polypropylene finds wide range of applications in areas such as household goods, automotive industry, fibers, domestic appliances, packaging, pipes, fittings etc. [Tripathi, 2002].

## **3.5 Characterizations of the Materials**

In polymeric nanocomposite studies, a series of analysis techniques are employed to gain insight of the nanofillers or nanocomposites. Followings are the characterization techniques used in this study to characterize the nanotubes and polymer–nanotube composites.

### **3.5.1 X-ray Diffraction (XRD)**

XRD is a method that has been widely used to understand the crystalline structures of solid substances and to identify the crystalline materials that exist in a solid specimen.

In XRD analysis, an X-ray beam that typically has a wavelength between 0.7 and 2 Å is sent onto a rotating sample. The X-ray beam is diffracted by the crystalline phases existing in the sample [Cao, 2004]. The diffraction of X-rays obeys the Bragg's law as follows,

$$n\lambda = 2d\sin\theta \quad (3.1)$$

where,  $d$  is the distance between the successive atom planes of the crystalline structure,  $\lambda$  is the wavelength of the incident X-ray beam,  $\theta$  is the angle between the atomic plane and the X-ray beam,  $n$  accounts for the order of diffraction [Callister, 1997]. The diffraction parameters of an X-ray beam diffracted from a crystalline phase is shown in Figure 3.9.

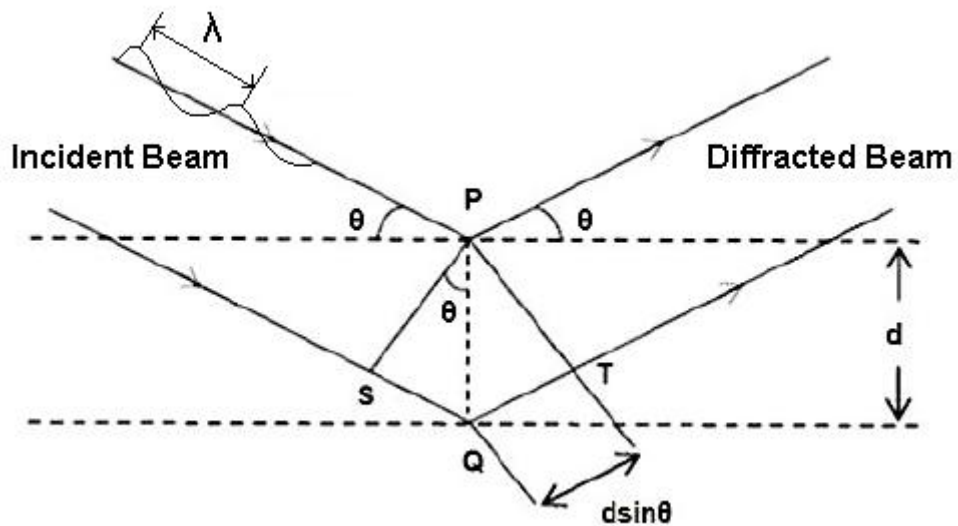


**Figure 3.9** Diffraction of X-ray beam from a crystalline material [Callister, 1997].

As the  $\theta$  angle is slowly increasing, recorder of the diffractometer transmits signals that are proportional to the intensity of the diffracted beam (Figure 3.9) and a plot of  $2\theta$  angle versus intensity is obtained. Every crystalline phase has characteristic peaks that are observed at specific  $2\theta$  values. Therefore, XRD pattern of any type of crystalline material is like a fingerprint. One can understand which crystalline phase exists in what proportion in a specimen by examining its XRD pattern. The diffraction pattern also gives information about the crystalline morphology of the specimen [Callister, 1997].

### 3.5.2 Fourier Transform Infrared (FTIR) Spectroscopy

Fourier Transform Infrared Spectroscopy is an analysis method used for identifying the chemical bonds or functional groups existing in a material. Middle range infrared spectrum ( $400 - 4000 \text{ cm}^{-1}$ ) is generally used for the characterization of samples. The absorption and transmission of infrared lights on the molecular level make it possible to obtain information about the chemical composition of an unknown material [Stuart, 1996].

### **3.5.3 Multi-Point BET Surface Analysis**

The most widely used method for projecting the surface characteristics of porous materials is the BET method. BET stands for Brunauer, Emmett and Teller, the initials of scientists who developed the technique in 1938. Properties of materials such as surface area or pore-size distribution can be determined by BET surface analysis.

BET analysis can be either single-point or multi-point. In multi-point BET surface analysis, nitrogen gas environment with controlled pressure is applied onto a specimen of known initial weight. The analysis is carried out under constant temperature. As the pressure of the nitrogen is increased, the nitrogen molecules are adsorbed by the pores and bulk free surface of the sample. As surfaces of the sample are fully covered, the pressure is decreased and the nitrogen molecules are desorbed. The adsorption and desorption isotherms of the sample give information about the surface characteristics of the analyzed specimen.

### **3.5.4 Scanning Electron Microscopy (SEM)**

SEM is a microscopic analysis technique, which is widely used in the characterization of materials' surface morphology. In this microscopic analysis technique, electron beam sent from an electron gun scans the surface of a sample. The interaction of electron beam with the surface atoms of the sample produces signals that are detected by a detector. The variations in the intensity of signals are processed and transformed to visible images.

The surface of the specimen should be electrically conductive. If the sample is electrically isolating, it should be made conductive by coating with an electrically conductive material such as carbon or gold [Bhattacharya, 2008].

The magnification ratio of the SEM images is higher than conventional optical microscopes, but lower than transmission electron microscopes. More than 50,000 times magnification is possible in SEM images [Bhattacharya, 2008].

### 3.5.5 Transmission Electron Microscopy (TEM)

TEM is used for detailed molecular morphology characterization of specimens. TEM is a more advanced technique with respect to SEM since it allows observing the internal molecular structures of a sample. The resolution of a TEM image is about 0.2 nm, which is much more detailed compared to 2 nm resolution of SEM images [McCulloch, Harland & Francis, 2003]. TEM provides high-resolution microscopic images, which give direct information about the atomic arrangements, distributions, defects and structures within a very small representative section of a specimen [Wischnitzer, 1989].

Preparing the specimen is the most crucial stage of TEM analysis. The specimen to be analyzed should be microtomed to very thin particles in order to obtain clear images. Besides, the specimen should be distributed throughout the surface of a carbon grid in a manner that it forms a single thin layer of specimen particles. Thick agglomerates of specimen particles should be avoided in a TEM specimen [Wischnitzer, 1989]. A schematic illustration of a TEM apparatus is shown in Figure 3.10.

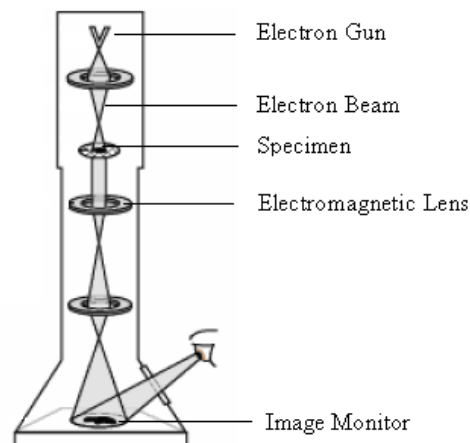


**Figure 3.10** Schematic illustration of a TEM apparatus\*.

\*Retrieved from <http://nobelprize.org/educational/physics/microscopes/tem>, last access: 12.9.2010



### 3.5.6 Mechanical Characterization

#### 3.5.6.1 Tensile Test

The tensile test is used to obtain information about tensile properties of materials such as elongation at break, Young's modulus, yield and tensile strength. To conduct a tensile test, standard test specimens should be prepared from the material to be analyzed. These specimens are generally in the shape of dog bones, both ends of which are clamped to the moving heads of the testing machine. As the tensile test begins, the moving heads of testing machine are separated at a constant speed rate by applying an increasing force. The force applied to elongate the specimen is continuously recorded. The test continues until the specimen breaks. Finally, force vs. elongation plot of the specimen is obtained. Figure 3.11 shows the schematic representation of a tensile test machine.

The output data of a tensile test is a plot of tensional force versus elongation. This raw data is transformed into a standard stress vs. strain plot by utilizing the dimensions of the specimen.

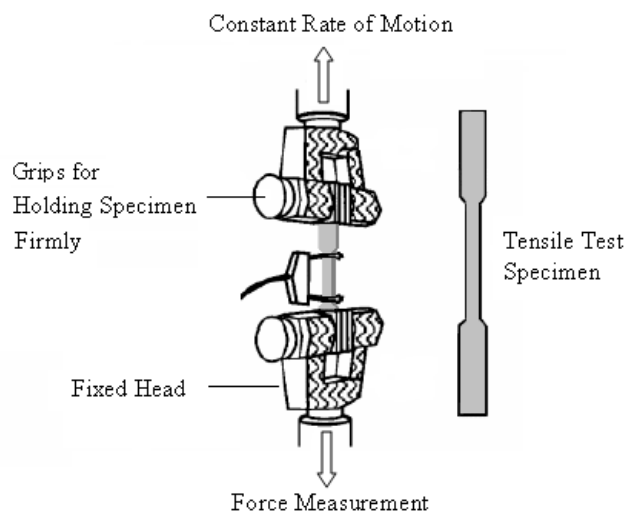


**Figure 3.11** Tensile test apparatus [Seymour, 1996].

Equations (3.2) and (3.3) are the associated equations for stress and strain, respectively.

$$\sigma = F / A_0 \quad (3.2)$$

$$\varepsilon = (L_i - L_0) / (L_i) \quad (3.3)$$

where  $F$  is the tensional force applied on the specimen,  $A_0$  is the initial cross-sectional area of the specimen,  $\sigma$  is the engineering stress in units of pressure, and  $\varepsilon$  is the dimensionless elongation of the specimen at any moment.

An important tensile property of materials is the Young's modulus. Young's modulus is the measure of stiffness of a material. Hooke's law (Equation 3.4) defines the Young's modulus ( $E$ ) as:

$$E = \varepsilon \cdot \sigma \quad (3.4)$$

The Young's modulus is the slope of the initial and linear region of a stress-strain plot.

Tensile strength of a material is the maximum stress that specimen can withstand until it breaks. Yield strength of a material is the maximum stress that specimen can withstand before it starts to deform plastically.

Two possible stress–strain plots for a hypothetical polymeric material are given in Figure 3.12. In Figure 3.12 (a), the tensile strength, which is the maximum point of the stress–strain curve, is observed at the fracture point. In this case, the first maxima, which is the maximum stress the specimen could carry before it plastically deforms, is the yield strength of the material. In Figure 3.12 (b), the specimen fractures before withstanding a higher stress than the yield point. In this case, the yield strength and the tensile strength of the specimen are the same value [Yeniova, 2009].

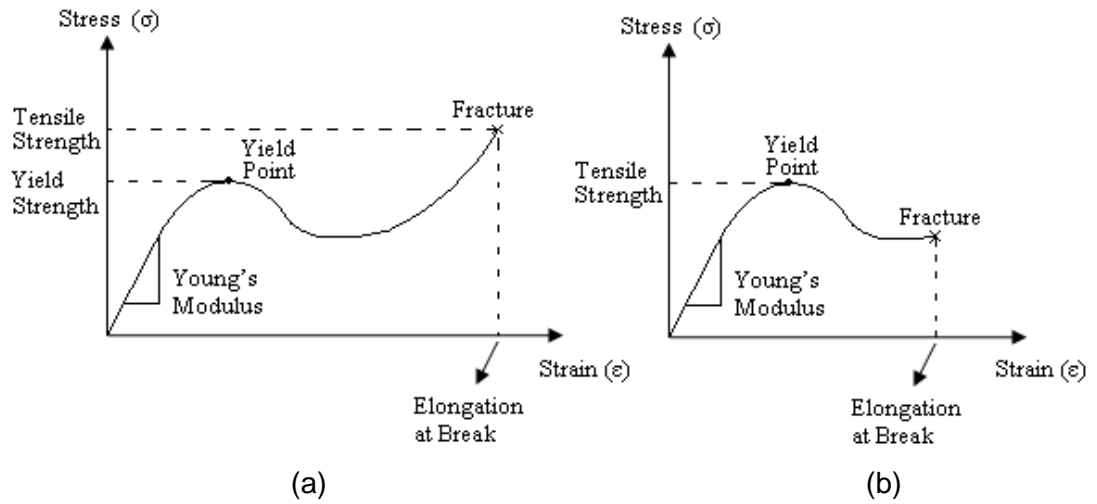


**Figure 3.12** Stress–strain curves: (a) Tensile strength at fracture (b) Tensile strength at yield.

Stress–strain curve of a material reveals its mechanical characteristics. Figure 3.13 shows some mechanical characteristics of materials according to their stress-strain curves.

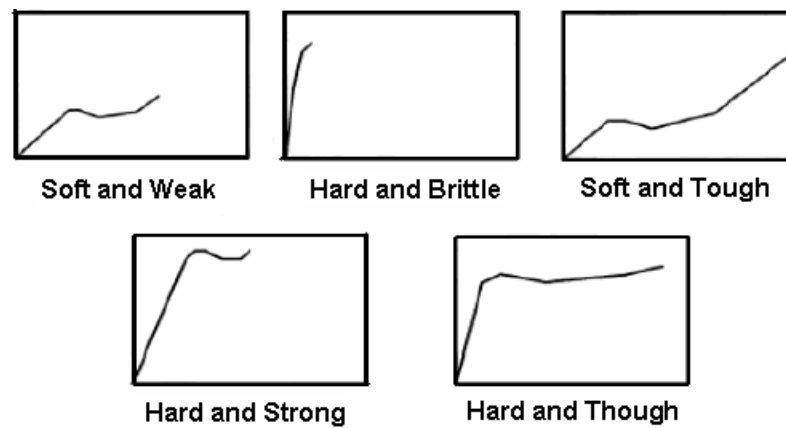


**Figure 3.13** Different stress–strain behaviors of materials [Yeniova, 2009].

### 3.5.7 Thermal Characterizations

#### 3.5.7.1 Differential Scanning Calorimetry (DSC)

DSC is a thermal analysis technique developed by S. Watson and J. O'Neill in 1960. Today, this technique is widely used to determine the glass transition, crystallization and melting temperatures of materials, especially those of polymeric materials.

In DSC analysis, the sample is placed inside a miniature pan, with another empty pan next to it (reference pan). Both pans are heated by applying thermal energy. The heat is conveyed to the pans in a manner that the temperature of both pans increases at the same rate. The difference between the rate of heat transferred to the sample pan and empty pan is recorded with respect to temperature. The difference in the heat flow is basically the energy absorbed by the sample to increase its own temperature.

When the sample undergoes physical changes such as melting, crystallization or glass transition, the plot starts to disorder from its normal trend since more or less heat is needed for the sample to undergo physical changes. In addition, the heat capacity and transition enthalpies of the analyzed specimen can be easily determined from this plot [Bhattacharya, 2008]. Figure 3.14 shows a typical DSC plot.

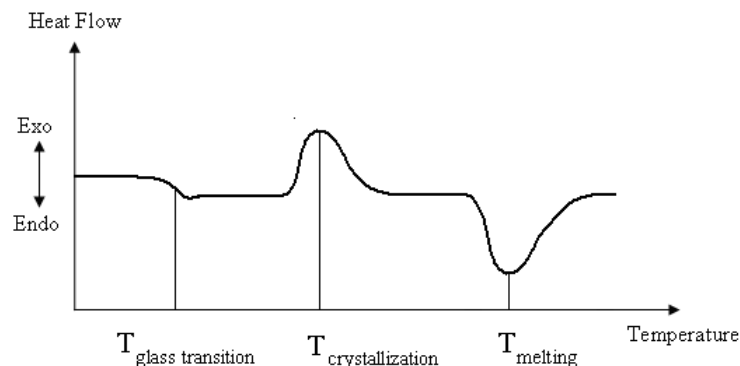


**Figure 3.14** A typical DSC plot.

### **3.5.7.2 Thermal Gravimetric Analysis (TGA)**

Thermal gravimetric analysis is a technique used to measure materials' resistance to heat. In this analysis technique, a sample is continuously weighed as its temperature is increased with a constant heating rate.

The analysis can be performed under a nitrogen (inert) or air atmosphere. As the temperature of the sample increases, the sample starts to evaporate or degrade, which results in a decrease in the initial weight of the sample. As the temperature further increases, the residual weight decreases. If a composite material is analyzed, the filler content of the composite may remain as the final residue [Bhattacharya et al., 2008].

### **3.5.7.3 Thermal Mechanical Analysis (TMA)**

Thermal mechanical analysis (also referred to as dilatometry) is a method that is used to analyze the mechanical expansion behavior of materials with respect to temperature. This analysis method is generally utilized for the determination of coefficient of thermal expansion, softening and transition temperatures of polymeric materials. In this technique, volumetric or dimensional elongation of a sample is measured with respect to increasing temperature. The plot of elongation vs. temperature gives direct information about the linear thermal expansion coefficient of the analyzed sample, which is the percent linear elongation of the specimen over the temperature gradient. The coefficient of thermal expansion (CTE) of polymeric materials can change with respect to temperature. CTE of polymeric materials generally increases with temperature since the polymers tend to lose structural integrity as they approach their melting points.

## CHAPTER 4

### LITERATURE SURVEY

The boom of interest in nanotube structures began with the discovery by Iijima [1991] that highly pure multi-wall carbon nanotubes could be produced by an arc discharge method. Studies on boron nitride nanotubes started with the reporting of synthesis by Chopra et al [1995]. Since then, boron nitride nanotubes have remained an active subject of materials science with increasing number of publications every year. However, BNNTs are still attracting less attention compared to their carbon counterparts. In Figure 4.1, the number of published articles on the nanotube structures of boron nitride and carbon are compared.

The studies on polymer–CNT composites are very common in the literature and being studied frequently since the discovery of carbon nanotubes by Iijima [1991]. However, the studies on polymer–BNNT composites are rare in the literature. There are many studies in the literature specifically about polypropylene (PP)–CNT composites. The PP–CNT composites in these studies were often prepared by using extrusion (melt blending) process. However, the polymer – BNNT composites in the associated studies were predominantly fabricated as thin films using solution dispersion method. This is mainly due to the difficulties in synthesizing sufficient amounts of purified BNNTs to process them via extrusion process.

The literature survey for this study is divided into three sections:

- 1- Production of boron nitride nanotubes
- 2- Polypropylene – carbon nanotube composites
- 3- Polymer – boron nitride nanotube composites

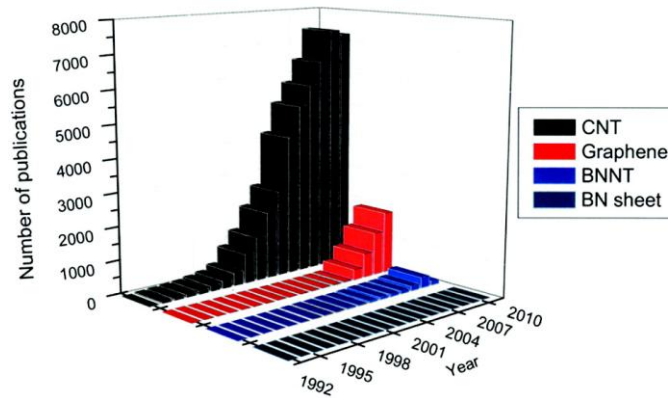


**Figure 4.1** Number of publications on the sheet and nanotube structures of carbon and boron nitride [Golberg, 2010].

#### 4.1 Production of Boron Nitride Nanotubes

Chopra et al. [1995] synthesized boron nitride nanotubes using an arc-discharge method. The length of the synthesized nanotubes was over 200 nm with inner diameter of between 1 - 3 nm and outer diameter of between 6 - 8 nm.

Tang et al. [2001] synthesized BNNTs by heating a mixture of elemental boron and iron oxide to high temperatures in a tubular furnace. Ammonia gas was used as the reaction gas. The study revealed that the reaction temperature and the weight ratio of boron to iron oxide in the initial mixture played an important role in the structure of synthesized BNNTs.

Tang et al. [2002] also synthesized BNNTs from a mixture of elemental boron and magnesium oxide. They observed a broad distribution in the diameter of synthesized nanotubes. Mg residues were removed from the final product and pure BNNTs were obtained.

Zhi et al. [2005] synthesized BNNTs using a mixture of elemental boron, iron oxide and magnesium oxide as the initial mixture. Highly pure BNNTs have been synthesized within a wide temperature range.

Lee et al. [2008] proposed a technique for growing high yield BNNTs in horizontal tubular furnaces. In their method, an alumina boat with a mixture of boron, iron oxide and magnesium oxide is placed in a quartz test tube, which is placed in the center of a tubular furnace and heated up to 1200 °C. Ammonia gas is fed at this temperature to react with the precursor gases. Long BNNTs are collected from the surfaces of test tube and the alumina boat.

Özmen [2008] has investigated the effect of synthesis parameters on the morphological properties of as-synthesized BNNTs. Elemental boron and iron oxide mixture was used as the initial mixture to synthesize BNNTs. The experiments were carried out on a horizontal tubular furnace. Ammonia was used as reaction gas. Different reaction temperatures and ratios of boron to iron oxide were experimented. It was concluded that a reaction temperature of 1300 °C and boron to iron oxide ratio of 15/1 yielded the highest concentration of BNNTs in the product.

#### **4.2 Polypropylene – CNT composites**

Kashiwagi et al. [2002] investigated the electrical, thermal and flammability properties of extruded PP–CNT composites. The cone calorimetry results revealed that 2 and 4 wt% of CNT addition significantly decreased the flammability of polypropylene. With 5 wt% of CNTs, the thermal conductivity of composites was increased. The electrical conductivity of polypropylene was dramatically increased with CNT addition.

Dondero and Gorga [2006] studied the morphological and mechanical properties of PP–CNT composites. Tensile tests revealed that by 0.25 wt% of multi-wall CNT addition, noticeable increase in the toughness of composites was achieved. Moreover, the elastic modulus was increased at same CNT loading. It was reported that CNTs are promising fillers for mechanical enhancement of polymers.

Manchado et al. [2005] studied the thermal and mechanical properties of extruded PP–CNT composites. It was reported that 0.5 – 1 wt% of CNT addition in neat PP matrix resulted in a noticeable increase in the elastic modulus and tensile strength.



The differential scanning calorimetry (DSC) curves indicated that CNT loading improves the thermal stability of neat polymer.

The study by Kim [2005] has showed that the usage of acid-treated carbon nanotubes were more effective than the non-treated CNTs in increasing the thermal properties of polypropylene.

Marosfoi et al. [2006] investigated the thermal properties of PP–CNT composites. Their study revealed that the allocation of CNTs increased the thermal stability of neat polypropylene.

Prashantha et al. [2008] investigated the role of polypropylene-graft-maleic anhydride (PP-g-MA) addition as a compatibilizer in the extruded PP–CNT composites. They used PP-g-MA in order to disperse CNTs more uniformly in the polymer matrix. It was reported that better dispersion of nanotubes was maintained with the usage of compatibilizer. Therefore, a better mechanical reinforcement was achieved.

### **4.3 Polymer – BNNT composites**

Zhi, Bando & Tang [2006] studied mechanical properties of Polystyrene(PS) – BNNT composite films that were prepared by solution dispersion method. It was observed that with 1 wt% addition of BNNTs, Young's modulus of composites was improved.

Harrison et al. [2007] studied the mechanical properties of extruded polyethylene (PE) – hexagonal boron nitride composites. They reported an improvement in the Young's modulus of neat polyethylene with the addition of 15 vol% of hexagonal boron nitride.

Zhi et al. [2008] studied thermal and mechanical properties of poly(methyl methacrylate) (PMMA) – BNNT composites prepared by solution dispersion method. With 1 wt% of BNNT addition, elastic modulus of composites was observed to improve. With 10 wt% of BNNT addition, thermal conductivity of

composites folded 3 times and coefficient of linear thermal expansion (CLTE) of composites were reduced. The composites remained electrically isolating.

Ravichandran et al. [2008] developed a novel polymer–BNNT composite for photovoltaic packaging applications. Saran (a co-polymer of vinylidene chloride and acrylonitrile) was used as the polymer matrix. Up to 1.5 wt% of BNNT loading in the composites was investigated. The resulting composites showed high transparency in the visible region, good barrier properties and thermal stability to be used as an encapsulating material for photovoltaic devices.

Zhi et al. [2009] studied the thermal, mechanical and electrical properties of composites of poly(methyl methacrylate) (PMMA), polystyrene (PS), poly(vinyl butyral) (PVB) and poly(ethylene vinyl alcohol) (PEVA) with purified BNNTs. With 18 - 37 wt% of BNNTs, dramatic increase in the thermal conductivity of polymers was observed. It was reported that BNNT loading decreased the coefficient of thermal expansion (CTE) of polymers. Electrically isolating nature of the polymers were kept in the resulting polymer–BNNT composites.

Terao et al. [2009] studied the thermal conductivity and thermal stability of polymer films with respect to BNNT concentration. With 1 wt% of BNNT addition, the thermal conductivity and thermal stability of the composites were improved.

#### **4.4 Objectives of the Study**

Even though studies about polymer–BNNT composites are rare in the literature, those studies proved the improving effect of BNNTs on several mechanical and thermal properties of polymers such as Young's modulus, strength, resistance to oxidation or thermal conductivity, while preserving the electrically isolating nature of the polymer matrix. However, most of the polymer – BNNT composites that have been studied to date were prepared as film specimens via a solution dispersion technique, which encompasses the dissolution of polymer and nanotubes inside a solution medium, followed by evaporation. This kind of a composite preparation approach is advantageous for research purposes since it allows a good dispersion of nanotubes inside the polymer matrix. On the other hand, it has drawbacks such as the complexity of the process and lacking commercial viability [McNally et al.,

2005]. Industrially, routine way of manufacturing polymeric commodities is the extrusion process.

The importance of this study is that the capability of BNNTs to improve the properties of polypropylene, which is an abundantly used thermoplastic polymer, was investigated for the first time. Moreover, the composites were prepared using extrusion process, which is a widely used process in industry to manufacture polymeric commodities.

The main objectives of this study are:

- To synthesize BNNTs from the reaction of ammonia gas with a mixture of elemental boron and iron oxide.
- To study the effect of inlet flow rate of ammonia gas on the production of BNNTs.
- To characterize the as-synthesized BNNTs using XRD, FTIR, multi-point BET, SEM and TEM analyses.
- To purify the as-synthesized BNNTs with successive acid treatments and to modify the surface of the nanotubes by grafting polyethylene glycol (PEG) moieties in order to improve their dispersion inside the polymer matrix.
- To prepare polypropylene–BNNT composites at different BNNT loadings using extrusion and injection molding processes.
- To investigate the effect of BNNT concentration on the mechanical and thermal properties of PP–BNNT composites by tensile testing, differential scanning calorimetry (DSC), thermal gravimetric analysis (TGA) and thermal mechanical analysis (TMA).
- To investigate the effect of purified and surface modified BNNT usage in the composites and to compare these effects with the as-synthesized BNNT usage.

## CHAPTER 5

### EXPERIMENTAL

The objectives of this study were to synthesize boron nitride nanotubes from the reaction of ammonia gas with a powder mixture of boron and iron oxide, to characterize the synthesized product with XRD, FTIR, multi-point BET surface, SEM and TEM analyses, to fabricate PP–BNNT composites with extrusion and melt injection processes, and to investigate the mechanical and thermal properties PP-BNNT composites as a function of BNNT concentration. Figure 5.1 summarizes the experimental work conducted in this study in order to achieve these objectives. Accordingly, experimental part of this study was represented in five sections:

- 1- Production of BNNTs
- 2- Characterization of BNNTs
- 3- Purification and modification of BNNTs
- 4- Fabrication of PP–BNNT composites
- 5- Characterization of PP–BNNT composites

First part covers the synthesis of boron nitride nanotubes from the reaction of ammonia gas with a powder mixture of boron and iron oxide to produce sufficient amounts of BNNTs for composite preparation. The second part covers the experiments that were carried out to characterize the synthesized BNNTs. Third part covers the purification and surface modification processes of as-synthesized BNNTs. Fourth part focuses on the fabrication of PP–BNNT composites using extrusion and injection molding processes. The last part is about the mechanical and thermal characterizations of PP–BNNT composites.

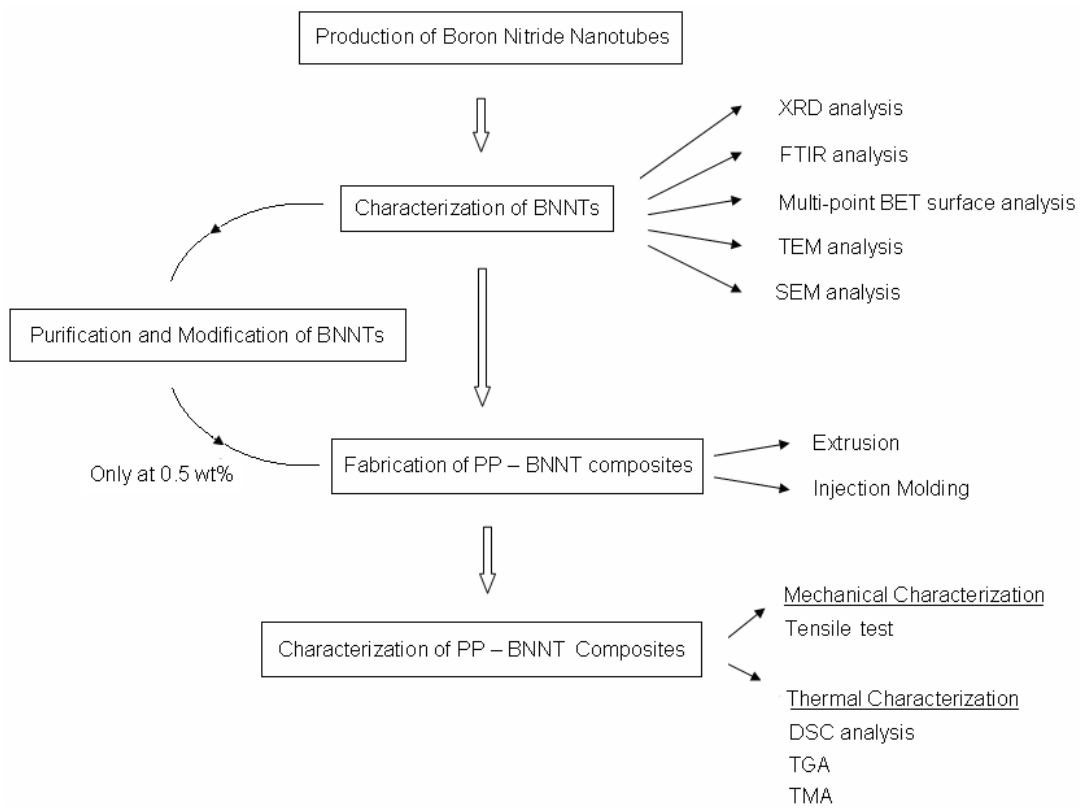


**Figure 5.1** Experimental work of the study.

## 5.1 Production of BNNTs

### 5.1.1 Experimental Set-Up

In this study, production of BNNTs was carried out by subjecting a powder mixture of elemental boron and iron oxide to ammonia gas flow inside a horizontal tubular furnace. Figure 5.2 shows the experimental set-up used for the synthesis of BNNTs in this study. The production of BNNTs was achieved in multiple batches.

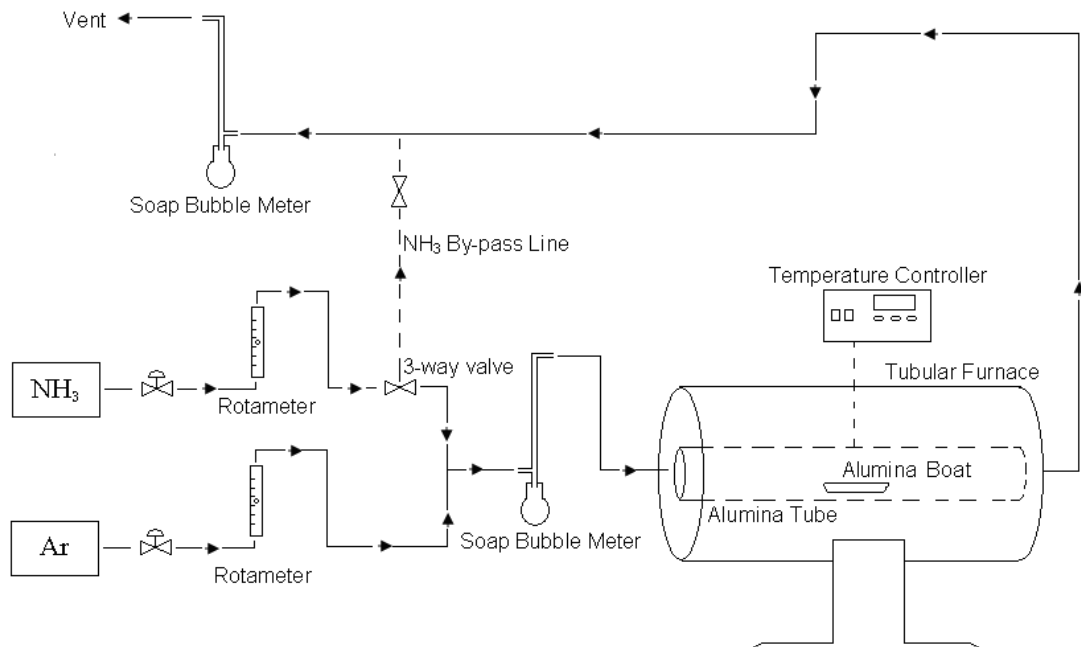


**Figure 5.2** Lay-out of the BNNT production system.

The BNNT production system consists of a Protherm PTF 16/50/450 horizontal tubular furnace, which can supply temperatures up to 1550 °C. The reaction chamber of the furnace is made from alumina and has an inner diameter of 50 mm. A temperature controller is connected to a Type B thermocouple, which measures the temperature at the inner center of the furnace. High purity argon and ammonia gases purchased from Oksan are connected to the furnace. The inlet flow rates of

the gases can be adjusted by rotameters. The actual inlet and outlet volumetric flow rates of the gases were measured with soap bubble meters. A 3-way valve was used in order to by-pass and to regulate the flow of ammonia gas while the furnace was being purged.

### **5.1.2 Experimental Procedure**

In a single BNNT synthesis batch, firstly, a mixture of elemental boron and iron oxide was prepared by dry mixing. The mixture was homogenized using an agate mortar and taken into an alumina boat with dimensions 120x30x15 mm. The mixture of boron and iron oxide was placed in the center of the horizontal tubular furnace. Following the placement, the temperature of the furnace was set to the reaction temperature by the temperature controller.

The regulators of argon and ammonia gas tubes were held at 2 bars. As the temperature of the furnace was increasing with a heating rate of 8 °C/min, argon gas was passed through the system at a flow rate of 50 cc/min in order to purge the furnace interior and clean the oxygen content. Temperature-time profile throughout a single BNNT synthesis batch is given in Figure 5.3. As the reaction temperature was reached, argon gas inlet to the system was shut off and the ammonia gas was fed into the system. The reaction period lasted for 2.15 hours.

When the reaction period was over, furnace was cooled at a rate of 5 °C/min with purging argon gas at 50 cc/min. After the cool down, the final product was taken out of the furnace. Color, physical appearance and the total weight of the product were recorded. The product from each batch was kept in a 60 cc specimen cap.

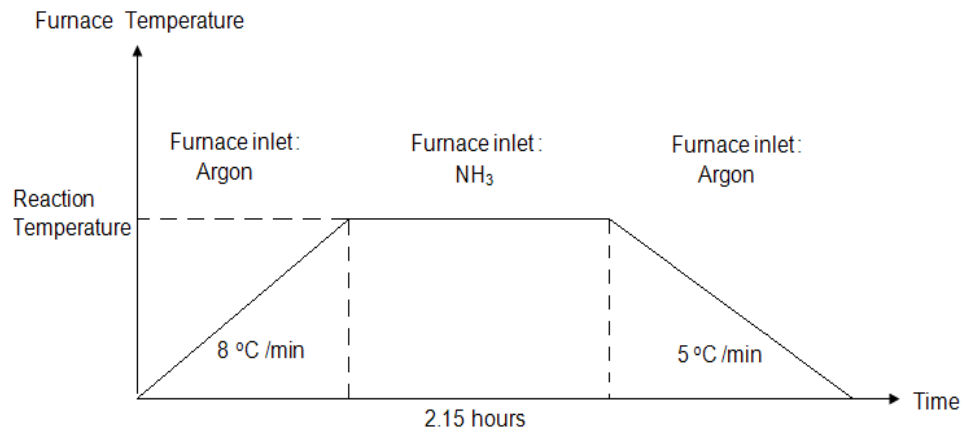


**Figure 5.3** Temperature–time profile of BNNT synthesis.

#### 5.1.2.1 BNNT Synthesis Parameters

There were five controllable synthesis parameters for the BNNT production in the explained system:

1. Total weight of the boron and iron oxide mixture
2. Boron to iron oxide weight ratio in the initial mixture
3. Reaction temperature
4. Reaction time
5. Inlet volumetric flow rate of ammonia gas

Second, third and fourth parameters were held constant in this study according to the formerly optimized values by the work of Özmen [2008]. Boron to iron oxide ratio of 15/1 and a reaction temperature of 1300 °C were reported to be optimum for the production of BNNTs in the cited study.

However, a higher amount of BNNT production was aimed in this study. Therefore, weight of the initial mixture and the inlet flow rate of ammonia gas were scaled up. The quality and the amount of the synthesized product were monitored with respect to initial mixture amounts and ammonia inlet flow rates in order to re-optimize the synthesis parameters. Ammonia inlet flow rates between 25 - 200



cc/min and initial mixture amounts of 0.8 and 1.2 grams were tested for optimization. The reaction time was 2.15 hours. Table 5.1 summarizes the initial mixture amount and ammonia inlet flow rate values tested to determine best conditions for BNNT production.

**Table 5.1** Tested parameters in BNNT production optimization runs.

Run No.	Total weight of initial mixture (g)	Ammonia inlet flow rate (cm <sup>3</sup> / min)
1	0.80	25
2	0.80	50
3	0.80	75
4	0.80	100
5	0.80	125
6	0.80	150
9	1.20	100
10	1.20	150
11	1.20	175
12	1.20	200

## 5.2 Purification and Modification of BNNTs

### 5.2.1 Purification of BNNTs

The purification of the as-synthesized BNNTs was carried out in order to get rid of the impurities in the as-synthesized product. In the purification process, 4 grams of as-synthesized BNNTs were poured into 400 mL of pure water and the mixture was sonicated for 30 minutes to separate iron particles by sedimentation. To get rid of remaining iron content, BNNTs were poured into a 500 mL of 2M HCl solution. The mixture was stirred for 3 hours at room temperature. BNNTs were retrieved from the mixture by filtration and washed with 500 mL of pure water.

In order to eliminate the boron content, HCl treated BNNTs were poured into a 500 mL of 2M HNO<sub>3</sub> solution. The mixture was stirred at 50 °C for 6 hours. BNNTs were retrieved from the mixture by filtration and rinsed with 500 mL of pure water. Finally, BNNTs were dried overnight at 100 °C in an oven.

### **5.2.2 Modification of BNNTs**

Surface modification of the purified BNNTs was carried out using polyethylene glycol (PEG). PEGylation process was carried out in order to graft PEG moieties on the nanotube surfaces and improve the dispersion of BNNTs inside the PP matrix.

For modification, 1 gram of purified BNNTs was poured into a 400 mL of 0.04 M NiCl<sub>2</sub> solution. 20 mL of PEG (M<sub>w</sub> ~ 600 g/mol) was added to the solution. The mixture was sonicated for 4 hours at 80 °C. After sonication, the mixture was filtered and surface modified BNNTs were rinsed with 1000 mL deionized water. Finally, BNNTs were dried overnight in a vacuum oven [Yeşil, 2010].

## **5.3 Characterizations of BNNTs**

Understanding the chemical and physical structure of the as-synthesized BNNTs was an important aspect of this study. The crystalline and chemical compositions of the synthesized BNNTs were investigated using XRD and FTIR analyses. Physical properties of the synthesized material such as surface area, pore distribution and average pore size were determined using multi-point BET surface analysis. The surface and molecular level morphology of the synthesized BNNTs were investigated with SEM and TEM analyses, respectively.

### **5.3.1 X-Ray Diffraction (XRD)**

To obtain information about the crystalline phases existed in the BNNT product, XRD analyses were performed with a Rigaku X-Ray Diffractometer between Bragg angles from 20° to 90° with a scanning rate of 1° /min. During the diffraction, voltage and current were held at 40 kV and 40 MA, respectively. Cu K $\alpha$  radiation source ( $\lambda=1.5418 \text{ \AA}$ ) was used.

### **5.3.2 Fourier Transform Infrared (FTIR) Spectroscopy**

FTIR Spectroscopy analysis was carried out to understand the chemical composition of the synthesized BNNTs. A Bruker Vertex 70 instrument was used for FTIR analysis of the synthesized BNNTs. Transmittance vs. wavenumber curves were obtained between wavenumbers from  $400\text{ cm}^{-1}$  to  $3900\text{ cm}^{-1}$ .

### **5.3.3 Multi-point BET Surface Analysis**

Multi-point BET surface analysis of the produced BNNTs was carried out with a Quantachrome Autosorb 1C Physical Adsorption instrument. BNNT specimen was dried in oven at  $110\text{ }^{\circ}\text{C}$  overnight, and degassed at  $300\text{ }^{\circ}\text{C}$  for 4 hours prior to the analysis. The purpose of degassing was to get rid of the moisture and other possible adsorbed gases in the pores of the specimen. Approximately 0.025 grams of sample was used for the analysis. Nitrogen adsorption/desorption isotherms of the BNNT specimen were obtained. Surface area and pore size data of the BNNT specimen were determined.

### **5.3.4 Scanning Electron Microscopy (SEM)**

SEM analysis was carried out with a FEI Quanta 400 scanning electron microscope to monitor the surface morphology of the synthesized BNNTs. The surface of BNNT specimen was coated with gold-palladium alloy to obtain an electrically conductive surface.

### **5.3.5 Transmission Electron Microscopy (TEM)**

TEM analysis of the BNNTs was carried out with a JEOL 200 kW transmission electron microscope to obtain images of BNNTs and understand the structure of the nanotubes. The BNNT specimen was dispersed in water medium and cast on the surface of a carbon grid for analysis.

## 5.4 Fabrication of Polypropylene – BNNT Composites

PP–BNNT composites were prepared using extrusion process. Following the extrusion process, composites were given standard shapes with melt injection process.

### 5.4.1 Materials

#### 5.4.1.1 Polymer Matrix

Isotactic polypropylene was used as the polymer matrix in this study. Polypropylene was supplied by Petkim Petrokimya Holding A.Ş., Turkey, in the form of white pellets, under trade names EH-241 and MH-418. Properties of EH-241 and MH-418 type polypropylene are given in Table 5.2.

**Table 5.2** Properties of EH-241 and MH-418 polypropylene.

Polymer	Melt Flow Index* (g/10min)	Density at 25 °C (g/cm <sup>3</sup> )	Tensile stress at yield (kg/cm <sup>2</sup> )**
EH-241	20 – 28	0.85	365
MH-418	4 – 6	0.85	350

\*According to ASTM D-1238 standard

\*\*According to ASTM-638 standard

#### 5.4.1.2 Antioxidant Agent

Antioxidant agent with trade name @IRGANOX 1010 (3-(3,5-di-tert-butyl-4-hydroxyphenyl)-propionate) (pentaerythritol tetrakis) was used in some of the composites prepared in this study in order to protect the composites from possible oxidative degradations that could be faced during the high-temperature processes.

Table 5.3 represents the structure and properties of antioxidant agent used in this study.

**Table 5.3** Properties of ©IRGANOX 1010 antioxidant [Ciba Specialty Products].

Structure	
Melting Range (°C)	110 – 125
Flashpoint (°C)	297
Specific Gravity	1.15

## 5.4.2 Extrusion of PP – BNNT Composites

### 5.4.2.1 Experimental Set-Up

In the fabrication of PP–BNNT composites, a Thermoprism TSE 16 TC model co-rotating twin-screw extruder was used. Figure 5.4 is the photograph of the twin-screw extruder with important parts designated. The extruder has a control panel, which was used to control the temperature profile along the barrel and the screw speed. In the barrel, composites were melt-mixed with the shear forces created by the motion of twin-screw. Mixtures of PP and BNNTs were fed from the feeding hole and the extruded composite was withdrawn from the die. Table 5.4 summarizes the properties of twin-screw extruder used in this study.

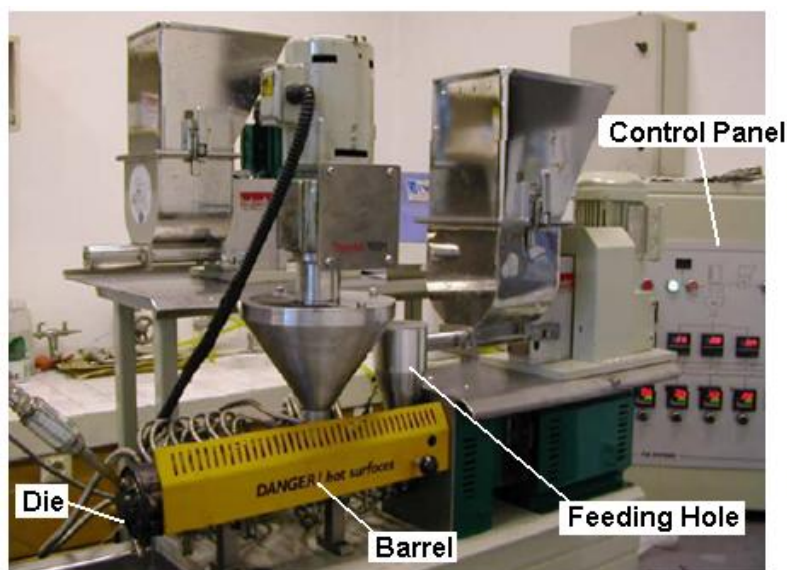


**Figure 5.4** Thermoprism TSE 16 TC model co-rotating twin-screw extruder.

**Table 5.4** Properties of the twin-screw extruder used in this study.

Property	Value
Screw Diameter (mm)	15.6
Barrel Length (mm)	384
Die Length (mm)	16
Max. Screw Speed (rpm)	500
Max. Torque (Nm)	12

#### 5.4.2.2 Experimental Procedure

Polypropylene, which was obtained in the form of small pellets, was ground into powder using an Arthur H. Thomas desktop hammer mill. The BNNTs were powdered using an agate mortar. The ground PP powder and powdered BNNTs were dried overnight in a vacuum oven at 100 °C. After the drying, PP powder and BNNTs were dry-mixed in varying weight percentages (Table 5.5). Dry-mixed

mixtures were mechanically homogenized prior to be fed into the extruder, where the melt mixing of BNNTs inside the polymer matrix was performed.

Before the extrusion process, several extrusion parameters were set by using the control panel of the extruder. The screw speed, which determines the speed of mixing, was set to a specific value (Table 5.5). The temperature profile along the barrel, which determines the melting profile of the polymer, was set by entering five consecutive values. These five temperature values were the temperatures of successive zones along the extruder barrel (Table 5.5).

The withdrawn extrudate was quickly immersed into a water pool in order to be cooled and solidified. The solidified extrudate was fed into a pelletizer where it is collected in the form of small pellets.

Table 5.5 represents all of the composite samples prepared in this study and the experimental parameters of their extrusion. For simplicity, all composite samples prepared in this study were given a code name in the format,

$$PPX + YA + ZWB$$

where **X** represents the type of polypropylene used as the polymer matrix, in a manner that one (1) is for EH-241 PP and two (2) is for MH-418 PP. **Y** and **Z** denote the weight percentages of antioxidant (@IRGANOX 1010) and BNNTs in the composite, respectively. If **Y** or **Z** was zero, associated part was not included in the code name. **W** denotes the treatment condition of BNNTs used in the composite and it was not included in the code name if the as-synthesized BNNTs were used. **W** = P was used for composites in which purified BNNT composites were used and **W** = M was used for composites in which purified and then surface modified BNNTs were used.

**Table 5.5** Compositions of all extruded materials and their extrusion parameters.

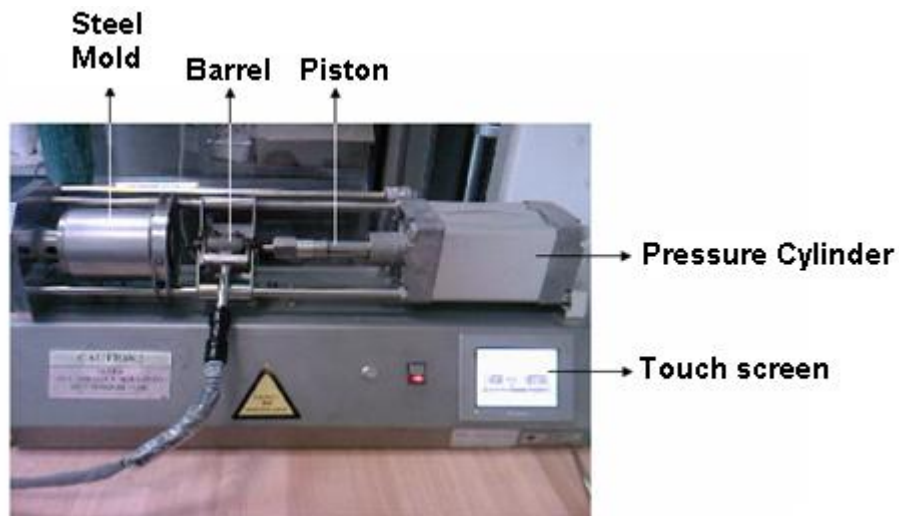
Group	PP Type	Composite name	Composition (wt%)				Extrusion Parameters	
			PP	BNNTs	@Irganox 1010	Screw Speed (rpm)	Barrel Temp. Profile (°C)	
1	EH-241	[PP1]	100	-	-	100	180-180-180-180-180	
		[PP1+1A]	99	-	1			
		[PP1+1A+1B]	98	1	1			
2	MH-418	[PP2]	100	-	-	150	180-185-195-205-215	
		[PP2+1A]	99	-	1			
		[PP2+1A+1B]	98	1	1			
		[PP2+1A+3B]	96	3	1			
3	MH-418	[PP2]	100	-	-	150	180-185-195-205-215	
		[PP2+0.5B]	99.5	0.5	-			
		[PP2+1B]	99	1	-			
		[PP2+3B]	97	3	-			
		[PP2+6B]	94	6	-			
		[PP2+0.5PB]	99.5	0.5	-			
[PP2+0.5MB]	99.5	0.5	-					



### 5.4.3 Injection Molding

#### 5.4.3.1 Experimental Set-Up

In order to carry out mechanical and thermal characterizations of PP–BNNT composites, standard composite specimens were molded using a DSM Xplore laboratory scale (10 cc) injection molding machine (Figure 5.5).

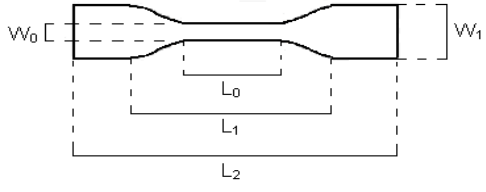


**Figure 5.5** DSM Xplore laboratory scale (10 cc) injection molding machine.

The injection molding machine contains a stainless steel mold, which functions as a template to fabricate two specimens in each injection batch, one of which is a tensile test specimen in the shape of a dog bone according to ISO 527-2 5A, and other is an impact test specimen according to ISO 178.

Table 5.6 represents the shape and dimensions of the injection molded tensile test specimen. Barrel of the injection machine is the part where polymer melts. Piston injects the molten polymer inside the barrel into the steel mold. Pressure cylinder stores the high-pressured  $N_2$  gas in order to push the piston.

**Table 5.6** Dimensions of the injection molded tensile test specimen.

Dimension	Value (mm)	Shape
Gauge Length ( $L_0$ )	20	 The diagram shows a tensile test specimen with a central narrow section and wider grip sections. The gauge length is $L_0$ , the distance between grips is $L_1$ , and the overall length is $L_2$ . The width of the narrow portion is $W_0$ and the width at the ends is $W_1$ .
Distance between grips ( $L_1$ )	50	
Overall Length ( $L_2$ )	80	
Width of narrow portion ( $W_0$ )	4	
Width at ends ( $W_1$ )	12.5	
Thickness	2	

#### 5.4.3.2 Experimental Procedure

Prior to melt injection, extruded polypropylene–BNNT composite pellets were dried in a vacuum oven at 100 °C overnight. Dried composite pellets were filled into the barrel of the injection machine, which had an inside temperature of 220 °C. The composite pellets were allowed to melt inside the barrel for 3 minutes. The piston pressed and injected the molten polymer into the steel mold with an injection pressure of 14 bars. The temperature of the steel mold was 25 °C. Pressure of the injection, barrel temperature and the temperature of the steel mold were controlled parameters of the melt injection process and adjusted using the integrated touch screen of the injection molding machine.

### 5.5 Characterizations of PP – BNNT Composites

#### 5.5.1 Mechanical Characterization (Tensile Testing)

Tensile tests were conducted with a Shimadzu AG-IS 100 kN testing machine. Stress-strain curves were obtained for each PP–BNNT composite specimen according to the standards of EN-ISO 527-1. Six specimens for each of the composites (Table 5.5) were tested in order to minimize the experimental error.

Crosshead speed (rate of strain) was held constant throughout the tests as 15 mm/min. Distance between the clamped points of tensile specimens was 30 mm. Engineering stress versus the elongation in the gauge length (20 mm initially) was recorded. Young's modulus, yield strength, tensile strength and elongation at break values of each composite were determined as the average of six specimens from the stress–strain curves

## **5.5.2 Thermal Characterizations**

In order to understand the effect of BNNT addition on the thermal properties of composites, differential scanning calorimetry (DSC), thermal gravimetric analysis (TGA), and thermal mechanical analysis (TMA) were performed.

### **5.5.2.1 Differential Scanning Calorimetry (DSC)**

In this study, a Perkin Elmer Diamond DSC analyzer was used for the DSC analysis. The temperature of the reference pan and the sample pan was increased from -40 °C to 200 °C with a heating rate of 10 °C/min, under nitrogen flow with a flow rate of 50 cc/min. Then, the sample was cooled back to -40 °C. Melting temperature, crystallization temperature, heat of fusion and percent crystallinity of the composites were determined from the DSC curves. DSC specimens were obtained from tensile test specimens of composites. DSC analysis was repeated three times for neat MH-418 polypropylene and the mean value for each thermal property were taken.

### **5.5.2.2 Thermal Gravimetric Analysis (TGA)**

In this study, a Perkin Elmer Pyris Thermal Gravimetric Analyzer was used for the TGA of first and second group composites (Table 5.5) and a Shimadzu DTG–60/60H TGA device was used for the TGA of third group composites (Table 5.5). The composite samples were continuously weighed while being heated from room temperature to 600 °C with a constant heating rate of 5 °C/min. The samples were held under nitrogen atmosphere during the analysis. The flow rate of the nitrogen gas was held at 50 cc/min. TGA specimens were obtained from the tensile test specimens of composites.

### **5.5.2.3 Thermal Mechanical Analysis (TMA)**

In this study, a Setaram Labsys Thermal Mechanical Analyzer (dilatometer) was used for thermal mechanical analysis. Composites' coefficients of linear thermal expansion (CLTE) were determined according to ASTM-D696. Injection molded impact test specimens were used as TMA specimens. The specimens were cut into standard sizes and rubbed with emery for surface flattening. A vitreous silica rod detected the change in the width of the specimen ( $W_i \sim 4$  mm) and recorded with respect to temperature from 25 °C to 150 °C. During the tests, the temperature of the samples was increased with a heating rate of 5 °C/min. TMA was repeated three times for neat MH-418 polypropylene and the mean CLTE values were taken.

## CHAPTER 6

### RESULTS AND DISCUSSION

In this study, BNNTs were synthesized from the reaction of ammonia gas with a powder mixture of boron and iron oxide. The synthesized BNNTs were characterized in terms of XRD, FTIR, multi-point BET, SEM and TEM analyses. PP-BNNT composites were prepared using extrusion and injection molding processes. Thermal and mechanical properties of the composites were investigated with respect to BNNT concentration.

#### 6.1 Production of BNNTs

##### 6.1.1 Effect of ammonia flow rate on BNNT production

BNNT production experiments were carried out at different inlet flow rates of ammonia gas and different amounts of initial powder mixtures in order to determine the best conditions for the production of BNNTs.

Test runs were held at a reaction temperature of 1300 °C and a B/Fe<sub>2</sub>O<sub>3</sub> weight ratio of 15/1 since those parameters were reported to yield the highest amount of nanotubes in the synthesized product by Özmen [2008]. However, higher amounts of BNNTs were required in this study in order to match the needed amounts for polymer composite preparation. Therefore, alumina boats with the largest possible size for the existing system were used. Due to scale up, varying ammonia inlet flow rate and weight of initial powder mixture values were tested to determine the best combination of production parameters.

Figure 6.1 shows the amounts of synthesized products with respect to different ammonia inlet flow rates when 0.8 g of boron and iron oxide mixture was used as

the initial mixture. Standard deviations of the produced amounts are shown in the graph representation.

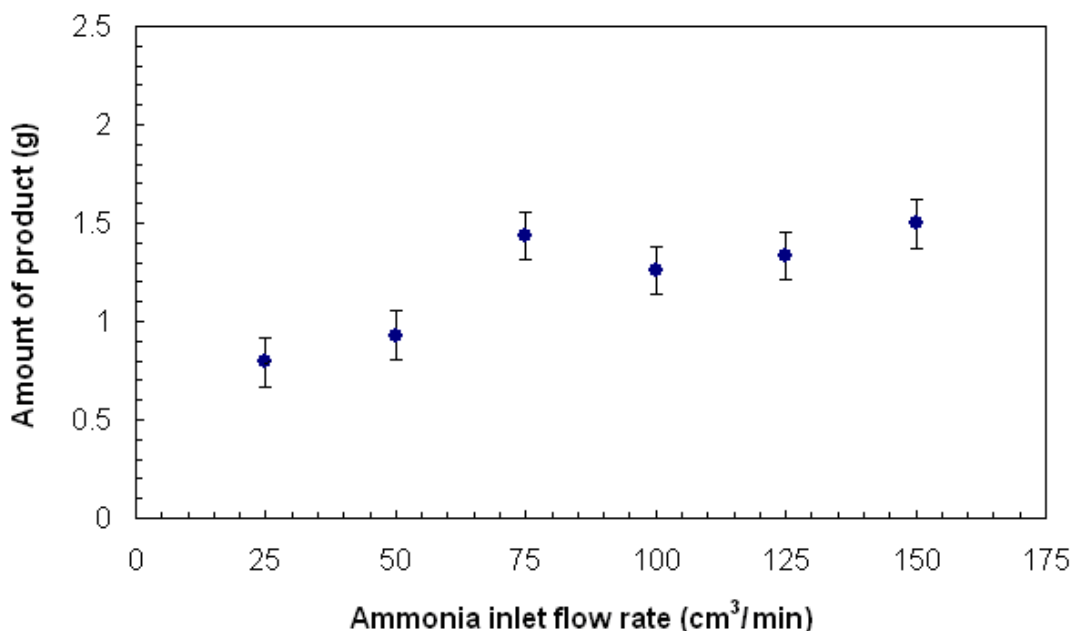


**Figure 6.1** Effect of ammonia inlet flow rate on the amount of synthesized product ( $W_B+W_{Fe_2O_3} = 0.8$  g).

From Figure 6.1, it was observed that the amount of the synthesized product increased with increasing ammonia inlet flow rates. However, produced amount values were stabilized as the inlet flow rate exceeded a certain value. Beside the amount of the synthesized product, color and the appearance of the product was of major significance for the BNNT synthesis optimization.

The whiteness of the product was a visual measure of hexagonal boron nitride concentration in the synthesized product. The gray color indicated the existence of impurities such as unreacted boron, iron or iron oxides. Therefore, whiteness of the product was evaluated as the main criterion of optimization. Table 6.1 represents the color of the products with respect to ammonia inlet flow rate values. In terms of

physical appearance, all of the synthesized products were in the form of powder and small particulates.

**Table 6.1** Color of synthesized materials with respect to ammonia inlet flow rate.

Flow rate of inlet ammonia gas (cm <sup>3</sup> /min)	Color of the synthesized material
25	Gray
50	White-gray
75	White-gray
100	White-gray
125	White
150	White-gray

The most desirable BNNT product was obtained when 0.8 g of boron and iron oxide mixture was subjected to an ammonia inlet flow rate of 125 cm<sup>3</sup>/min. The white color of the product indicated to a high concentration of hexagonal boron nitride. Optimum synthesis conditions for BNNTs are given in Table 6.2. Figure 6.2 is the photograph of a BNNT product synthesized under optimum synthesis conditions.

**Table 6.2** Optimum synthesis conditions for BNNT production.

Production Parameter	Substrate weight (g)	B / Fe <sub>2</sub> O <sub>3</sub> weight ratio	Reaction temperature (°C)	Reaction time (hours)	Ammonia Inlet flow rate (cm <sup>3</sup> / min)
<b>Value</b>	0.80	15	1300	2.15	125



**Figure 6.2** Photograph of the product synthesized under optimum conditions.

When initial mixture amounts higher than 0.8 grams were used, the products tended to have a grayish color, which indicated poor boron nitride yield. It can be postulated that, as the depth of powder mixture in the alumina boat exceeded a certain thickness, suitable ammonia – powder mixture interfacial area was lacked for the effective growth of boron nitride structures.

The concentration of ammonia gas inside the furnace and the diffusion of ammonia gas into the boron and iron oxide powder mixture were important factors for the formation mechanism of BNNTs. It was observed that under low ammonia inlet flow rates, the ammonia concentration inside the furnace remained insufficient to diffuse into the mixture and react with the precursor materials to form boron nitride structures. The increasing flow rate of ammonia enhanced the formation of BNNTs up to a certain extent. However, above a certain ammonia inlet flow rate, a grayish appearance was again ensued, which indicated poor formation of boron nitrides. It is possible that high ammonia gas flow swept away the boron nitride precursor gases that are formed on the surface of the powder mixture.



## 6.2 Characterizations of BNNTs

### 6.2.1 X-Ray Diffraction (XRD) Analysis

BNNTs were synthesized according to the synthesis conditions given in Table 6.2. Since the mass produced BNNTs were used in composite production process, the reproducibility of the BNNT product was an important task. Since the BNNTs were produced in repeated batches of the same conditions, the product obtained from each batch was expected to have the same properties. For that reason, XRD analysis of each synthesized material was carried out between  $2\theta$  angles of  $20^\circ$ – $90^\circ$ . XRD patterns of the BNNT samples were quite similar to each other. Figure 6.3 represents a typical XRD pattern of the as-synthesized BNNTs.

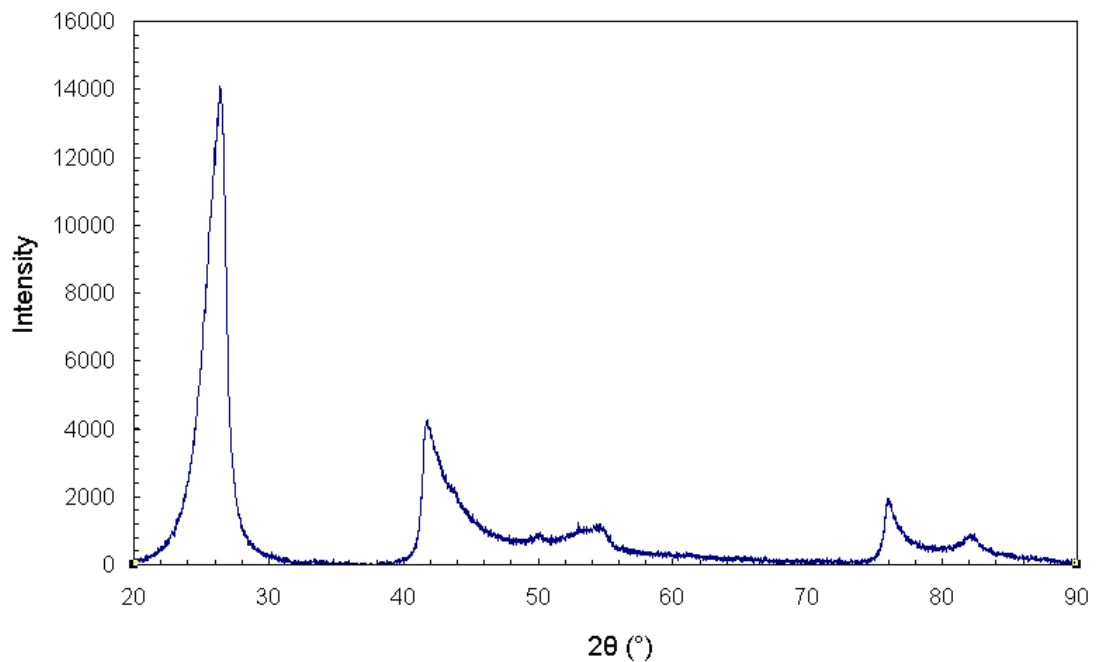


**Figure 6.3** Typical XRD pattern of the as-synthesized BNNTs.

Peaks were observed at  $2\theta$  angles of  $26.48^\circ$ ,  $41.82^\circ$ ,  $50.38^\circ$ ,  $54.74^\circ$ ,  $76.20^\circ$  and  $82.48^\circ$ . Those peaks belong to hexagonal boron nitride. An extra peak was observed around  $2\theta$  degree of  $44.7^\circ$ , the intensity of which varied from specimen to specimen. This peak originated from the presence of cubic iron ( $\alpha$ -Fe) in the specimen.

No presence of iron oxide ( $\text{Fe}_2\text{O}_3$ ) in the synthesized product was revealed by XRD pattern since the main characteristic peak of iron oxide, which typically forms at  $33.15^\circ$ , was not detected in any of the XRD patterns. It was concluded from the XRD results that, hexagonal boron nitride and cubic iron were the crystalline materials existed in the synthesized product. XRD data of boron nitride (hexagonal and rhombohedral), iron, iron oxide and the as-synthesized BNNTs are given in Appendix A.

### **6.2.2 Fourier Transform Infrared (FTIR) Spectroscopy Analysis**

FTIR spectroscopy analysis of the as-synthesized BNNTs was carried out between wavenumbers from  $400\text{ cm}^{-1}$  to  $3900\text{ cm}^{-1}$ . Figure 6.4 represents a typical FTIR spectrum of the BNNT product synthesized according to the conditions given in Table 6.2.

The major peaks observed at wavenumbers of  $1380\text{ cm}^{-1}$  and  $810\text{ cm}^{-1}$  are associated with the B–N stretching vibrations and B–N–B bending vibrations, respectively [Nyquist & Kagel, 1971]. Those two peaks confirmed the presence of predominant boron nitride in the synthesized material, which was in agreement with the XRD results. The peak observed around  $3210\text{ cm}^{-1}$  belongs to water molecules which are adsorbed on the synthesized material [Özmen, 2008]. The small peaks observed at wavenumbers of  $2800$ ,  $2530$  and  $2300\text{ cm}^{-1}$  indicate the existence of boron in the synthesized material. The FTIR spectra of elemental boron and iron oxide that are used in the production of BNNTs are included in Appendix B.

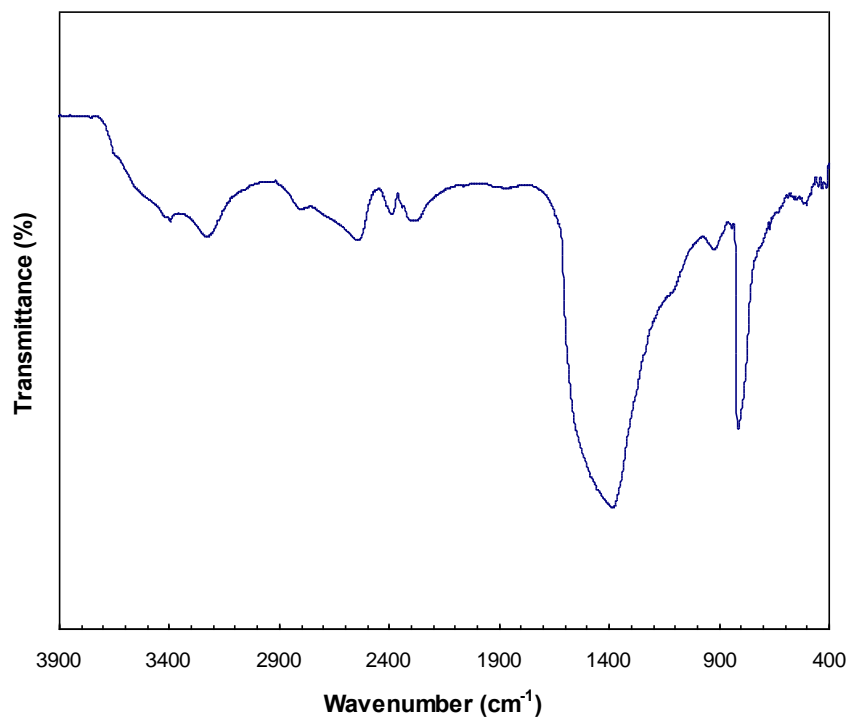


**Figure 6.4** Typical FTIR Spectrum of the as-synthesized BNNTs.

### 6.2.3 Multi-point BET Surface Analysis

Multi-point BET surface analysis of the as-synthesized BNNTs was carried out. Figure 6.5 represents nitrogen adsorption/desorption isotherms of the synthesized BNNTs. Full dots in Figure 6.5 represent the adsorption of nitrogen molecules by the BNNT specimen. Empty dots represent desorption of nitrogen molecules from sample surfaces.

The isotherm of the as-synthesized BNNT sample (Figure 6.5) corresponds to type II isotherm according to BDDT (Brauner, Deming, Deming, Teller) classification [Branauer et al., 1940]. Type II isotherm is typically formed when adsorption occurs on nonporous powders or on powders with pore diameters larger than micropores [Lowell et al., 2006].

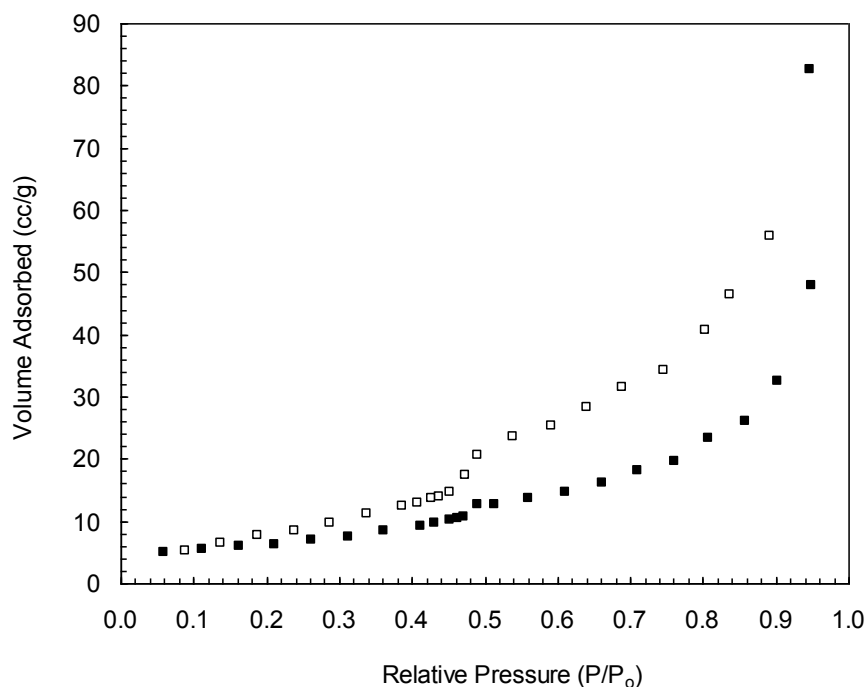


**Figure 6.5** Adsorption/desorption isotherms of the as-synthesized BNNTs.

A hysteresis was observed at a relative pressure of 0.24 (Figure 6.5). This hysteresis resembled both Type A and B hysteresis according to the De Boer classification [De Boer, 1958]. Type A hysteresis indicates the existence of cylindrical pore channels in the materials. Type B hysteresis is associated with slit-shaped pores or the space between parallel plates [Lowell et al., 2006].

Type A behavior of the BNNT sample was probably induced by the hollow cylindrical shape of nanotubes acting as cylindrical pore channels. The reason for Type B behavior may be the voids between multi-wall nanotubes, which induced a slit-shaped pore opening behavior.

The adsorption first starts with the trapping of nitrogen molecules on the inner walls of micropores, then continues with mesopores [Branauer, Emmett & Teller, 1938]. In mesopores, adsorption and desorption mechanism followed different ways. The filling of the mesopores occurs by the condensation on the walls of pores with formation of layers. On the other hand, desorption occurs by moving away from

pore openings with evaporation. The volume of the adsorbed nitrogen gas under the  $P/P_0$  value of 0.01 was very small with respect to the volume of nitrogen gas adsorbed around  $P/P_0$  value of 1.0 (Figure 6.5). Therefore, it was understood that the BNNT specimen has negligible amount of micropores and abundant amount of mesopores in its structure.

Multi-point BET surface area of the as-synthesized material was  $22.52 \text{ m}^2/\text{g}$ , which is a low value for a nanotube sample. The reason for the low specific surface area was the agglomeration of the nanotubes. Details of specific surface area calculation using BET method is given in Appendix C. Meso and micro pore volume of the BNNT specimen was  $0.078 \text{ cc/g}$  and the average mesopore diameter of the BNNT specimen was  $38.78 \text{ \AA}$ .

Figure 6.6 shows the pore size distribution of the as-synthesized BNNTs. The main peak formed at  $38.78 \text{ \AA}$  corresponded to average mesopore diameter. However, small peaks observed at pore diameters around  $110 \text{ \AA}$  and  $60 \text{ \AA}$  indicated the presence of little amount of macropores in the synthesized material. The pore size distribution of the synthesized material was in agreement with the nitrogen adsorption/desorption isotherms.

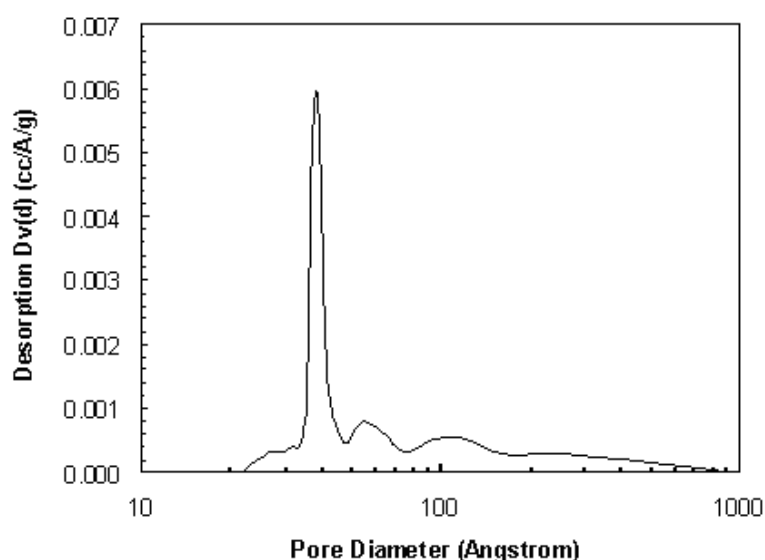


**Figure 6.6** Pore size distribution of the as-synthesized BNNTs.

## 6.2.4 Scanning Electron Microscopy Analysis

SEM analysis was carried out in order to monitor the surface morphology of the as-synthesized BNNTs. Figures 6.7 and 6.8 show SEM images of the as-synthesized BNNTs. From Figure 6.7, it was observed that the as-synthesized BNNTs were agglomerated. The agglomeration is a result of the nanotube entanglements during the growth stage of nanotubes. High aspect ratios and low bending stiffness of nanotubes are major reasons of their tendency to agglomerate [Shi et al., 2004]. From Figure 6.8 (b), outer diameters of the nanotubes were observed to vary between 50–130 nm. Presence of iron was detected on the bulbous ends of the nanotubes by EDS analysis, which was in agreement with the XRD analysis results. It is probable that tip growth mechanism was displayed in the formation of nanotubes rather than root growth mechanism since the bulbous tips of the nanotubes were observed at suspending ends of the nanotubes (Figure 6.8 (b)).

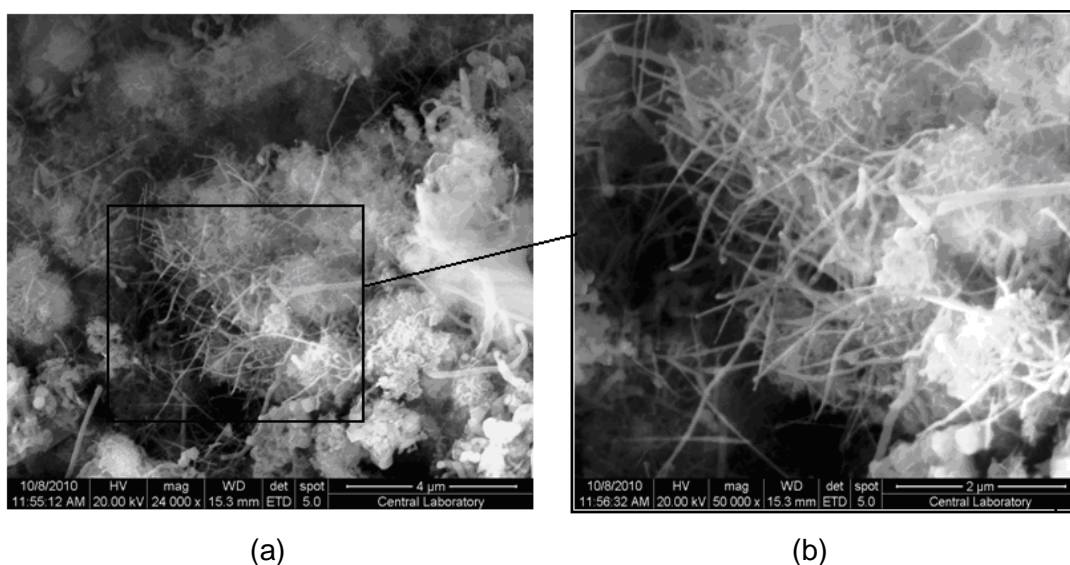


**Figure 6.7** SEM images of the as-synthesized BNNTs (a) 24,000x magnification (b) 50,000x magnification.

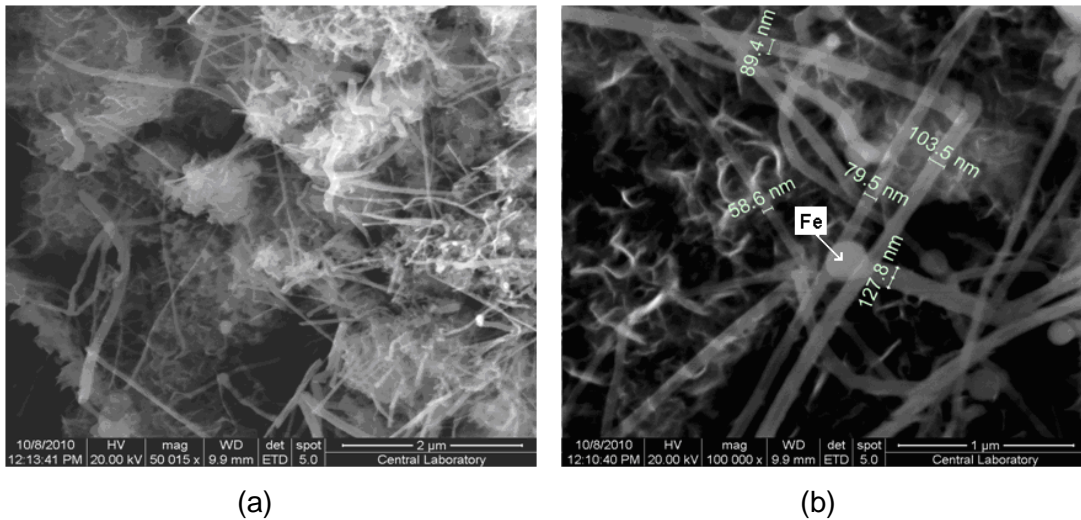


**Figure 6.8** SEM images of the as-synthesized BNNTs (a) 50,000x magnification (b) 100,000x magnification.

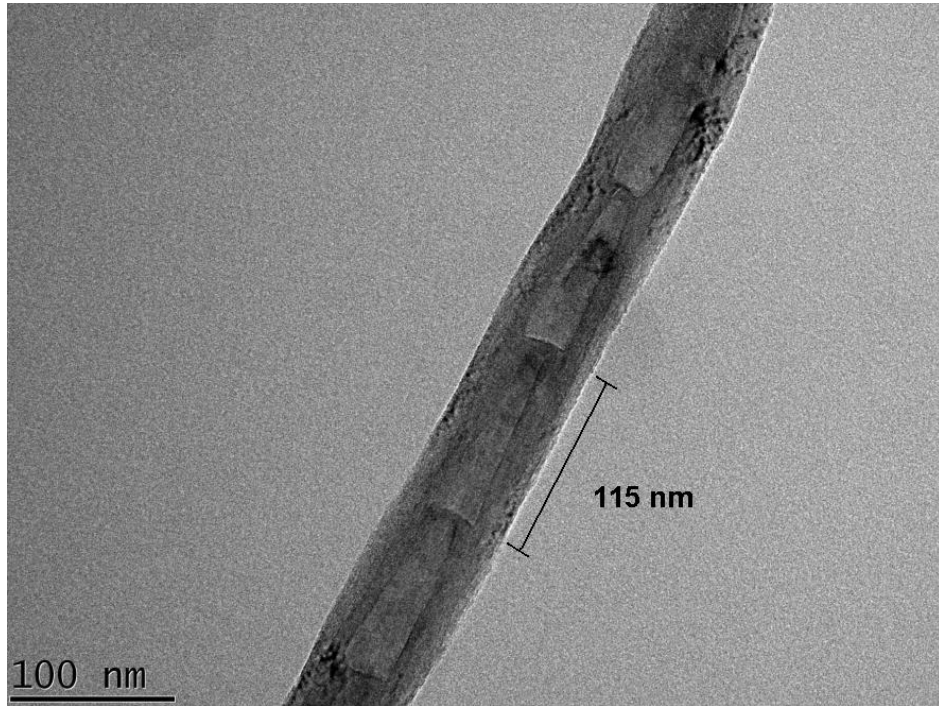
### 6.2.5 Transmission Electron Microscopy Analysis

With TEM analysis, molecular level morphology of the boron nitride nanotubes was monitored. Loose tubular structures of hexagonal boron nitride that suspend freely in the carbon grid media were targeted for imaging. TEM images of the as-synthesized BNNTs are shown in Figures 6.9, 6.10 and 6.11.

In Figure 6.9, TEM image of a bamboo-like, multi-wall BNNT is represented. Subsequent conical shapes, each of which has a length about 115 nm, form the bamboo-like nanotube. The outer diameter of the nanotube is about 65 nm. The inner diameter of the nanotube was about 30 nm in the widest region and 12 nm in the narrowest region.

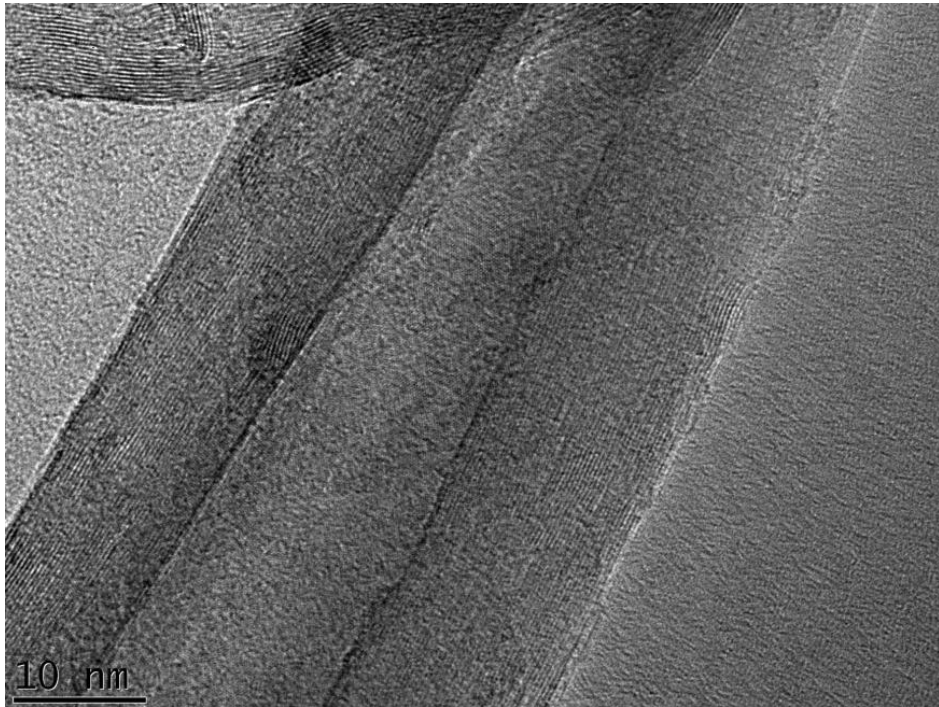
Figure 6.10 represents the structure of a nanotube with a hollow cylinder shape. The outer diameter of the nanotube was about 43 nm. The inner diameter of the nanotube varies between 11 and 17 nm. It was observed that nanotubes in the as-grown product were multi-wall type. The parallel lanes seen in Figure 6.10 are boron nitride sheets that are concentrically rolled over and over to form a multi-wall nanotube.

Figure 6.11 represents a bamboo-like nanotube that is broken from the ends. This may be a result of forging the product in an agate mortar for powdering. The black dots seen on the nanotubes may be due to either local irregularities in the boron nitride structure or impurities [Golberg, 2009].



**Figure 6.9** TEM image of a bamboo-like multi-wall BNNT.





**Figure 6.10** TEM image of a hollow cylinder multi-wall BNNT.

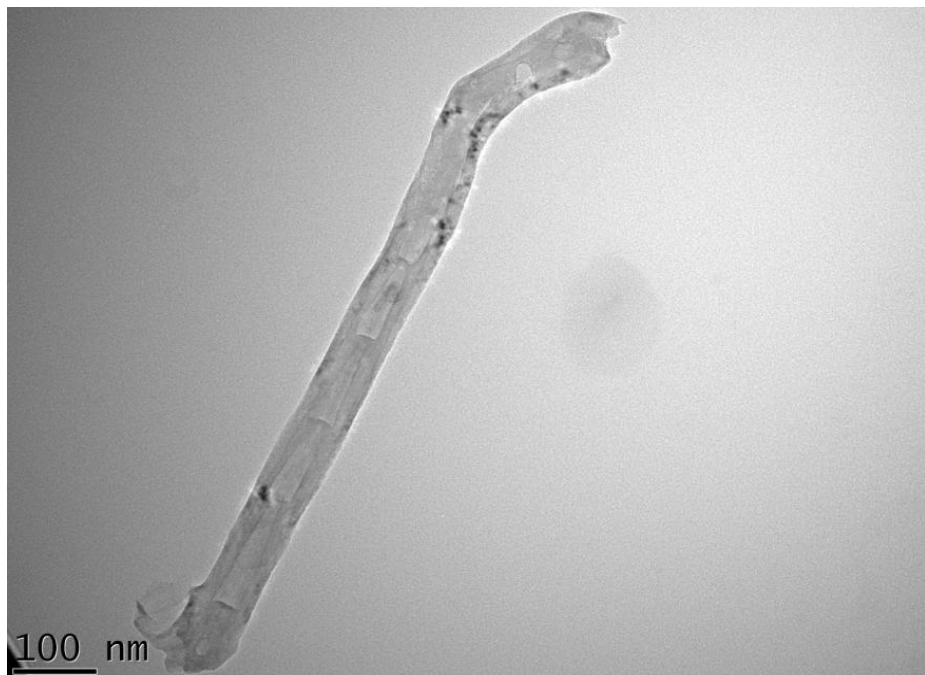


**Figure 6.11** TEM image of a bamboo-like multi-wall BNNT that is broken from ends.

## 6.3 Characterizations of PP – BNNT Composites

Mechanical and thermal characterizations of polypropylene–BNNT nanocomposites were carried out using tensile testing, differential scanning calorimetry (DSC), thermal gravimetric analysis (TGA) and thermal mechanical analysis (TMA). All composites prepared in this study and their compositions are given in Table 5.5.

Three groups of PP – BNNT composites were prepared and characterized:

- **Group 1:** Effects of 1 wt% antioxidant and 1 wt% as-synthesized BNNTs on the composites were investigated using EH-241 type PP.
- **Group 2:** Effects of 1 wt% antioxidant, 1 and 3 wt% as-synthesized BNNT loadings on the composites were investigated using MH-418 type PP.
- **Group 3:** Effects of the as-synthesized BNNT loadings (0.5, 1, 3 and 6 wt%), purified BNNT loading (0.5 wt%) and, purified and then surface modified BNNT loading (0.5 wt%) on the composites were investigated using MH-418 type PP.

### 6.3.1 Mechanical Characterization (Tensile Testing)

Tensile testing of PP–BNNT composites was carried out and associated stress-strain curves were obtained. Representative stress-strain curves that belong to the composites shown in Figure 6.12 are given in Appendix E. Young's modulus, tensile strength, yield strength and elongation at break values of each sample were determined as the mean of six specimens. Tensile properties of all samples obtained from tensile tests are given in Appendix D.

Figure 6.12 is the photograph of six replicates of injection molded tensile test specimens at different BNNT loadings. Codes of the composites are designated on Figure 6.12. It was noticed that the color of transparent PP became white with an increase in the BNNT loading.

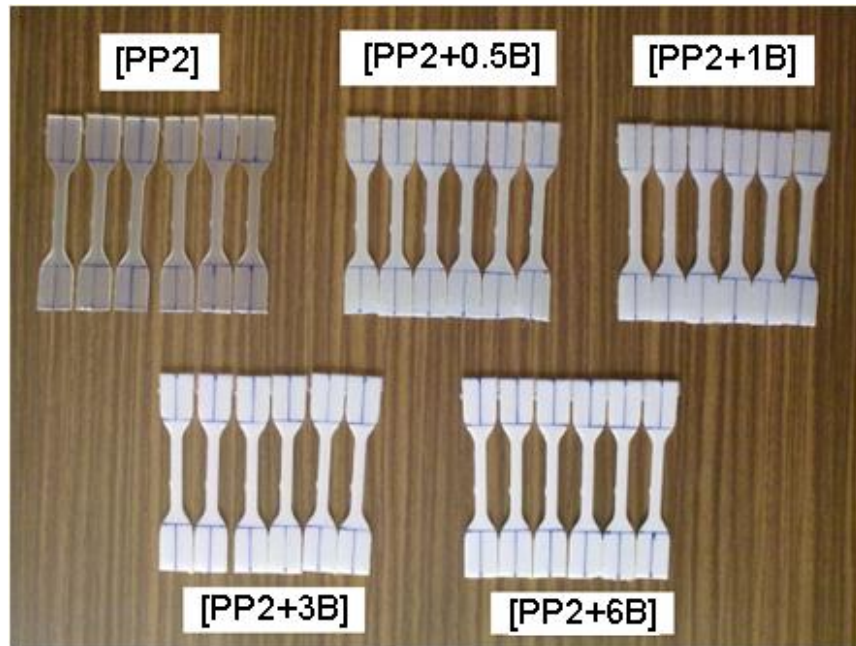


**Figure 6.12** Six replicates of tensile test specimens at different BNNT loadings.

### 6.3.1.1 First Group Composites

Tensile test results of first group composites are represented in Figure 6.13 as bar graph representations. Standard deviations of the measurements are shown on the graphs.

The presence of 1 wt% antioxidant positively affected the tensile and yield strength of neat PP, whereas the effect on Young's modulus was minor. The positive effect of antioxidant on the strength of neat PP might be due to the preservation of polymer chains from oxidative degradations during high-temperature processes of extrusion and injection molding.

1 wt% BNNT addition slightly improved the Young's modulus and yield strength of neat PP due to the adhesion between the nanotubes and the polymer matrix. However, BNNT addition caused a decrease in the elongation at break value, which indicated that the flexibility of neat PP was hindered by the BNNT presence.

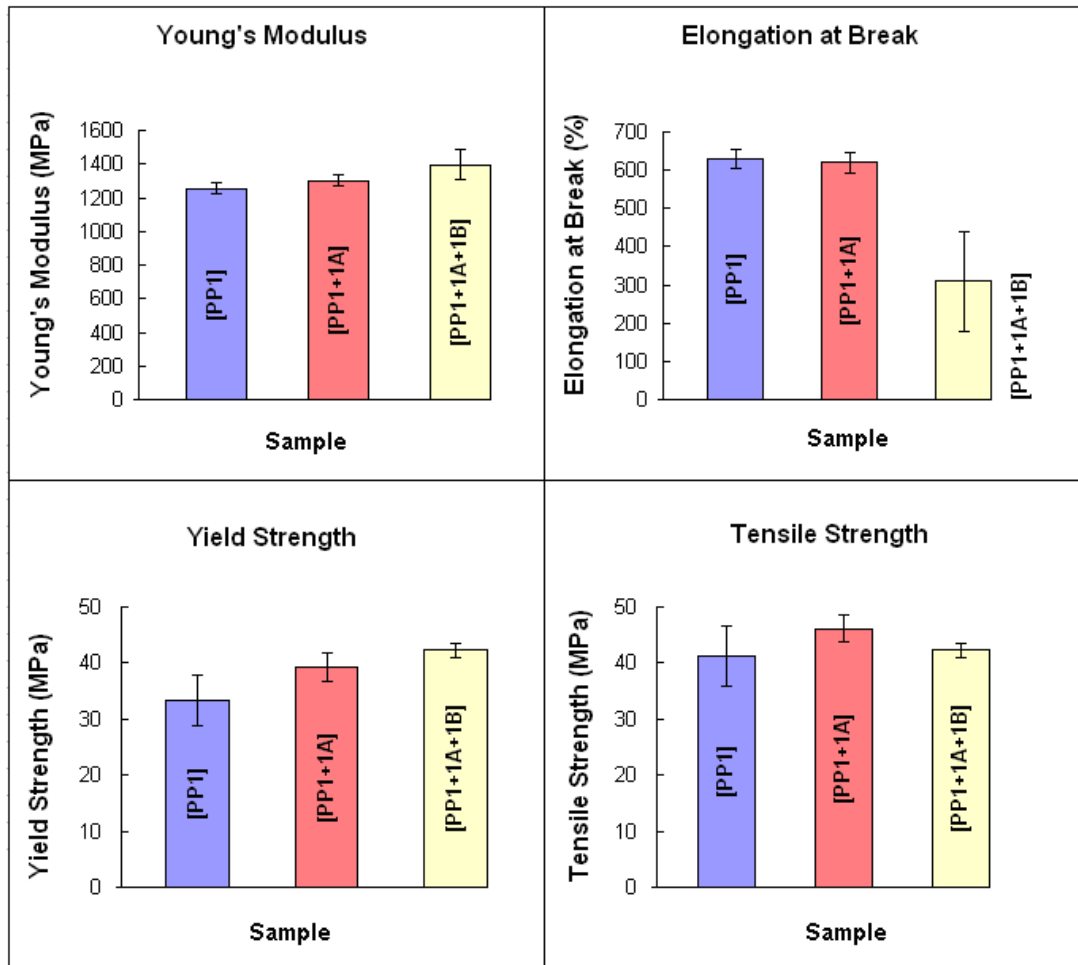


**Figure 6.13** Tensile properties of first group composites.

A decline in the tensile strength value with nanotube addition was due to the poor dispersion of nanotubes inside the polymer matrix, which is a common shortage of using as-synthesized nanotubes in polymer composites [Moniruzzaman & Winey, 2006]. Nanotubes' tendency to form bundles inside the PP matrix prevented the uniform dispersion of fibers. The agglomeration of nanotubes caused stress concentrated areas, which resulted in decrease in the strength of the composites.

### **6.3.1.2 Second Group Composites**

MH-418 polypropylene was used in the second group composites considering that the lower melt flow index of MH-418 might induce a more uniform dispersion of nanotubes with respect to EH-241 by creating stronger shear forces inside the polymer medium during the extrusion. The impact of antioxidant and BNNT additions on neat PP were investigated. Figure 6.14 is the bar graph representation of the tensile properties of second group composites.

The Young's modulus of neat MH-418 PP increased with both antioxidant and BNNT additions. The yield strength of neat PP did not change significantly with respect to antioxidant or BNNT addition. The elongation at break value of neat PP remained same in antioxidant presence. However, the addition of BNNTs decreased the elongation at break and the tensile strength values of neat PP. 3 wt% of BNNT addition did not make any positive contribution to the mechanical properties of neat PP over the 1 wt% BNNT composite. On the contrary, 3 wt% of BNNT addition decreased the tensile strength value due to cluster formations inside the matrix, which was a result of the increase in the as-synthesized BNNT concentration. The decrease in the elongation at break and tensile strength values can be attributed to the poor dispersion of the as-synthesized BNNTs inside the PP matrix. Due to agglomeration of BNNTs inside the matrix, defects were formed in the polymer structure, which caused early fractures during tensile tests.

It was also observed that MH-418 type PP exhibited higher Young's modulus, tensile and yield strength with respect to EH-241 type PP. MH-418 PP might have undergone better mixing in the extrusion stage due to its lower melt flow index, which means its higher viscosity. Higher barrel temperature and screw speed in the extrusion of MH-418 PP might have also promoted the better mixing.

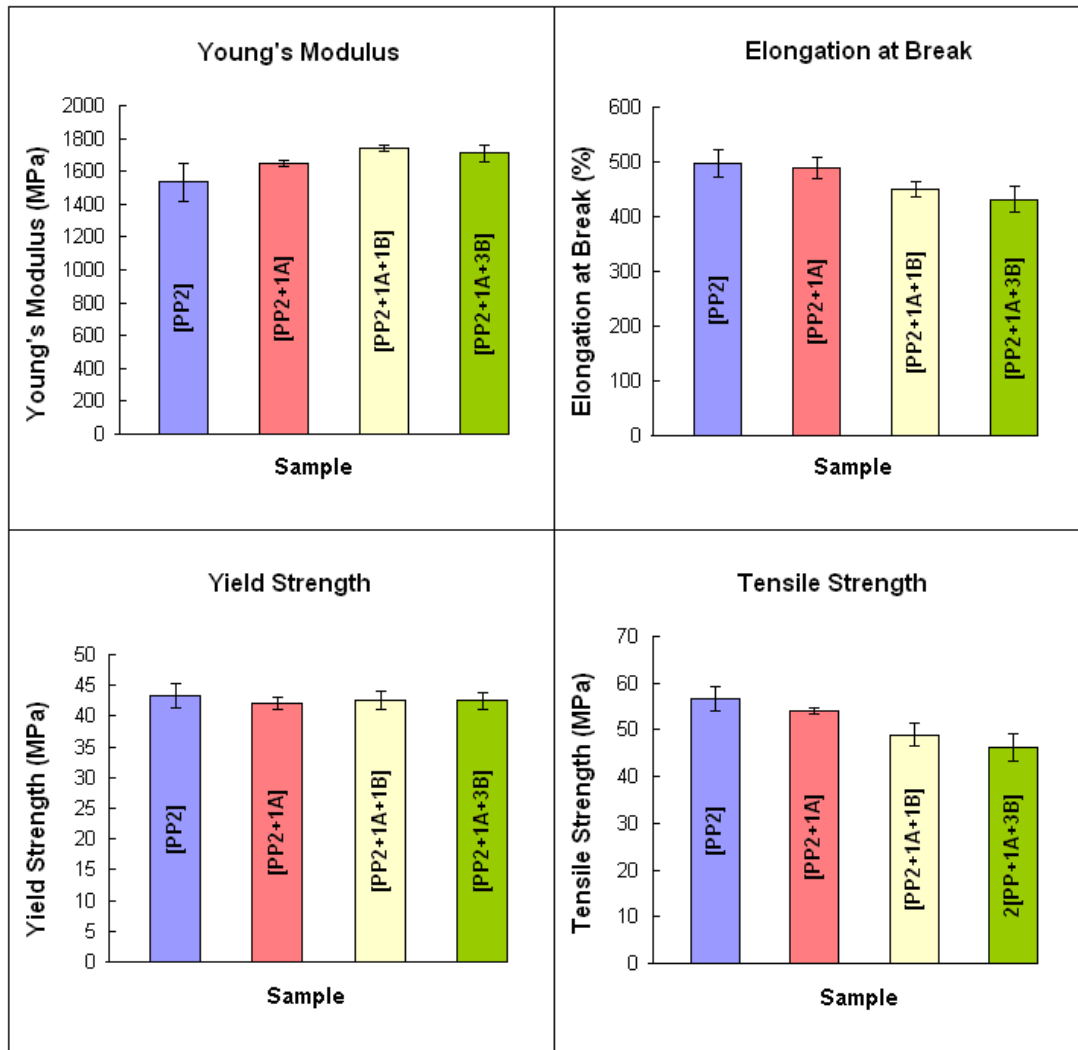


**Figure 6.14** Tensile properties of second group composites.

### 6.3.1.3 Third Group Composites

In the third group composites, 0.5, 1, 3 and 6 wt% BNNT additions in neat PP were investigated. Among studied BNNT loadings, 0.5 wt% BNNT addition gave the best results in terms of tensile property improvement. Therefore, effects of 0.5 wt% loadings of purified BNNTs, and purified – surface modified BNNTs were investigated with respect to same loading of the as-synthesized BNNTs. Figure 6.15 is the bar graph representation of Young's modulus values of third group composites.

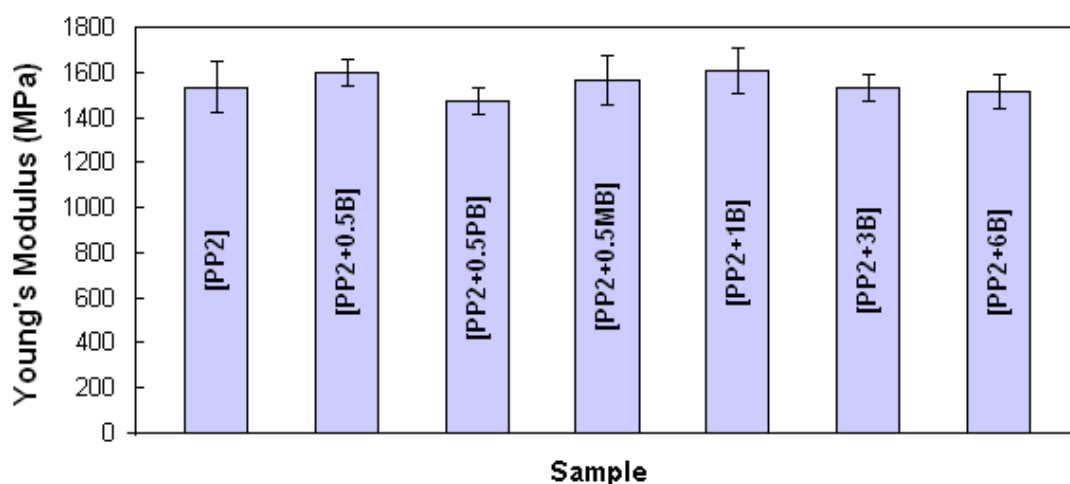


**Figure 6.15** Young's modulus of third group composites.

The Young's Modulus of neat PP increased slightly with 0.5 and 1 wt% of the as-synthesized BNNT additions. The increase might be due to high modulus of nanotubes. However, at higher concentrations of the as-synthesized BNNTs (3 and 6 wt%), the modulus started to decrease when compared to low nanotube loadings. Associated with the increase in BNNT loading, an increase in the formation of BNNT bundles inside the PP matrix may have caused this decrease.

Composite with 0.5 wt% of purified BNNTs ([PP2+0.5PB]) did not exhibit higher Young's modulus with respect to PP having 0.5 wt% as-synthesized BNNTs. On the other hand, Young's modulus of the composite with 0.5 wt% of purified and then surface modified BNNTs ([PP2+0.5MB]) exhibited slight improvement over neat PP. This was probably a result of better adhesion between the surface modified nanotubes and polymer matrix.

The yield strengths of third group composites are shown in Figure 6.16. It was observed that no increase or very slight increases with respect to neat PP were induced by BNNT loadings.

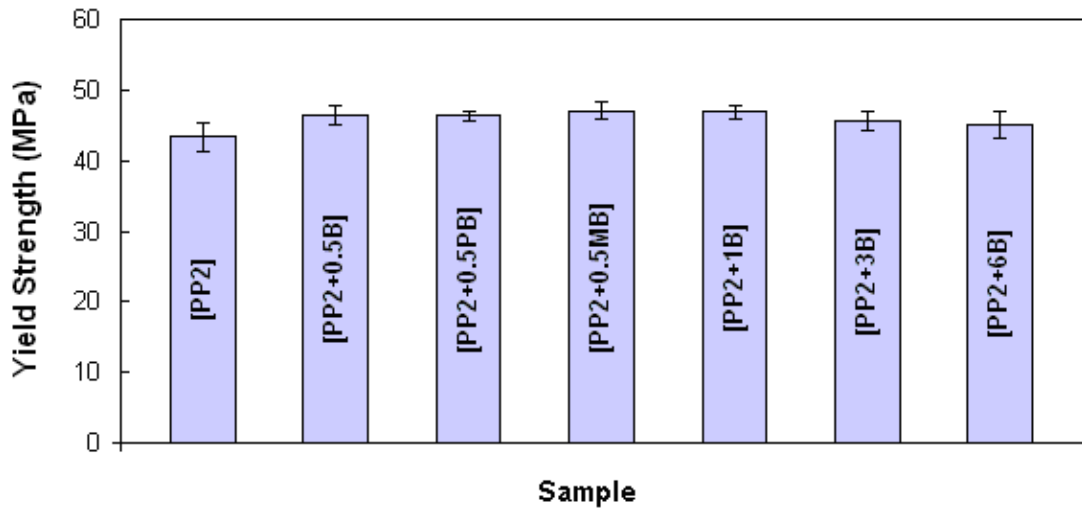


**Figure 6.16** Yield strength of third group composites.

Elongation at break values of third group composites are given in Figure 6.17. Elongation at break values of composites were observed to be inversely related with the as-synthesized BNNT concentration. At higher weight fractions of the as-synthesized BNNTs, tensile specimens exhibited earlier fractures due to defects induced by the bundles of BNNTs. However, the flexibility of the neat PP was not affected by the addition of purified and then surface modified BNNTs, which means



that cluster formations by BNNTs were prevented to an extent by purification and modification processes.

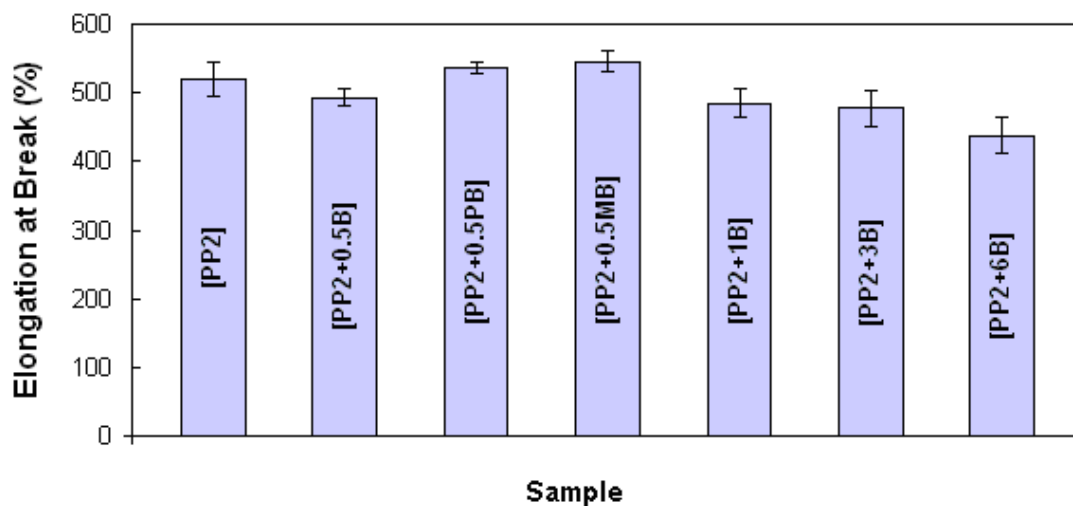


**Figure 6.17** Elongation at break of third group composites.

Tensile strengths of third group composites are given in Figure 6.18. The highest tensile strength was obtained for the composite with 0.5 wt% of purified and then surface modified BNNTs, which was evidence that grafting the nanotubes with polyethylene glycol (PEG) moieties improved the dispersion of BNNTs inside the polymer matrix. It was also observed that the [PP2+0.5MB] composite displayed a homogeneous appearance, which should be indication of the successful dispersion. Only by the usage of purified and then surface modified BNNTs, slight improvements in all mechanical properties of neat PP were achieved. Yeşil [2010] previously reported the positive effect of the similar nanotube modification process on the strength of PET – carbon nanotube composites.

The composite with 0.5 wt% of purified BNNTs ([PP2+0.5PB]) also displayed slightly higher tensile strength with respect to neat polypropylene, which might be associated with the elimination of impurities from the BNNT product, such as iron particles.

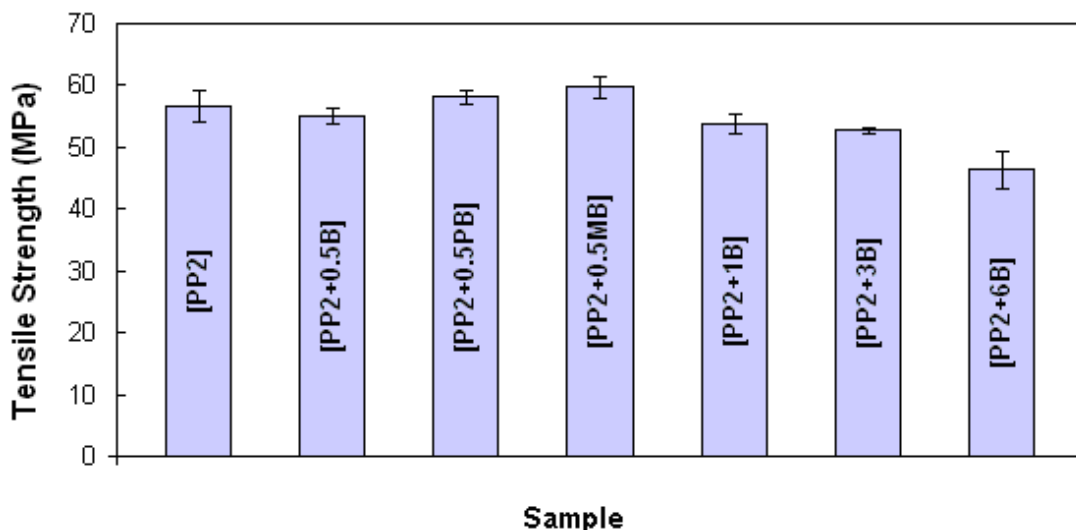


**Figure 6.18** Tensile strength of third group composites.

The addition of the as-synthesized BNNTs slightly decreased the tensile strength values due to the BNNT bundle formations. It was observed in this study that, in order to overcome problems related to dispersion and to obtain promising mechanical property improvements in polymer–BNNT composites, the as-synthesized BNNTs should be subjected to purification and also surface modification processes.

The slight decreases in tensile strength of neat PP with the as-synthesized BNNT additions might also be associated with the length of the nanotubes. As postulated by Wang et al. [2008], the strength of a polymer–nanotube composite depends on the length of filler fibers. Since the as-synthesized nanotubes can be easily broken in the composite manufacturing stages, they could end up being shorter than a critical value under which they lack contributing to the mechanical strength.

Generally, it was observed that low loadings (0.5 and 1 wt%) of the as-synthesized BNNTs caused slight increases in the Young’s modulus and yield strength of neat PP due to high stiffness of BNNTs, while preserving the tensile strength of neat PP. On the other hand, high loadings of the as-synthesized BNNTs (3 and 6 wt%) decreased the elongation at break and tensile strength values of neat PP.

Probable reason of these decreases was the BNNT bundle formations inside the PP matrix, which acted as mechanical defects to decrease flexibility of neat matrix. This problem is frequently addressed in polymer-nanotube composites since nanotubes tend to agglomerate inside polymer matrixes due to their high aspect ratios and low bending stiffness [Shi et al., 2004].

### 6.3.2 Differential Scanning Calorimetry (DSC)

Melting and crystallization behaviors of composite samples were investigated by DSC analysis. Melting temperature ( $T_m$ ), crystallization temperature ( $T_c$ ), enthalpy of fusion ( $\Delta H_f$ ) and percent crystallinity ( $X_c$ ) values for each sample were determined. The glass transition temperature ( $T_g$ ) could not be determined from the DSC curves since the  $T_g$  peaks were uncertain. Calculation of  $X_c$  is given in Appendix F. DSC plots of all samples are included in Appendix G. Table 6.3 tabulates the thermal properties of all samples prepared in this study.

**Table 6.3** Thermal properties of PP–BNNT composites.

Composite	PP wt%	$T_c$ (°C)	$T_m$ (°C)	$\Delta H_f$ (J/g)	$X_c$ (%)
[PP1]	100	121.85	164.65	85.09	40.71
[PP1+1A]	99	120.50	163.81	74.80	36.15
[PP1+1A+1B]	98	126.55	164.47	83.77	40.90
[PP2]	100	119.40	164.94	80.77	38.65
[PP2+1A]	99	117.72	164.73	77.11	37.27
[PP2+1A+1B]	98	124.70	164.30	82.22	40.14
[PP2+1A+3B]	96	127.42	165.00	76.65	38.20
[PP2+0.5B]	99.5	124.24	165.50	83.23	40.02
[PP2+0.5PB]	99.5	123.21	166.07	88.16	42.39
[PP2+0.5MB]	99.5	124.19	166.23	74.83	35.98
[PP2+1B]	99	124.88	164.79	73.24	35.40
[PP2+3B]	97	125.39	164.63	69.57	34.32
[PP2+6B]	94	126.38	164.64	61.90	31.51

The melting temperature of neat PP and the composites did not change significantly. On the other hand, it was observed that as the concentration of BNNTs in the polymer matrix was increased, crystallization temperature ( $T_c$ ) of the composites increased. The increase in the  $T_c$  indicates faster crystallization of polymer chains upon cooling, which resembles the nucleating agent effect. The addition of nucleating agents provides sites for the initiation of crystallization, which increases the crystallization temperature [Maier & Calafut, 1998]. It can be said that BNNTs functioned in a similar manner with nucleating agents. A similar nucleating mechanism was previously reported when carbon nanotubes were added as fillers into polyethylene matrix [Bhattacharyya, 2003].

A controversial result was observed in the degree of crystallinity ( $X_c$ ) values. Even though the BNNT filler is abundantly crystalline,  $X_c$  of the composites decreased as the BNNT concentration was increased. This was an unexpected result. However, the calculation of  $X_c$  by utilizing the method given in Appendix F is disputed since this method assumes simplifications that might not conform the real case if the specific heat of the polymeric material is altered by the addition of a filler. This kind of an alteration might have been induced by the BNNTs, which have quite different thermal properties than the polypropylene matrix. Moreover, the  $X_c$  values calculated using this method represent the percent crystallinity close to the melting point, not at the room temperature. Due to the reasons explained, the  $X_c$  values of the PP–BNNT composites might be misleading [Kong & Hay, 2002].

### **6.3.3 Thermal Gravimetric Analysis (TGA)**

Thermal degradation behaviors of composites were observed using TGA by heating samples from room temperature to 600 °C under  $N_2$  atmosphere in order to investigate the effect of BNNT loading on the thermal stability of PP based composites.

### 6.3.3.1 First Group Composites

Figure 6.19 shows the TGA plots of first group composites. Neat EH-241 PP shows a steep weight loss in the temperature range of 380–465 °C. This weight loss might be due to chain degradation of PP. The same steep weight loss for 1 wt% antioxidant composite was also observed with a little shift towards to higher temperatures. Antioxidant presence could have stabilized the PP chains against degradation, thus enhanced the thermal stability. 1 wt% of the as-synthesized BNNT addition did not make further improvement over the composite having 1 wt% of antioxidant. Weight fractions of final residues were in agreement with antioxidant and BNNT concentrations in the composites.

It was experimentally proved that BNNTs have quite high chemical and thermal inertness. The oxidation of BNNTs was reported to start at 800 °C under air atmosphere [Chen et al., 2004]. TGA of the as-synthesized BNNTs was carried out under nitrogen atmosphere. The resulting TGA curve was given in Appendix H. It was observed that BNNTs did not undergo any thermal degradation in the temperature range of 25–600 °C.

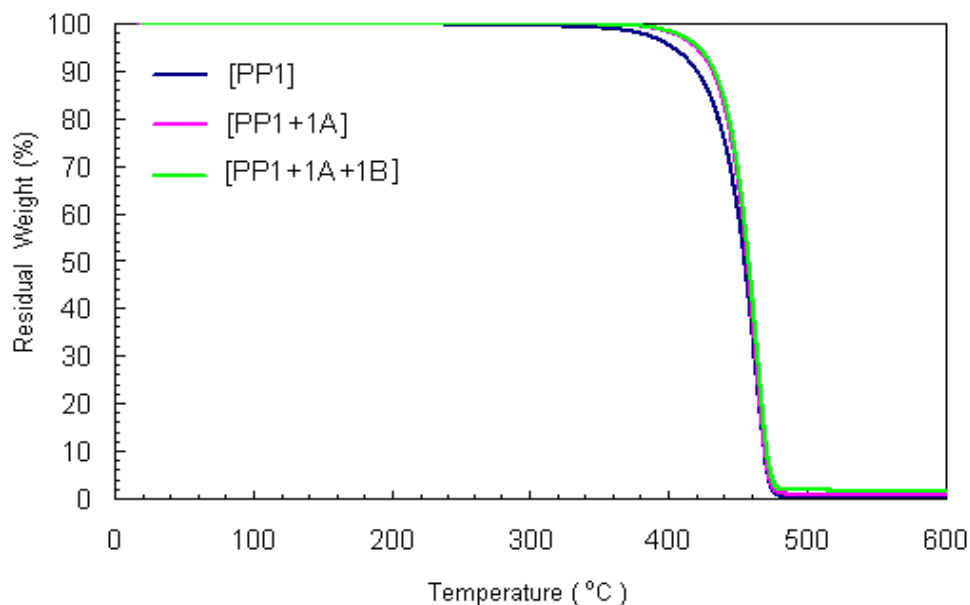


**Figure 6.19** TGA plots of first group composites.

### 6.3.3.2 Second Group Composites

Figure 6.20 shows the TGA plots of second group composites. The steep weight loss for this polymer type (MH-418) was observed in the temperature range of 310–420 °C. Seemingly, this indicated the lower thermal stability of MH-418 type PP when compared to that of EH-241 PP. Neat MH-418 PP might have undergone more thermal degradation under the higher barrel temperature used in the extrusion stage when compared to EH-241.

The presence of 1 wt% antioxidant caused a more pronounced improvement in the thermal stability of neat MH-418 PP for the possible reason explained above. 1 wt% BNNT addition made no significant enhancement over the composite having 1 wt% of antioxidant. However, when the BNNT loading was increased to 3 wt%, the composite somehow exhibited lower thermal stability with respect to composite having 1 wt% of BNNTs. This was an unexpected result since the BNNTs were proven robust in the temperature range of analysis. This behavior could be resulted from the experimental errors in the TGA analysis.

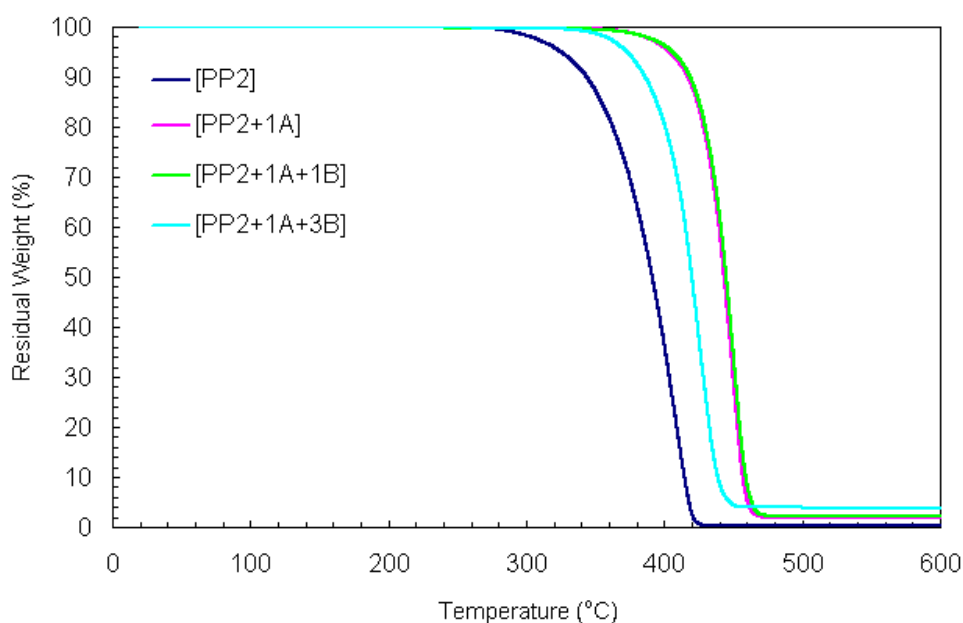


**Figure 6.20** TGA plots of second group composites.

### 6.3.3.3 Third Group Composites

Figure 6.21 represents the TGA plots of third group composites. In the absence of antioxidant, the steep weight loss region was shifted to higher temperatures with BNNT additions, which indicated that BNNT presence stabilized the neat PP against degradation. In other words, BNNT addition improved the thermal stability of neat PP at all studied concentrations. This was an expected result due to the high chemical and thermal stability of BNNTs [Chen et al., 2004].

Slight thermal improvement with respect to neat PP was obtained with 1 wt% of the as-synthesized BNNT loading. PP having 0.5 and 3 wt% of as-synthesized BNNT loadings induced higher thermal stability improvements with respect to PP having 1 wt% of BNNTs. PP having 6 wt% of BNNT addition induced the highest thermal improvement among the all of the BNNT additions, which indicated that the thermal stability improvement of neat PP was related with the BNNT loading.

The effect of 0.5 wt% loading of purified and purified – surface modified BNNT additions were investigated with respect to same loading of the as-synthesized BNNTs. It was observed that the usage of purified BNNTs did not make any improvement over the usage of as-synthesized BNNTs. However, a slight extra improvement in the thermal stability of neat PP was achieved by the usage of purified and then surface modified BNNTs with respect to the usage of as-synthesized BNNTs. This was probably due to the uniform dispersion of BNNTs inside the PP matrix. Nicely dispersed nanotubes might have induced an extra stabilizing effect to the polymer matrix.

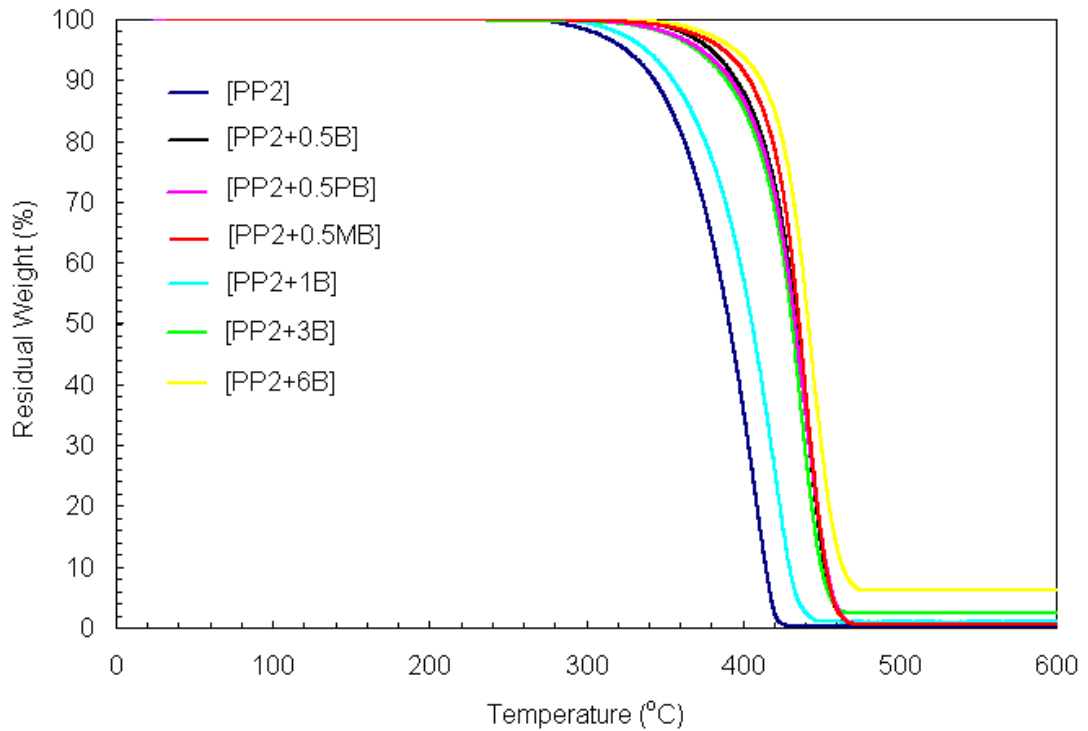


**Figure 6.21** TGA plots of third group composites.

### 6.3.4 Thermal Mechanical Analysis (TMA)

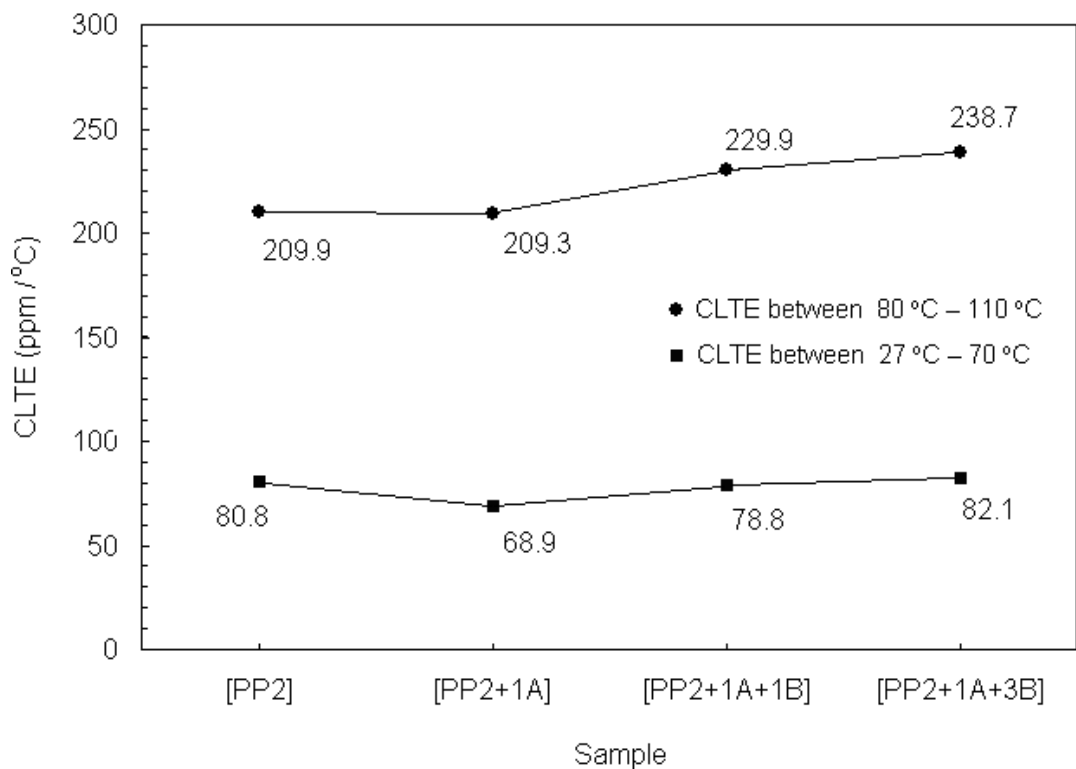
Thermal mechanical analysis (dilatometry) was performed according to ASTM-D696 on second and third group composites (Table 5.5) in order to obtain information about composites' coefficient of linear thermal expansion (CLTE). As the BNNTs are envisioned to be fillers for composites that endure high operating temperatures, estimating their effect on the thermal expansion of polymer composites is crucial. TMA analysis curves of second and third group composites obtained from the software of Setaram Labsys dilatometer are included in Appendix I.

Figure 6.22 shows the coefficients of linear thermal expansion (CLTE) of second group composites calculated in two different temperature intervals: from 27 °C to 70 °C and from 80 °C to 110 °C, in order to represent different ranges of application temperatures.



In second group composites, addition of 1 wt% antioxidant reduced the CLTE of neat PP between 27 °C and 70 °C and did not affect between 80 °C and 110 °C. On the other hand, addition of 1 wt% and 3 wt% BNNTs did not affect the CLTE at lower temperatures but slightly increased the CLTE at higher temperatures (Figure 6.22).

Figure 6.23 represents the CLTE of composites with respect to the as-synthesized BNNT loadings in the absence of antioxidant. The CLTE of neat PP was not significantly affected with the addition of BNNTs in lower temperature interval except the BNNT loading of 0.5 wt%, which seemed to slightly increase the CLTE of neat PP. In the higher temperature interval, CLTE of neat PP showed slight increases in all BNNT loadings with respect to neat PP.



**Figure 6.22** CLTE of second group composites.

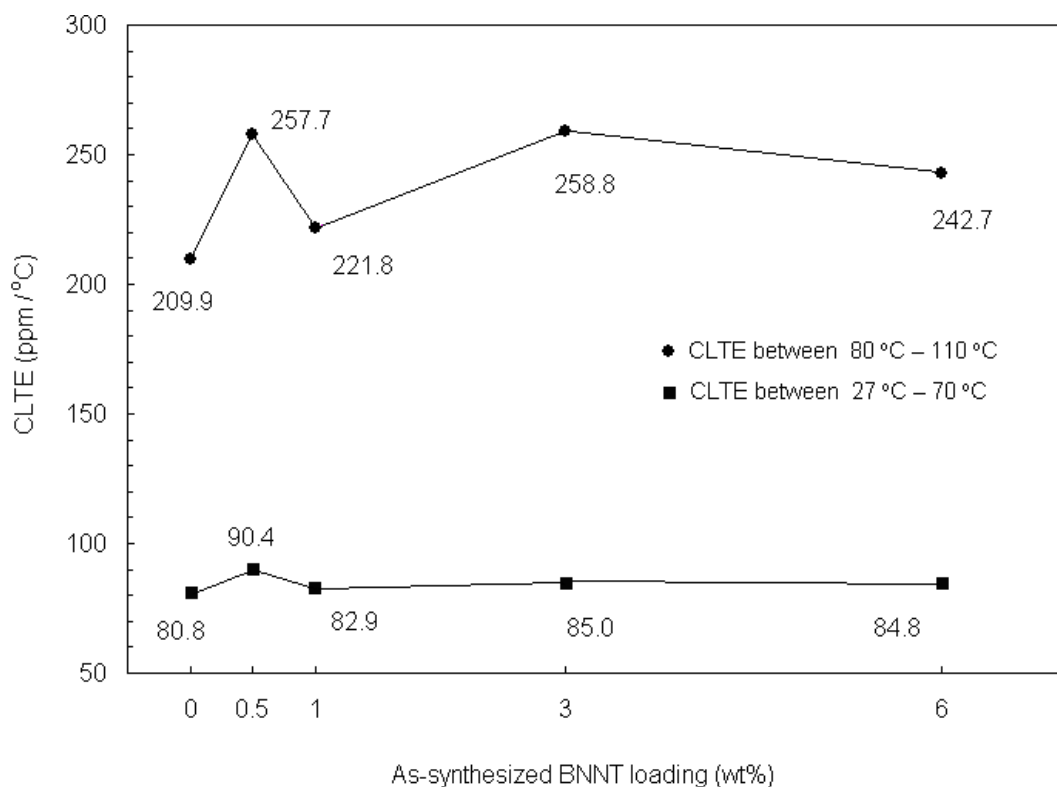


**Figure 6.23** CLTE of composites with respect to the as-synthesized BNNT loadings.

The effect of adding purified and surface modified BNNTs in neat PP was also investigated. Figure 6.24 shows the CLTE of neat PP, and PP - BNNT composites with 0.5 wt% of the as-synthesized (PP2+0.5B), purified (PP2+0.5PB), purified and then surface modified (PP2+0.5MB) BNNTs. It was observed that composites with purified and purified–surface modified BNNTs exhibited lower CLTE with respect to the composite with the as-synthesized BNNTs.

The slight increase in the CLTE of composites with nanotube addition can be due to several reasons. The entrapped air inside the nanotube agglomerates could have increased the expansion with temperature. Wei et al. [2002] reported an increase in the CLTE of neat polyethylene when carbon nanotubes were added as fillers. According to Wei et al. [2002], the source of thermal expansion in a polymer–nanotube composite is solely the polymer chains, which is the total volume of the composite excluded by the volume occupied by the nanotube fillers.

However, the phonon modes (which are the source of remarkably high thermal conductivities of nanotubes) and Brownian motions induced by the nanotube fillers to the polymer matrix cause an increase in the CLTE of composites. In this study, a similar mechanism might have been the source of slight increases in CLTE with the as-synthesized nanotube additions (Figure 6.23).

However, when there was a homogeneous dispersion of the nanotubes inside the PP matrix as considered to exist in the composite [PP2+0.5MB], the interfacial area between polymer chains and nanotubes might have been high enough to resist towards the thermal–mechanical expansion, hence compensating the effect of phonon mode induced mechanism. Zhi et al. [2009] reported decreases in the CLTE of polymers with uniform dispersion of BNNTs inside the matrix, which was postulated to be due to the adhesion between the polymer matrix and individual nanotubes.

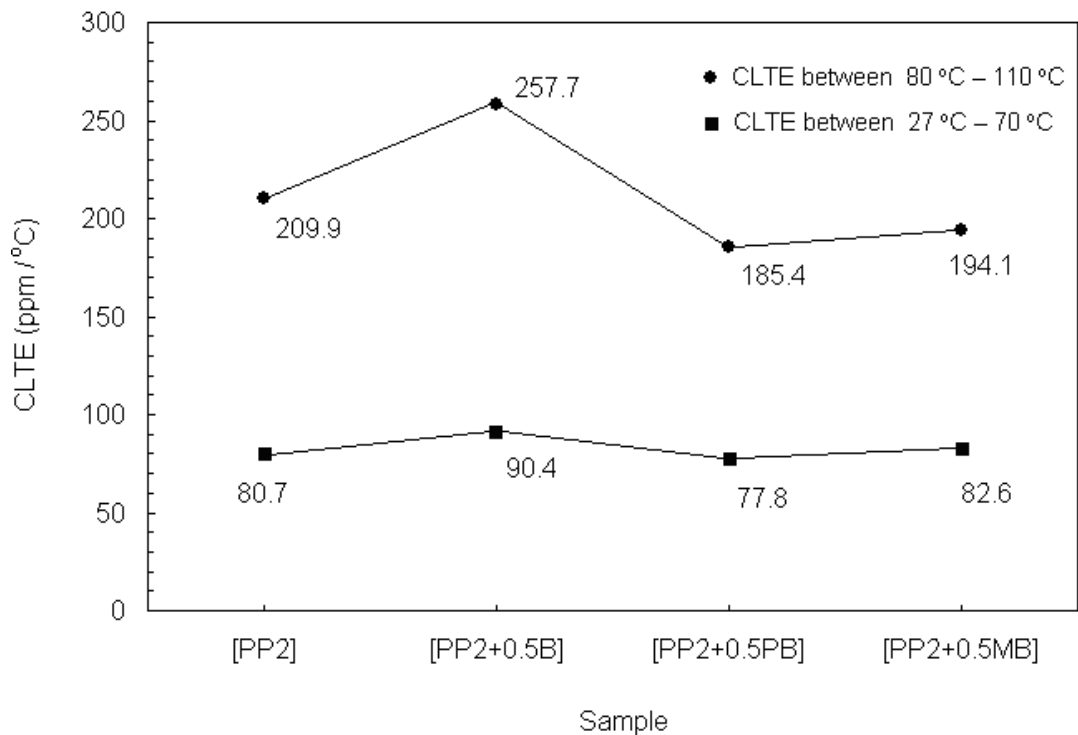


**Figure 6.24** CLTE of composites with respect to 0.5 wt% of the as-synthesized, purified and purified – surface modified BNNT additions.

## CHAPTER 7

### CONCLUSIONS

- BNNTs were successfully synthesized by reacting ammonia gas with a powder mixture of boron and iron oxide.
- Initial mixture amount of 0.8 g and ammonia inlet flow rate of 125 cm<sup>3</sup>/min were observed to yield the product with the whitest appearance, which indicated to high concentration of boron nitride in the as-synthesized material.
- XRD and FTIR analyses revealed that the synthesized material predominantly consisted of hexagonal boron nitride. Presence of iron and boron was also observed.
- Multi-point BET surface area of the as-synthesized BNNT sample was 22.53 m<sup>2</sup>/g.
- TEM analysis revealed the presence of multi-wall nanotubes with both bamboo-like and hollow cylindrical shapes in the synthesized product.
- With SEM analysis, agglomeration of BNNTs was observed. The outer diameters of the nanotubes varied between 50–130 nm.
- Tensile test results revealed that the addition of 0.5 and 1 wt% of the as-synthesized BNNTs slightly increased the Young's modulus and yield strength of neat PP. Higher loadings of the as-synthesized BNNTs (3 and 6 wt%) decreased the Young's modulus and yield strength values when compared to low BNNT loadings, due to the BNNT bundle formations.

- The elongation at break and tensile strength values of PP–BNNT composites were inversely related with the as-synthesized BNNT concentration.
- Contrary to the 0.5 wt% addition of the as-synthesized BNNTs, usage of purified (acid-treated) BNNTs in the same loading did not decrease the elongation at break and tensile strength values of neat PP.
- By the usage of purified and then surface modified BNNTs in a 0.5 wt% loading, all mechanical properties of neat PP were improved slightly.
- DSC plots revealed a noticeable increase in the crystallization temperature ( $T_c$ ) of composites with BNNT addition, due to the BNNTs acting as nucleating sites for the initiation of crystallization.
- When the as-synthesized BNNTs were added to neat PP in the absence of antioxidant, the thermal stability of neat PP was improved in all BNNT loadings. In other words, BNNT loadings stabilized the neat PP against thermal degradation.
- Usage of purified and then surface modified (PEGylated) BNNTs induced a slight extra thermal stability improvement of neat PP when compared to the usage of the as-synthesized BNNTs.
- TMA analysis revealed that addition of the as-synthesized BNNTs in PP matrix did not significantly affect the coefficient of linear thermal expansion (CLTE) of composites between 27 °C and 70 °C, but caused slight increases in the CLTE between 80 °C and 110 °C with respect to neat PP.
- CLTE of the composites having 0.5 wt% of purified and then surface modified BNNTs were lower than that of composite with 0.5 wt% of as-synthesized BNNTs.

## REFERENCES

**Ajayan**, P.M., Zhou, O.Z., (2001), "Applications of carbon nanotubes", Carbon Nanotubes, *Topics Appl. Phys.*, vol. 80, pp. 391–425.

**Bhattacharya**, S.N., Gupta, R.K., Kamal, M.R., (2008), "Polymeric nanocomposites: Theory and practice", Hanser Verlag, Munich.

**Bhattacharyya**, A.R., Sreekumar, T.V., Liu, T., Kumar, S., Ericson, L.M., Hauge, R.H., Smalley, R.H., (2003), "Crystallization and orientation studies in polypropylene/single wall carbon nanotube composite", *Polymer*, vol. 44, pp. 2373–77.

**Brunauer**, S., Deming, L., Deming, W., E. Teller, (1940), "On a theory of the Van der Waals adsorption of gases", *J. Am. Chem. Soc.*, vol. 62, pp. 1723–32.

**Brunauer**, S., Emmett, P. H., Teller, E., (1938), "Adsorption of gases in multimolecular layers", *J. Am. Chem. Soc.*, vol. 60, pp. 309–19.

**Callister**, W., (1997), "Materials science and engineering: An Introduction", 4th Edition, John-Wiley & Sons, USA.

**Cao**, G., (2004), "Nanostructures and nanomaterials: Synthesis, properties and applications", Imperial College Press, UK.

**Ceresena** Research, (2007), "Market study: Polypropylene (UC 805)", <http://www.ceresana.com/en/market-studies/plastics/polypropylene/>, last accessed: 03. 08. 2010.

**Chen**, Y., Fitzgerald, J., Williams, J. S., Bulcock, S., (1999), "Synthesis of boron nitride nanotubes at low temperatures using reactive ball milling", *Chem. Phys. Lett.*, vol. 299 (3-4), pp. 260-64.

**Chen**, Y., Zou, J., Campbell, S.J., Le Caer, G., (2004), "Boron nitride nanotubes: Pronounced resistance to oxidation", *Appl. Phys. Lett.*, vol. 84 (13), pp. 2430–32.

**Chopra**, N.G., Luyken, R.J., Cherrey, K., Crespi, V.H., Cohen, M.L., Louie, S.G., Zettl, A., (1995), "Boron nitride nanotubes", *Science*, vol. 269 (5226), pp. 966–67.

**Chopra**, N.G., Zettl, A., (1998), "Measurement of the elastic modulus of a multi-wall boron nitride nanotube", *Sol. St. Comm.*, vol. 105 (5), pp. 297–300.

**Ciba Specialty Products**, ®Irganox 1010  
<http://www.polivinilplastik.com/urunler/I1010.pdf>, last accessed: 24.09.2010.

**Collister**, J., (2001), "Commercialization of polymer nanocomposites", In: "Polymer nanocomposites, synthesis characterization and modelling", Krishnamoorti, R., Vaia R.A., (eds), *American Chemical Society*, pp. 7–14.

**Crawford**, R. J., (1998), "Plastics Engineering", 3rd edition, BH., Oxford.

**De Boer**, J.H., (1958), "The shapes of capillaries", In *The Structure and Properties of Porous Materials*, in Proceedings of the Tenth Symposium, Colston Research Society, University of Bristol, Everett, D.H., Stone, F.S. (eds.), Butterworths Science Publications, London, pp. 68–94.

**Dondero**, W.E., Gorga, R.E., (2006), "Morphological and mechanical properties of carbon nanotube / polymer composites via melt compounding", *Journal of Polymer Science: Part B: Polymer Physics*, vol. 44, pp. 864 – 78.

**Ebewele**, R.O., (2000), "Polymer science and technology", 1st edition, CRC Pres, New York.

**Garcia**, M., Vliet, G. , Jain, S., Schrauwen, B. A. G. , Sarkissov, A. van Zyl, W.E., Boukamp, B., (2004), "Polypropylene/SiO<sub>2</sub> nanocomposites with improved mechanical properties", *Rev. Adv. Mater. Sci*, vol. 6, pp. 169–75.

**Golberg**, D., Bando, Y., Huang, Y., Terao, T., Mitome, M., Tang, C.C., Zhi, C.Y., (2010), "Boron nitride nanotubes and nanosheets", *ACS Nano*, vol. 4 (6), pp. 2979–93.

**Golberg**, D., Bando, Y., Tang, C.C., Zhi, C.Y., (2009), "Functional boron nitride nanotubes", <http://www.cityu.edu.hk/ieeeneec/abstract/golberg.pdf>, last accessed: 09.11.2010

**Harrison**, C., Weaver, S., Bertelsen, C., Burgett, E., Hertel, N., Grulke, E., (2007), "Polyethylene/boron nitride composites for space radiation shielding", *Journal of Applied Polymer Science*, vol. 109 (4), pp. 2529–38.

**Hong**, S., Myung, S., (2007), "Nanotube electronics: A flexible approach to mobility", *Nature Nanotechnology*, vol. 2, pp. 207–8.

**Iijima**, S., (1991), "Helical microtubules of graphitic carbon", *Nature*, vol. 354, pp. 56-58.

**Ishigami**, M., Aloni, S., Zettl, A., (2003), "Properties of boron nitride nanotubes", Scanning tunneling microscopy / spectroscopy and related techniques: 12th international conf., edited by Koenraad, P.M., Kemerink, M., pp. 94–99.

**Jiang**, H., Liu, B., Huang, Y., (2004), "Thermal expansion of single wall carbon nanotubes", *J. Eng. Mater. Technol.*, vol. 126(3), pp. 265–71.

**Jones**, R.M., (1999), "Mechanics of composite materials", 2nd edition, Taylor & Francis, Philadelphia.

**Jordan**, J., Jacob, K., Tannenbaum, R., Shara, M., Jasiuk, I., (2005), "Experimental trends in polymer nanocomposites - A Review", *Materials Science and Engineering*, vol. 393 (1-2), pp. 1-11.

**Kashiwagi**, T., Grulke, E., Hilding, J., Harris, R., Awad, W., Douglas, J., (2002), "Thermal degradation and flammability properties of poly(propylene)/carbon nanotube composites", *Macromol. Rapid Commun.*, vol. 23 (13), pp. 761–65.

**Kaw**, K., (1997), "Mechanics of composite materials", 1st edition, CRC Press, New York.

**Kawasumi**, M., (2004), "The discovery of polymer – clay hybrids", *J. Polym. Sci. Part A, Polym. Chem.*, vol. 42, pp. 819–24.

**Kim**, S.W., (2005), "Thermal properties of multi-walled carbon nanotube-reinforced polypropylene composites", The 9th Russian-Korean International Symposium on Science and Technology (KORUS 2005), pp. 284–87.

**Koi**, N., Oku, T., Inoue, M., Suganuma, K., (2008) "Structures and purification of boron nitride nanotubes synthesized from boron-based powders with iron particles", *J. Mater. Sci.*, vol. 43 (8), pp. 2955–61.

**Kong**, Y., Hay, J.N., (2002), "The measurement of the crystallinity of polymers by DSC", *Polymer*, vol. 43 (2002), pp. 3873–78.



**Kopeliovich**, D., "Classification of Composites",  
[http://www.substech.com/dokuwiki/doku.php?id=classification\\_of\\_composites](http://www.substech.com/dokuwiki/doku.php?id=classification_of_composites),  
last accessed: 12.09.2010.

**Kroschwitz**, J.I., Mark H.F., (2003), "Encyclopedia of polymer science and technology", 3rd Edition, Wiley Interscience.

**Lee**, C.H., Wang, J., Kayatsha, V.K., Huang, J.Y., Yap, T.K., (2008), "Effective growth of boron nitride nanotubes by thermal chemical vapor deposition", *Nanotechnology*, vol.19 (45), id: 455605.

**Lourie**, O., Yu, M.F., Dyer, M.J., Moloni, K., Kelly, T.F., Ruoff, R.S., (2000), "Strength and breaking mechanism of multiwalled carbon nanotubes under tensile load", *Science*, vol. 287 (5453), pp. 637–40.

**Lowell**, S., Shields, J. E., Thomas, M. A., Thommes, M., (2006), "Characterization of porous solids and powders: Surface area, pore size and density", Springer, Netherlands.

**Maier**, C., Calafut, T., (1998), "Polypropylene: The definitive user's guide and databook", 1<sup>st</sup> edition, William Andrew Inc., NY.

**Manchado**, M.A., Valentini, L., Biagiotti, J., Kenny, J.M., (2005), "Thermal and mechanical properties of single-walled carbon nanotubes–polypropylene composites prepared by melt processing", *Carbon*, vol. 43 (7), pp. 1499–1505.

**Mark**, J.E., (2007), "Physical properties of polymers handbook", 2nd edition, Springer, New York.

**Marosfoi**, B.B., Szabó, A., Marosi, G., Tabuani, D., Camino, G., Pagliari, S., (2006), "Thermal and spectroscopic characterization of polypropylene – carbon nanotube composites", *Journal of Thermal Analysis and Calorimetry*, vol. 86 (3), pp. 669–73.

**Mazumdar**, S. K., (2002), "Composites manufacturing materials, product, process engineering", CRC press, USA.

**McCulloch**, D., Harland, J., Francis, P., (2003), "Notes on transmission electron microscopy" RMIT Microscopy and Micro-analysis Facility, Depart. Appl. Phys., RMIT University (Australia).

**Middleman** S., (1997), "Fundamentals of polymer processing", McGraw-Hill, USA.

**Milev**, A.S., Kannangara, G. S. K., (2005), "Nanotechnology", In: Kroschwitz, J.I., Seidel, A., (Eds), Kirk-Othmer Encyclopedia of Chemical Technology, 5th Edition, vol. 17, pp. 1-29, Wiley, NJ.

**Moniruzzaman**, M., Winey, K.I., (2006), "Polymer nanocomposites containing carbon nanotubes", *Macromolecules*, vol. 39, pp. 5194–205.

**Nyquist**, R. A., Kagel, R. O., (1971), "Infrared spectra of inorganic compounds (3800 - 45 cm<sup>-1</sup>)", Academic Press, New York and London, 1971.

**Owen**, J.H.G., "Nanotubes and fullerenes for quantum computing", [http://homepage.mac.com/jhgowen/research/nanotube\\_page/nanotubes.html](http://homepage.mac.com/jhgowen/research/nanotube_page/nanotubes.html), last accessed: July, 2010

**Özmen**, D., (2008), "Production and characterization of boron nitride nanotubes", Chemical Engineering MS Thesis, Middle East Technical University, Ankara, Turkey.

**Prashantha**, K., Soulestin, J., Lacrampe, M.F., Claes, M., Dupin, G., Krawczak, P., (2008), "Multi-walled carbon nanotube filled polypropylene nanocomposites based on masterbatch route: Improvement of dispersion and mechanical properties through PP-g-MA addition", *Express Polymer Letters*, vol. 2 (10), pp. 735–45.

**Ravichandran**, J., Manoj, A.G., Liu, J., Manna, I., Carroll, D.L., (2008) "A novel polymer nanotube composite for photovoltaic packaging applications", *Nanotechnology*, vol. 19, id: 085712.

**Rinzler**, A.G., Liu, J., Dai, H., Nikolaev, P., Huffman, C.B., Rodriguez-Macias, F.J., Boul, P.J., Lu, A.H., Heymann, D., Colbert, D.T., Lee, R.S., Fischer, J.E., Rao, A.M., Eklund, P.C., Smalley, R.E., (1998) "Large-scale purification of single-wall carbon nanotubes: process, product, and characterization", *Appl. Phys. A. Material Science and Processing*, vol. 67 (1), pp. 29–37.

**Seymour**, R.B., (1996), "Polymer chemistry: An introduction", 4nd edition, New York.

**Seymour**, R. B., Carraher C. E., (1984), "Structure-property relationships in polymers", Plenum Press, New York.

**Shi**, D.L., Feng, X.Q., Huang, Y.Y., Hwang, K.C., Gao, H., (2004), "The effect of nanotube waviness and agglomeration on the elastic property of carbon nanotube reinforced composites", *Journal of Engineering Materials & Technology*, vol. 126, pp. 250–57.

- Stuart**, B., (1996), "Modern Infrared Spectroscopy", John Wiley & Sons Inc., UK.
- Terao**, T., Bando, Y., Mitome, M., Zhi, C.Y., Tang, C.C., Golberg, D., (2009), "Thermal conductivity improvement of polymer films by catechin-modified boron Nitride Nanotubes", *J. Phys. Chem. C*, vol. 113 (31), pp. 13605–609.
- Terrones**, M., Romo-Herrera, J.M., Cruz-Silva, E., López-Urías, F., Muñoz-Sandoval, E., Velázquez-Salazar, J.J., Terrones, H., Bando, Y., Golberg, D., (2007), "Pure and doped boron nitride nanotubes", *Materials Today*, vol. 10 (5), pp. 30–38.
- Treacy**, M.M.J., Ebbesen, T.W., Gibson, J.M., (1996), "Exceptionally high Young's modulus observed for individual carbon nanotube", *Nature*, vol. 381, pp. 678–80.
- Tripathi**, D., (2002), "Practical Guide to Polypropylene", 1st edition, Rapra Technology Ltd., UK.
- Tang**, C., Bando, Y., Sato, T., Kurashima, K., (2002), "A novel precursor for synthesis of pure boron nitride nanotubes", *Chem. Commun.*, vol. 2002 (12), pp. 1290-91.
- Tang**, C. C, Lamy de la Chapelle, M., Li, P., Dang, H., Y., Fan, S. S., (2001), "Catalytic growth of nanotube and nanobamboo structures of boron nitride", *Chem. Phys. Lett.*, vol. 342 (5-6), pp. 492–96.
- Wang**, W., Ciselli, P., Kuznetsov, E., Peijs, T., Barber, A.H., (2008), "Effective reinforcement in carbon nanotube – polymer composites", *Phil. Trans. R. Soc. A*, vol. 366, pp. 1613–26.
- Wei**, C., Srivastava, D., Cho, K., (2002), "Thermal expansion and diffusion coefficients of carbon nanotube – polymer composites", *Nano Letters*, vol. 2(6), pp. 646–50.
- Wilson**, M., Kannangara, K., Smith, G., Simmons, M., Raguse, B., (2002), "Nanotechnology, Basic science and emerging technologies", 1st edition, Chapman & Hall / CRC, Australia.
- Wischnitzer**, S., (1989), "Introduction to Electron Microscopy", 3rd Edition, Pergamon Press, New York.

**Yang**, D.J., Zhang, Q., Chen, G., Yoon, S. F., Ahn, J., Wang, S. G., Zhou, Q., Wang, Q., Li, J. Q. (2002), "Thermal conductivity of multiwalled carbon nanotubes", *Physical Review B*, vol. 66, id: 165440.

**Yayla**, S., (2007), "Production and characterization of polypropylene/organoclay nanocomposites", Chemical Engineering MS Thesis, Middle East Technical University, Ankara, Turkey.

**Yeniova**, C., (2009), "Impact modified polystyrene based nanocomposites", Chemical Engineering MS Thesis, Middle East Technical University, Ankara, Turkey.

**Yeşil**, S., (2010), "Processing and characterization of carbon nanotube based conductive polymer composites", Chemical Engineering Ph. D. Thesis, Middle East Technical University, Ankara, Turkey.

**Zhi**, C.Y., Bando, Y., Tang, C.C., Golberg, D., (2005), "Effective precursor for high yield synthesis of pure BN nanotubes", *Sol. St. Comm.*, vol. 135 (1-2), pp. 67–70.

**Zhi**, C.Y., Bando, Y., Tang, C.C., (2006), "Boron nitride nanotubes/polystyrene composites", *J. Mater. Res.*, vol. 21 (11), pp. 2794–800.

**Zhi**, C.Y., Bando, Y., Tang, C., Honda, S., Sato, K., Kuwahara, H., Golberg, D., (2006), "Purification of boron nitride nanotubes through polymer wrapping", *J. Phys. Chem. B*, vol. 110 (4), pp. 1525–28.

**Zhi**, C.Y., Bando, Y., Wang, W.L., Tang, C.C., Kuwahara, H., Golberg, D., (2008), "Mechanical and thermal properties of polymethyl methacrylate-BN nanotube composites", *Journal of Nanomaterials*, vol. 2008, id: 642036.

**Zhi**, C.Y., Bando, Y., Tang, C.C., Huang, Q., Golberg, D., (2008), "Boron nitride nanotubes: Functionalization and composites", *Journal of Materials Chemistry*, vol. 18, pp. 3900–08.

**Zhi**, C.Y., Bando, Y., Terao, T., Tang, C.C., Kuwahara, H., Golberg, D., (2009), "Towards thermoconductive, electrically insulating polymeric composites with boron nitride nanotubes as fillers", *Adv. Funct. Mater.*, vol. 19 (12), pp. 1857–62.

## APPENDIX A

### XRD DATA

XRD data of hexagonal BN, rhombohedral BN, Fe, Fe<sub>2</sub>O<sub>3</sub> and the as-synthesized BNNTs are tabulated in Tables A.1 - A.5. XRD data was retrieved from the catalog of International Centre for Diffraction Data (ICDD) for inorganic materials.

**Table A.1** XRD data of hexagonal BN.

Catalog no: 34-0421 Hexagonal BN Rad:CuK $\alpha$ 1 ( $\lambda$ :1.5406 Å)					
d (Å)	2 $\theta$ (°)	Intensity	h	k	l
3.328	26.76	100	0	0	2
2.169	41.59	23	1	0	0
2.062	43.87	10	1	0	1
1.817	50.14	16	1	0	2
1.663	55.16	12	0	0	4
1.550	59.55	<2	1	0	3
1.319	71.41	5	1	0	4
1.252	75.93	13	1	1	0
1.172	82.17	14	1	1	2
1.134	85.51	<3	1	0	5
1.109	87.94	<3	0	0	6
1.084	90.53	<3	2	0	0
1.031	96.66	3	2	0	2
1.000	100.68	10	1	1	4

**Table A.1 (cont'd)** XRD data of hexagonal BN.

0.908	115.93	<4	2	0	4
0.831	135.63	<4	0	0	8
0.830	136.14	4	1	1	6

**Table A.2** XRD data of rhombohedral BN.

<b>Catalog no: 45-1171</b>					
<b>Rhombohedral BN</b>					
<b>Rad:CuK<math>\alpha_1</math> (<math>\lambda</math>:1.5406 Å)</b>					
<b>d (Å)</b>	<b>2<math>\theta</math> (°)</b>	<b>Intensity</b>	<b>h</b>	<b>k</b>	<b>l</b>
3.334	26.71	100	0	0	3
2.119	42.61	20	1	0	1
1.989	45.56	12	0	1	2
1.666	55.06	8	0	0	6
1.638	56.07	4	1	0	4
1.470	63.18	2	0	1	5
1.251	75.95	8	1	1	0
1.193	80.41	<3	1	0	7
1.172	82.11	11	1	1	3
1.112	87.66	<3	0	0	9
1.077	91.23	<3	0	2	1
1.059	93.22	<3	2	0	2
1.001	100.62	7	1	1	6
0.831	135.85	4	1	1	9
0.816	141.13	4	2	1	1
0.808	144.53	4	1	2	2

**Table A.3** XRD data of cubic iron ( $\alpha$ -Fe).

<b>Catalog no: 87-0722</b>					
<b>Cubic Fe</b>					
<b>Rad: CuK<math>\alpha</math>1 (<math>\lambda</math>:1.5406 Å)</b>					
<b>d (Å)</b>	<b>2<math>\theta</math> (°)</b>	<b>Intensity</b>	<b>h</b>	<b>k</b>	<b>l</b>
2.022	44.76	100	1	1	0
1.430	65.16	16	2	0	0
1.167	82.52	30	2	1	1

**Table A.4** XRD data of iron oxide ( $\text{Fe}_2\text{O}_3$ ).

<b>Catalog no: 33-0664</b>					
<b><math>\text{Fe}_2\text{O}_3</math></b>					
<b>Rad:CuK<math>\alpha</math>1 (<math>\lambda</math>:1.5406 Å)</b>					
<b>d (Å)</b>	<b>2<math>\theta</math> (°)</b>	<b>Intensity</b>	<b>h</b>	<b>k</b>	<b>l</b>
3.684	24.14	22	0	1	2
2.700	33.15	100	1	0	4
2.519	35.61	75	1	1	0
2.292	39.28	4	0	0	6
2.207	40.85	24	1	1	3
2.077	43.52	4	2	0	2
1.840	49.48	59	0	2	4
1.694	54.09	72	1	1	6
1.636	56.15	2	2	1	1
1.603	57.43	8	1	2	2
1.485	62.45	17	0	1	8
1.453	63.99	55	2	1	4
1.349	69.60	6	2	0	8
1.311	71.94	21	1	0	10
1.306	72.26	12	1	1	9
1.259	75.43	17	2	2	0
1.227	77.73	9	3	0	6

**Table A.4 (cont'd)** XRD data of iron oxide (Fe<sub>2</sub>O<sub>3</sub>).

1.189	80.71	11	1	2	8
1.163	82.94	12	0	2	10
1.141	84.91	17	1	3	4
1.103	88.54	17	2	2	6
1.076	91.34	5	0	4	2
1.055	93.71	18	2	1	10
1.042	95.24	<3	1	1	12
1.039	95.66	8	4	0	4
0.989	102.28	11	3	2	8
0.971	104.91	<3	2	2	9
0.960	106.61	14	3	2	4
0.958	107.02	11	0	1	14

**Table A.5** XRD data of the as-synthesized BNNTs.

Rad: CuKa1 ( $\lambda$ :1.5418 Å)		
d (Å)	2 $\theta$ (°)	Intensity
3.362	26.48	100
2.163	41.82	30
1.807	50.38	5
1.667	54.74	7
1.254	76.20	12
1.169	82.48	6



## APPENDIX B

### FTIR SPECTRA OF BORON AND IRON OXIDE

FTIR spectra of boron and iron oxide used in this study are given in Figures B.1 and B.2.

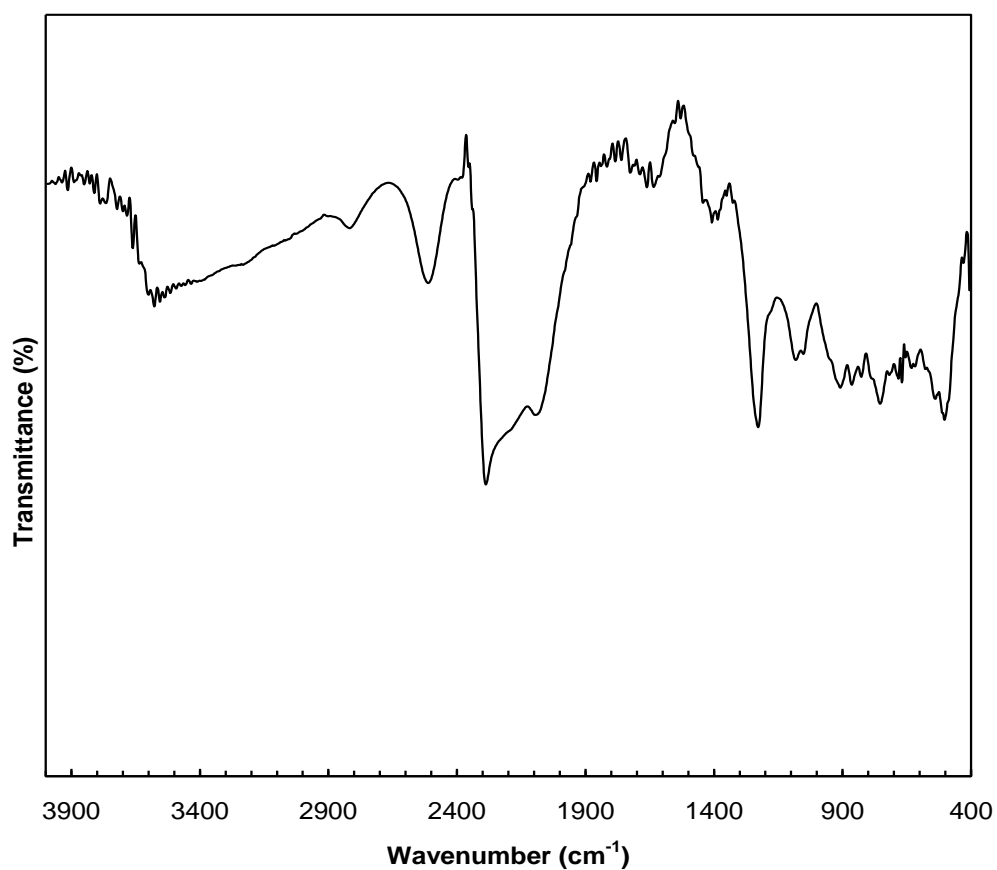


**Figure B.1** FTIR spectrum of boron [Özmen, 2008].

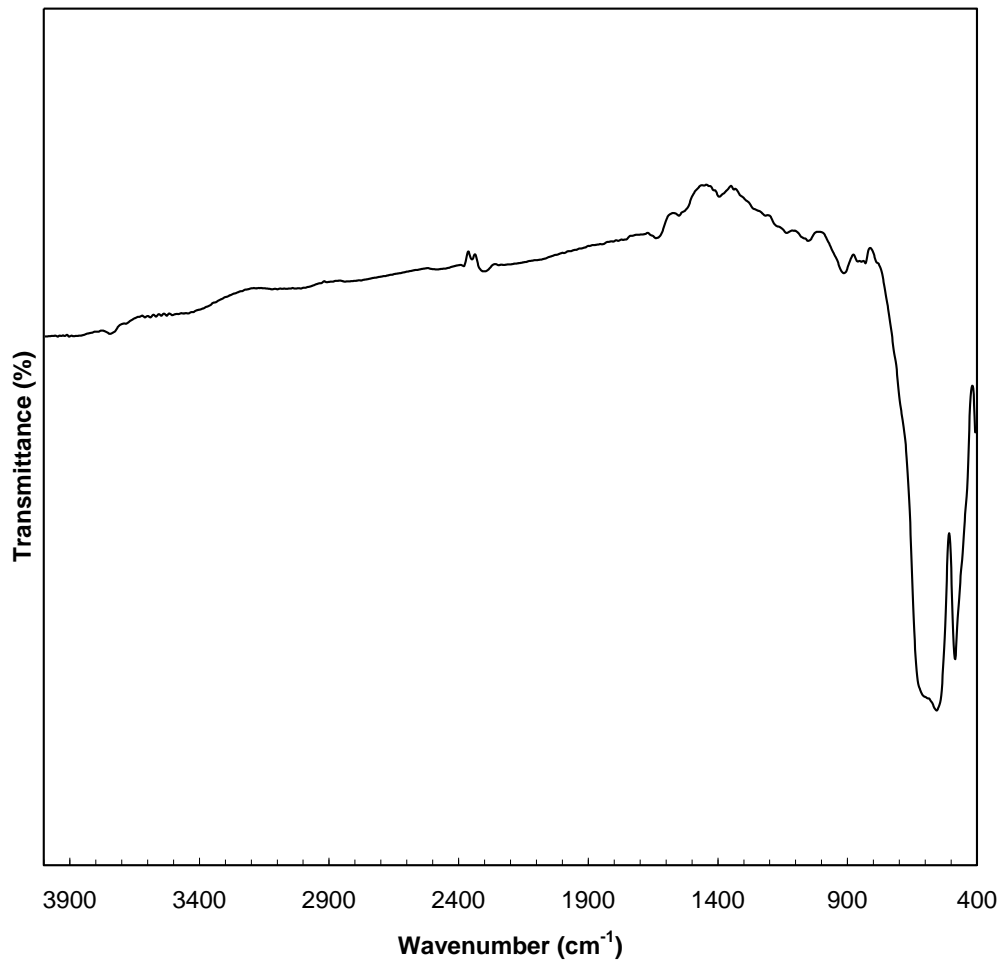


**Figure B.2** FTIR spectrum of iron oxide (Fe<sub>2</sub>O<sub>3</sub>) [Özmen, 2008]

## APPENDIX C

### BET METHOD FOR SURFACE AREA DETERMINATION

BET Method is used to determine surface areas of solid materials [Brunauer et al., 1938]. In multi-point BET surface analysis, surface areas of materials are calculated from BET equation (Eq. C.1). BET equation was derived by extending the Langmuir theory (for monolayer adsorption) to multilayer adsorption. According to BET method, physical adsorption occurs on multiple layers and there is no interaction between adsorption layers. Therefore, Langmuir theory is separately applied to each layer.

$$\frac{1}{V[(P_o/P)-1]} = \frac{C-1}{V_m C} \left( \frac{P}{P_o} \right) + \frac{1}{V_m C} \quad (\text{C.1})$$

where,

$C$  = Isotherm constant depending on the pore structure of the adsorbate

$V$  = Volume adsorbed

$V_m$  = Volume adsorbed for monolayer coverage

$P$  = Equilibrium pressure

$P_o$  = Saturation vapor pressure of the adsorbate.

If the system obeys BET model, plot of  $1/[V(1-P/P_o)]$  versus  $(P/P_o-1)$  gives a straight line for  $0.05 < P/P_o < 0.35$ , the slope of which is  $1/V_m C$ .

The total surface area is given by,

$$S_g = \left[ \frac{V_m N_o}{V} \right] \alpha \quad (\text{C.2})$$

where,

$S_g$  = total surface area

$V_m$  = volume adsorbed for monolayer coverage

$V$  = volume adsorbed

$N_o$  = Avogadro's number,  $6.02 \times 10^{23}$  molecules/mol

$\alpha$  = value for the area covered by one adsorbed molecule

$$\alpha = 1.09 \left[ \frac{M}{N_o \rho} \right]^{\frac{2}{3}} \quad (\text{C. 3})$$

where,

$M$  = molecular weight

$\rho$  = density of the adsorbed molecules

and  $\alpha = 0.162 \text{ nm}^2/\text{molecule}$  for nitrogen

## APPENDIX D

### TENSILE TEST RESULTS OF ALL SAMPLES

Table D.1 represents the tensile properties of all samples prepared in this study. The properties are given as the mean values of six specimens and the standard deviations of the measurements.

**Table D.1** Tensile properties of all samples.

Property Sample	Young's Modulus (MPa)	Tensile Strength (MPa)	Yield Strength (MPa)	Elongation at Break (%)
[PP1]	1256 ± 35	41 ± 5	33 ± 1	629 ± 25
[PP1+1A]	1303 ± 37	46 ± 3	39 ± 2	620 ± 27
[PP1+1A+1B]	1395 ± 90	42 ± 1	42 ± 1	310 ± 130
[PP2]	1533 ± 114	57 ± 3	43 ± 2	520 ± 24
[PP2+1A]	1648 ± 15	54 ± 1	42 ± 1	488 ± 19
[PP2+1A+1B]	1740 ± 22	49 ± 2	43 ± 1	450 ± 13
[PP2+1A+3B]	1708 ± 54	46 ± 3	42 ± 1	432 ± 24
[PP2+0.5B]	1599 ± 95	55 ± 1	46 ± 1	493 ± 13
[PP2+0.5PB]	1476 ± 59	58 ± 1	46 ± 1	537 ± 8
[PP2+0.5MB]	1563 ± 111	60 ± 2	47 ± 1	546 ± 15
[PP2+1B]	1608 ± 103	54 ± 2	47 ± 1	484 ± 23
[PP2+3B]	1533 ± 57	53 ± 1	46 ± 1	477 ± 27
[PP2+6B]	1514 ± 75	46 ± 3	45 ± 2	437 ± 26

## APPENDIX E

### REPRESENTATIVE STRESS-STRAIN CURVES

Figures E.1 – E.5 show representative stress-strain curves for neat MH-418 PP and third group composites with as-synthesized BNNT additions.

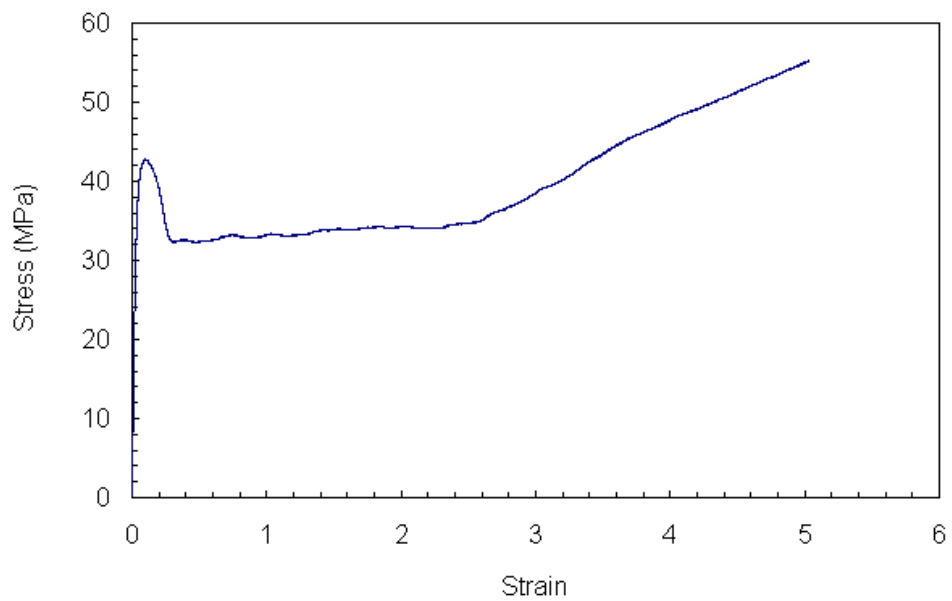


**Figure E.1** Representative stress-strain curve for [PP2].

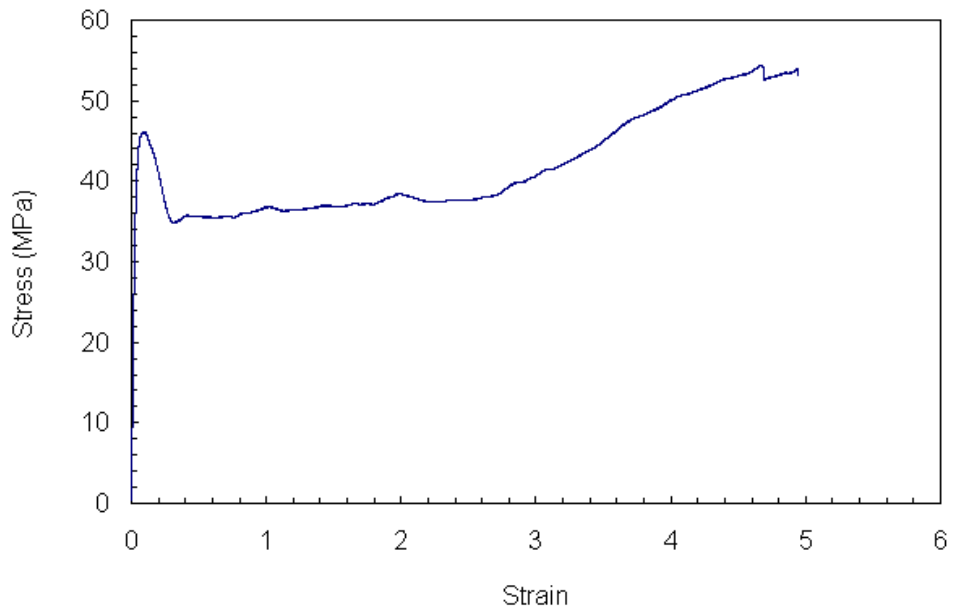


**Figure E.2** Representative stress-strain curve for [PP2+0.5B].

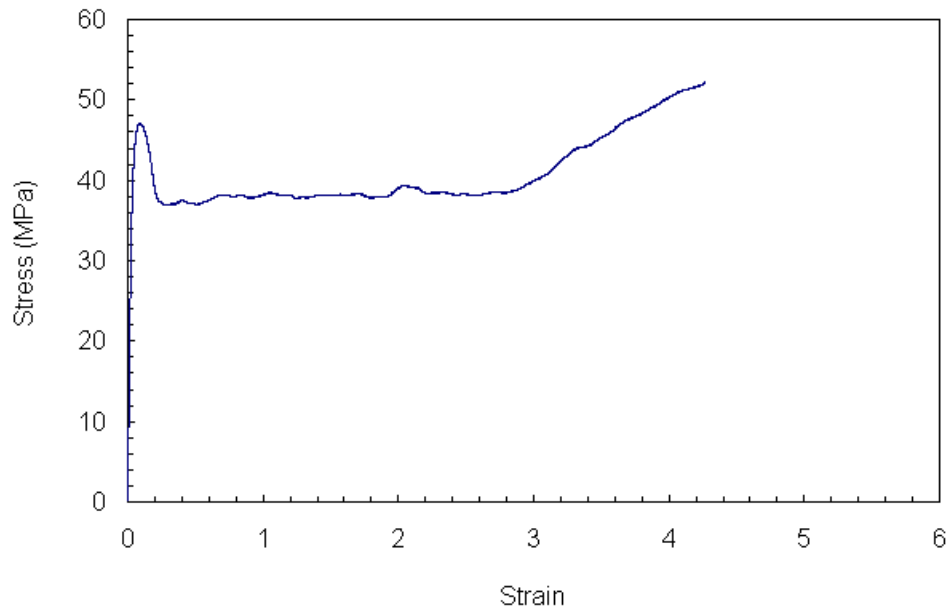


**Figure E.3** Representative stress-strain curve for [PP2+1B].

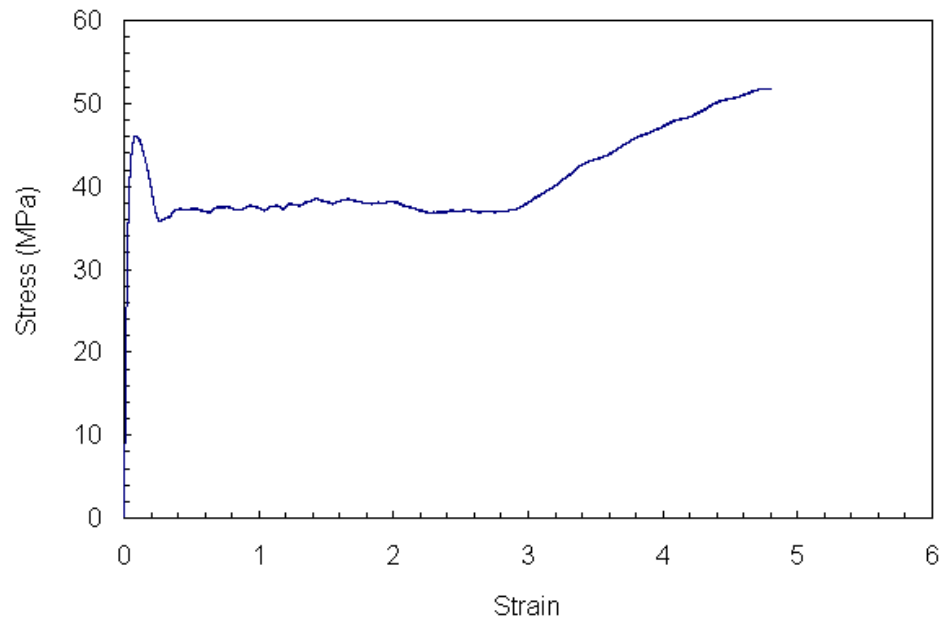


**Figure E.4** Representative stress-strain curve for [PP2+3B].

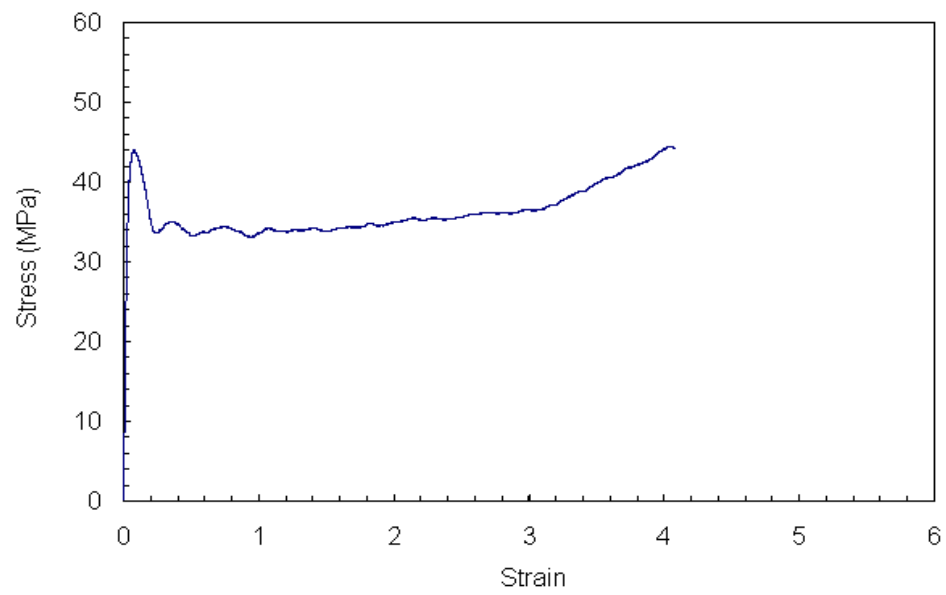


**Figure E.5** Representative stress-strain curve for [PP2+6B].



## APPENDIX F

### DETERMINATION OF PERCENT CRYSTALLINTY

The percent crystallinity ( $X_c$ ) of each composite was calculated from Equation F.1.

$$X_c = \frac{\Delta H_f / W_{pp}}{\Delta H_{fo}} \times 100 \quad (F.1)$$

where,

$X_c$  = Percent crystallinity (%)

$\Delta H_f$  = Enthalpy of fusion for composite (J/g)

$W_{pp}$  = Weight fraction of PP in the composite

$\Delta H_{fo}$  = Enthalpy of fusion value for the pure crystalline form of PP (J/g)

$\Delta H_{fo}$  value is taken as 209 J/g [Garcia et al., 2004].

## APPENDIX G

### DSC PLOTS OF ALL SAMPLES

DSC plots of all samples prepared in this study are given in Figures G.1 – G.15

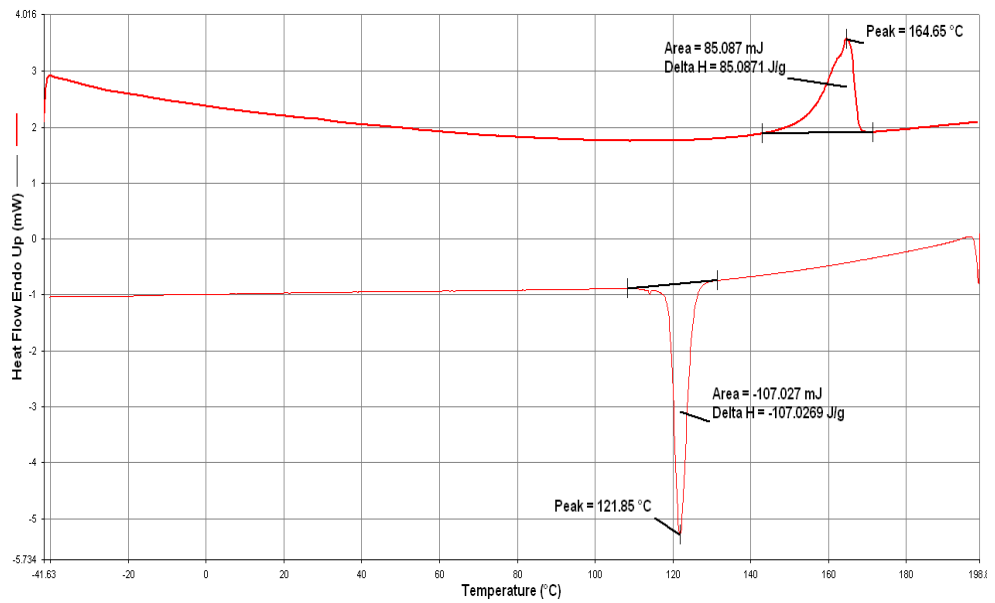


Figure G.1 DSC plot of [PP1].

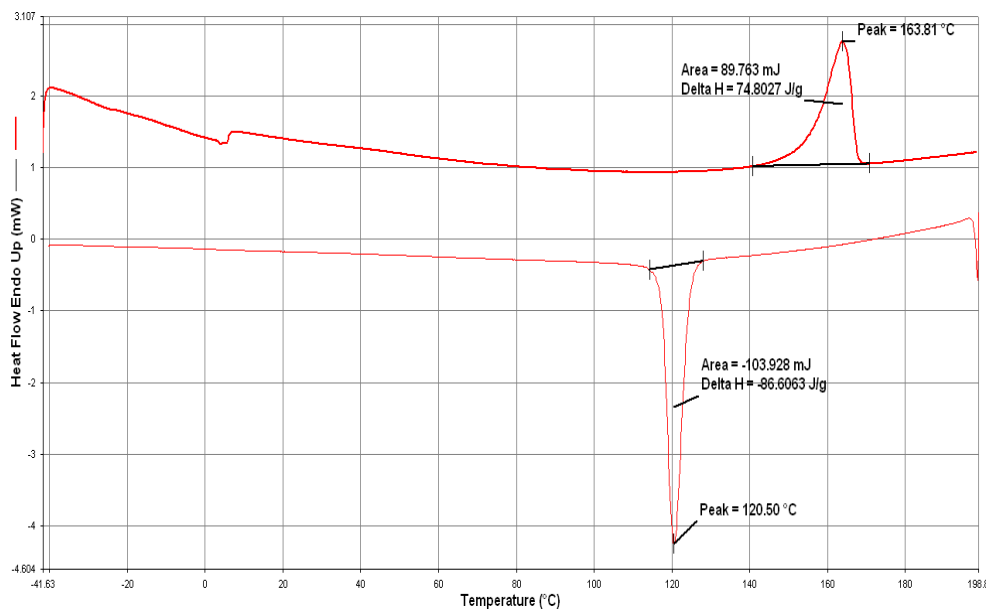


Figure G.2 DSC plot of [PP1+1A].

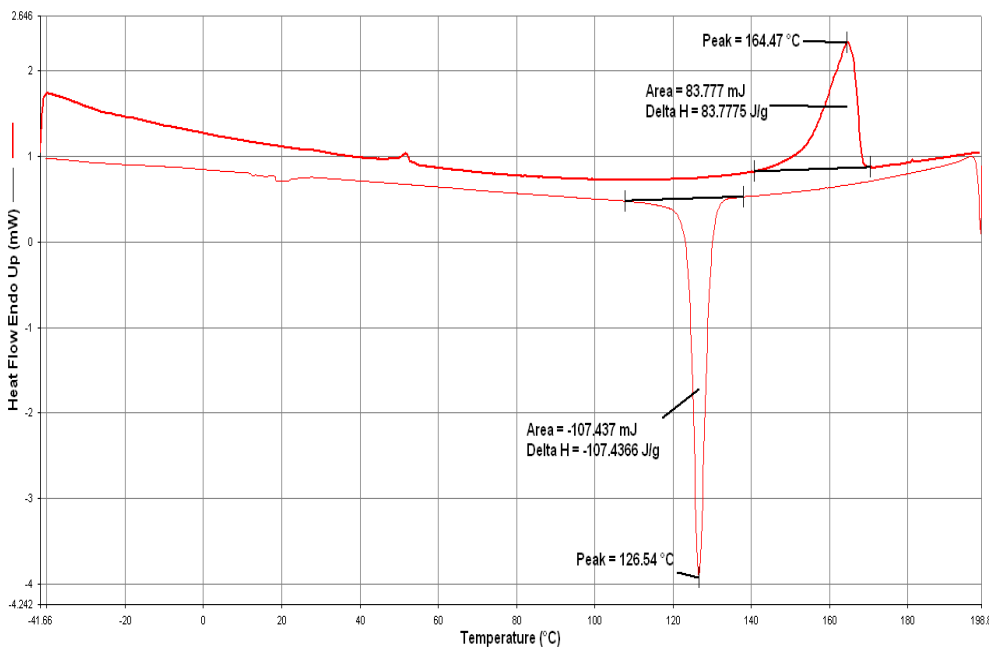


Figure G.3 DSC plot of [PP1+1A+1B].

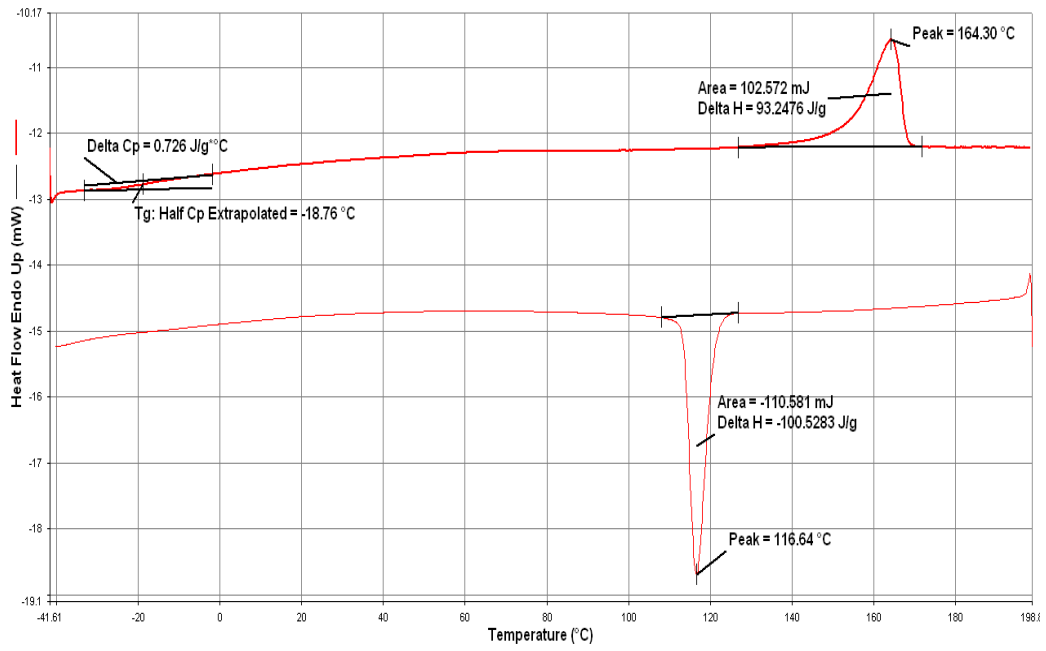


Figure G.4 DSC plot of [PP2] (1<sup>st</sup> analysis).

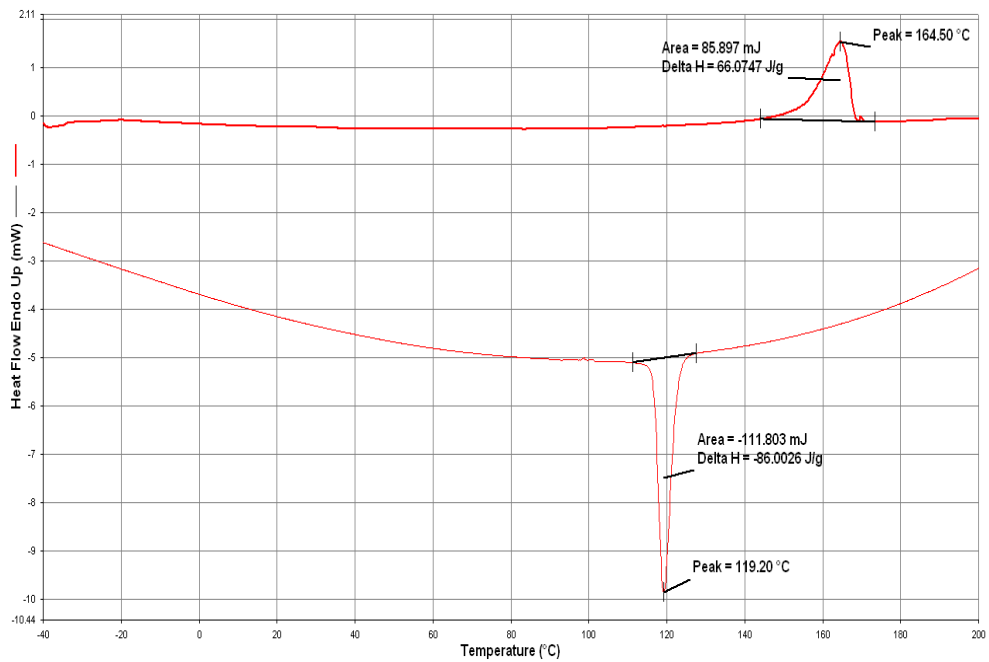


Figure G.5 DSC plot of [PP2] (2<sup>nd</sup> analysis).

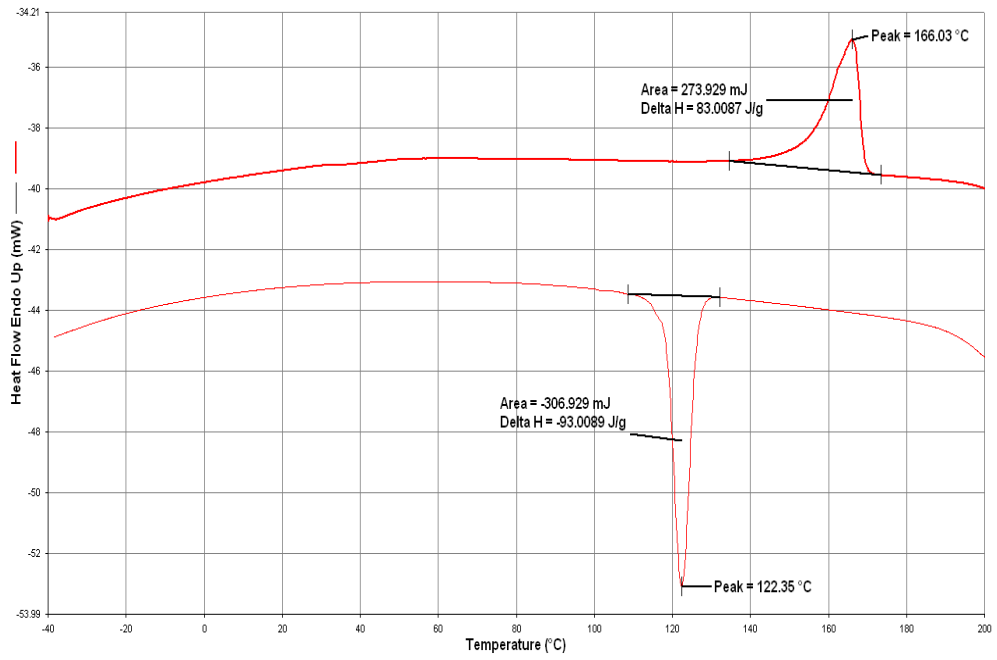


Figure G.6 DSC plot of [PP2] (3<sup>rd</sup> analysis).

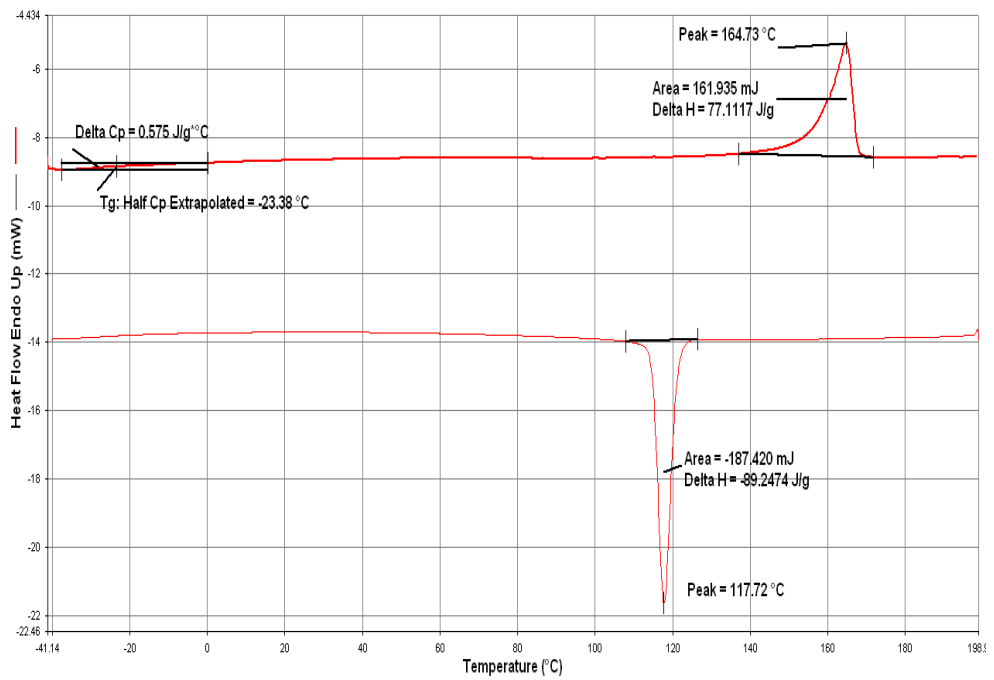


Figure G.7 DSC plot of [PP2+1A].

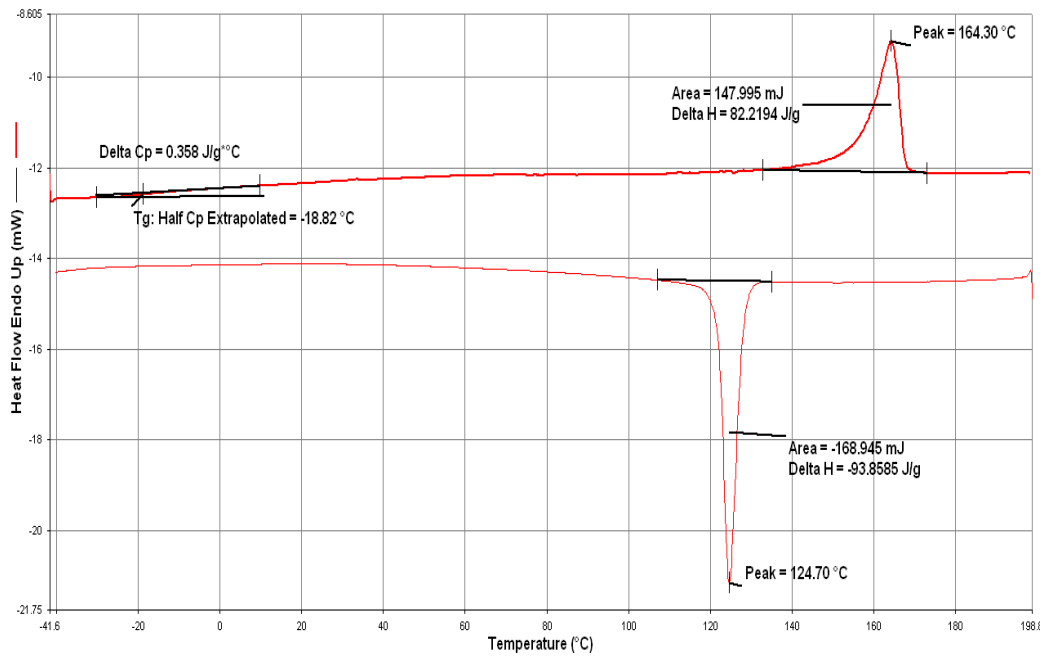


Figure G.8 DSC plot of [PP2+1A+1B].

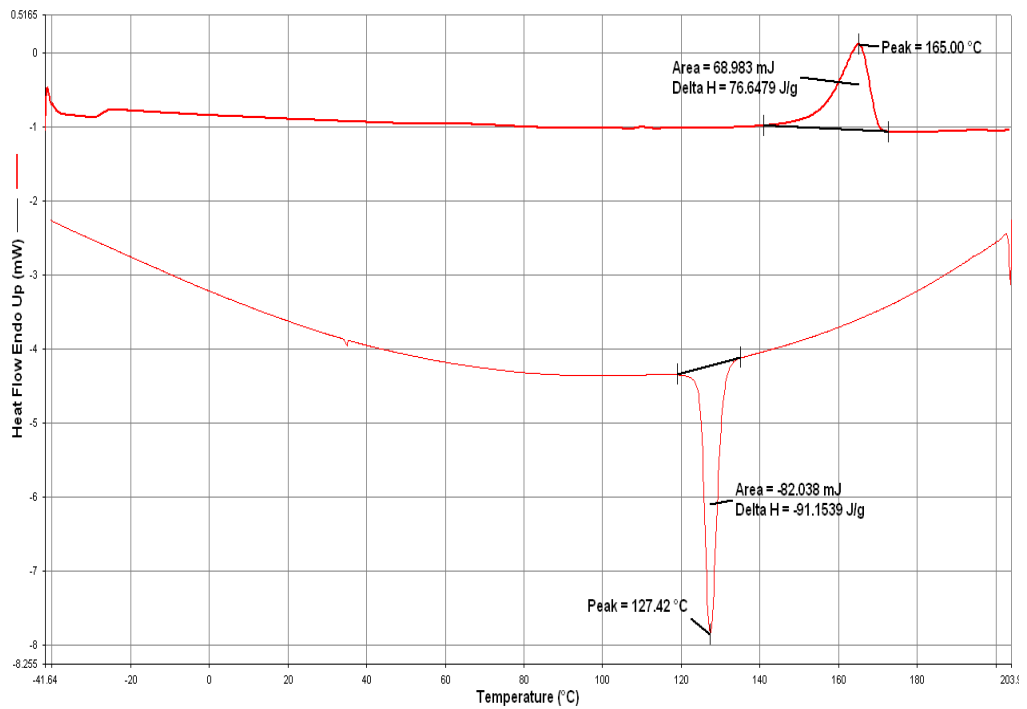


Figure G.9 DSC plot of [PP2+1A+3B].

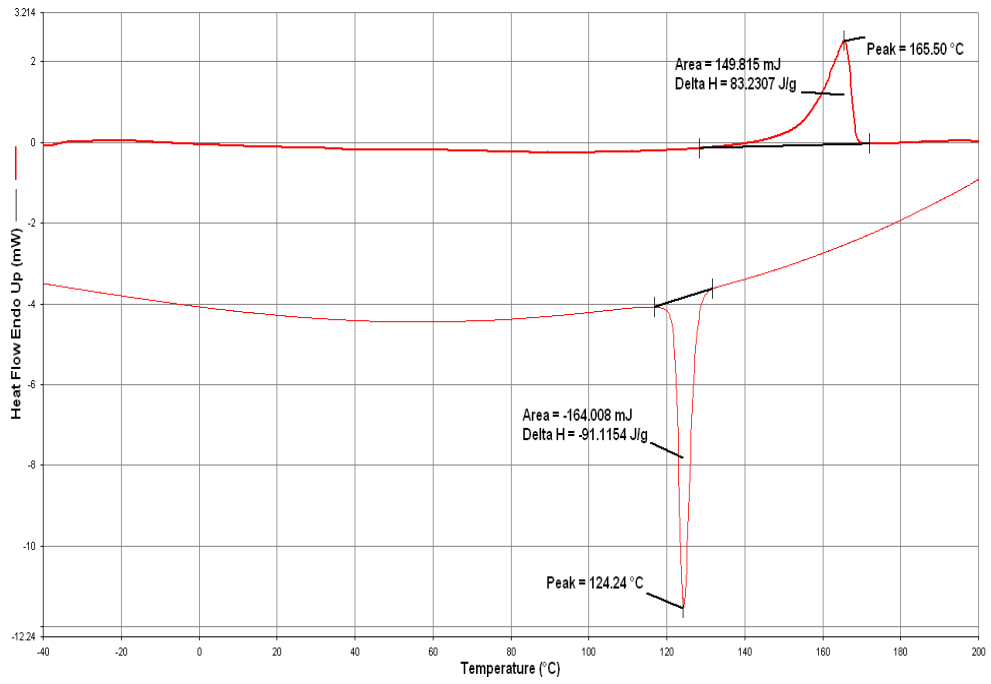


Figure G.10 DSC plot of [PP2+0.5B].

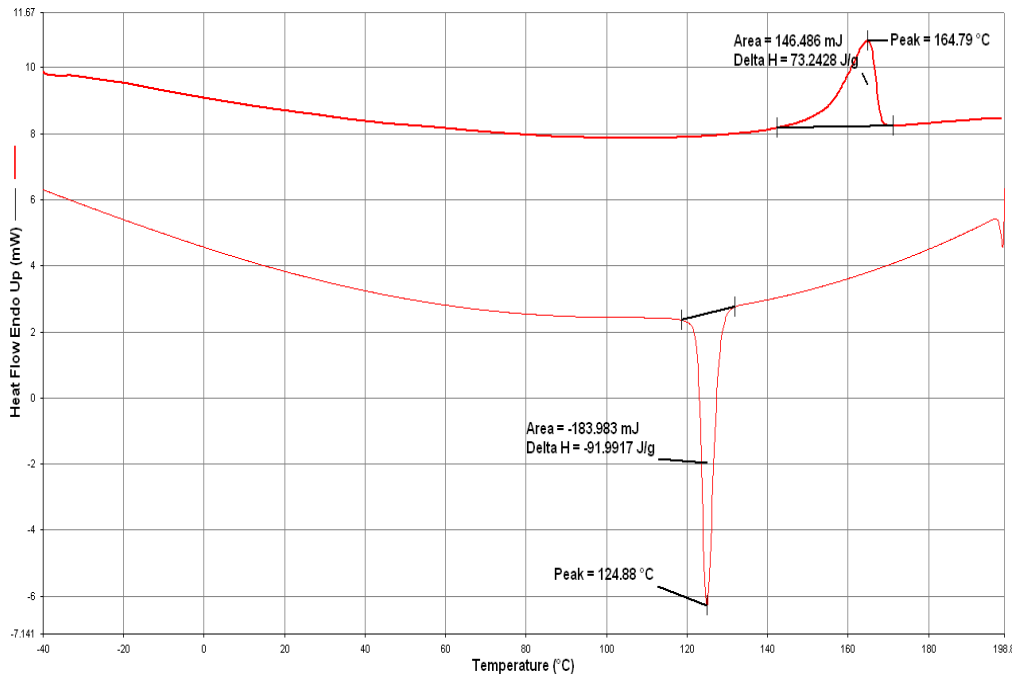


Figure G.11 DSC plot of [PP2+1B].

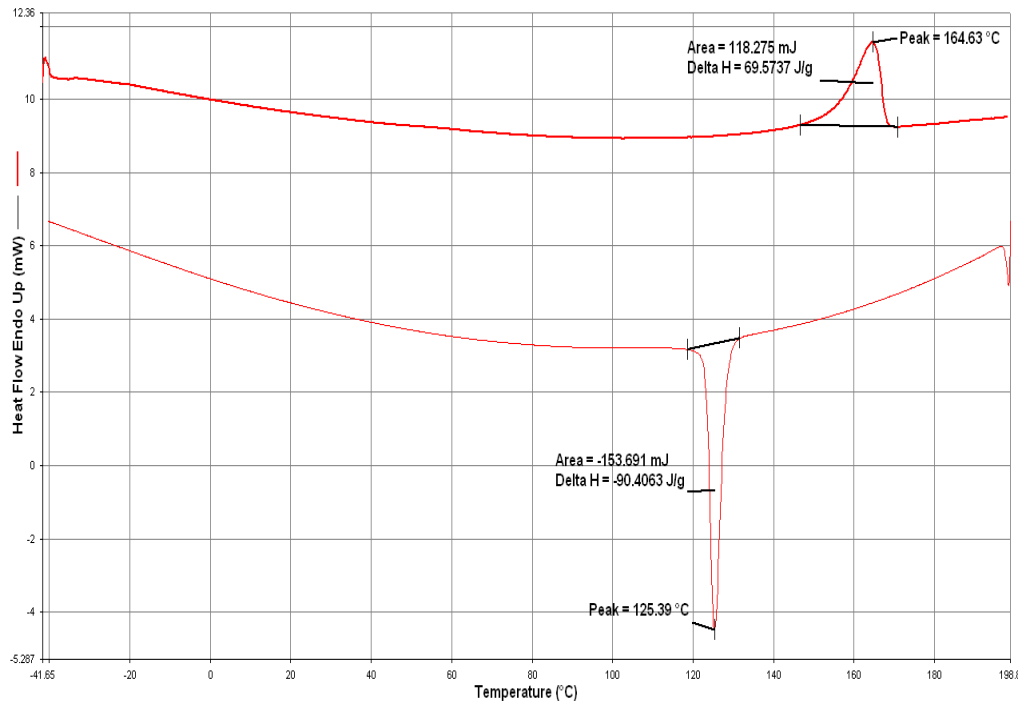


Figure G.12 DSC plot of [PP2+3B].

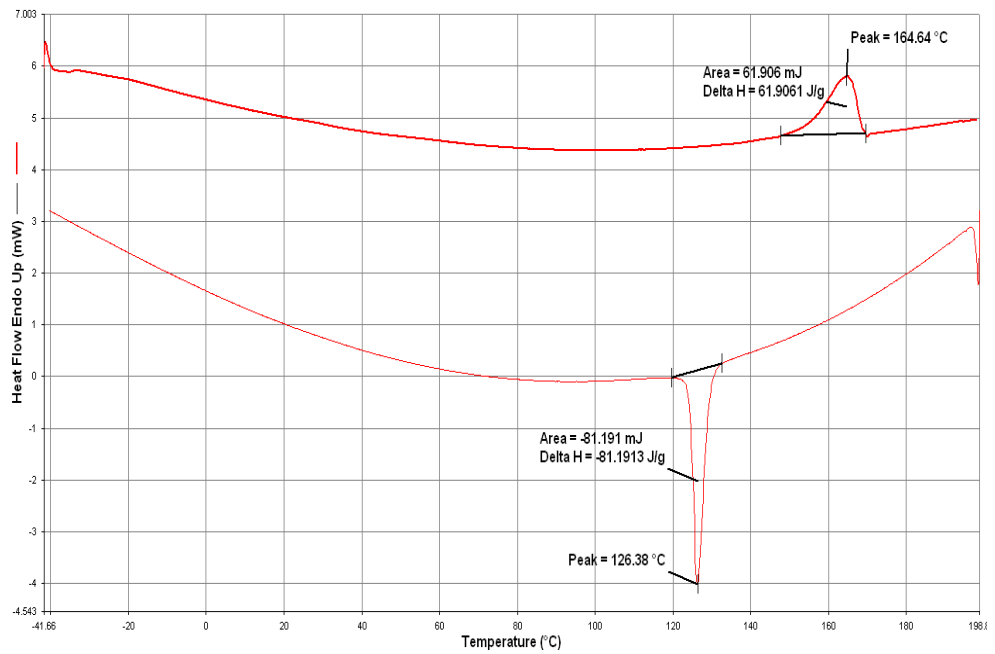
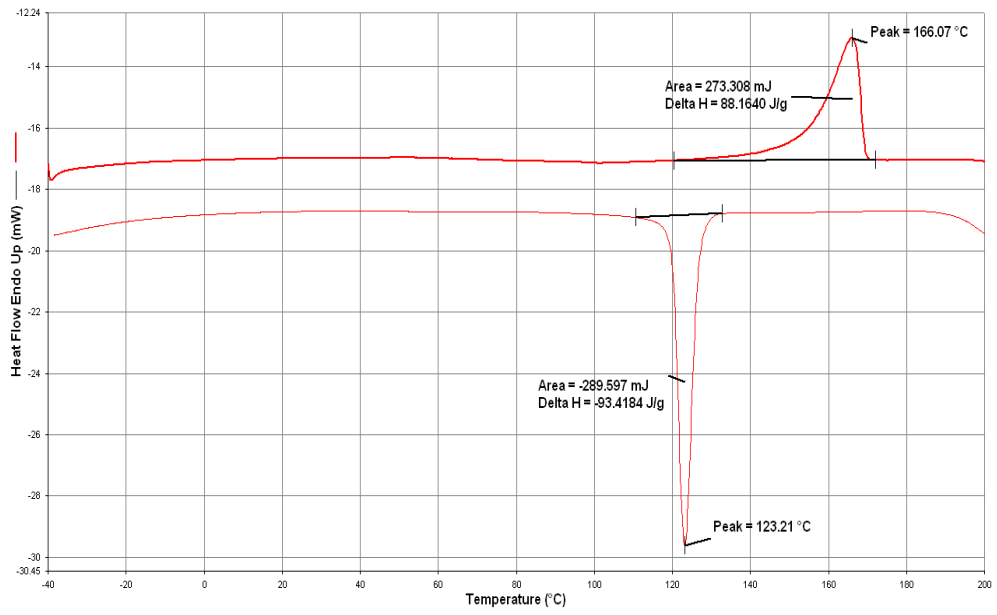
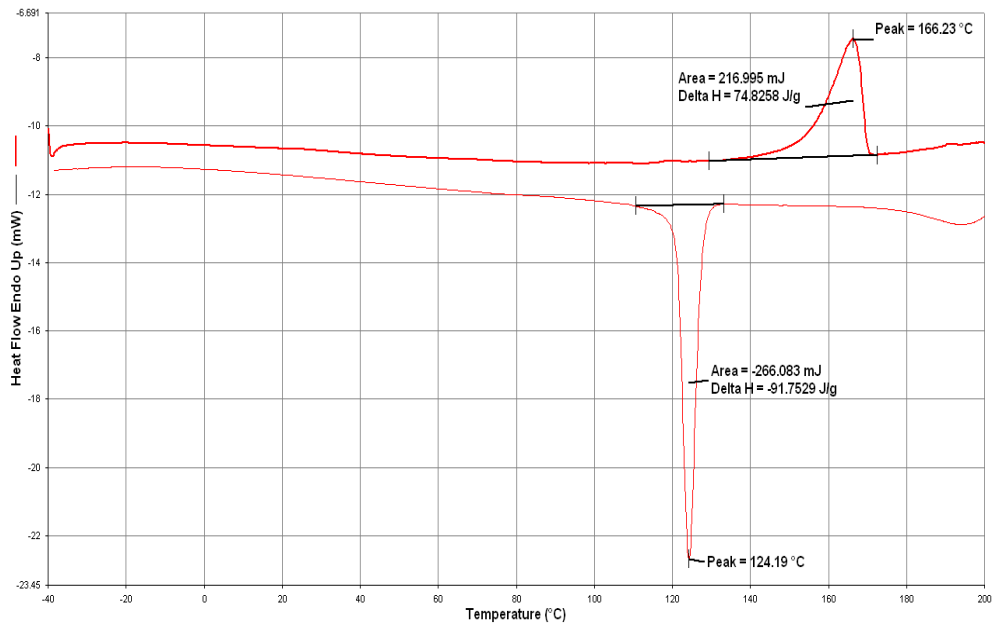


Figure G.13 DSC plot of [PP2+6B].





**Figure G.14** DSC plot of [PP2+0.5PB].



**Figure G.15** DSC plot of [PP2+0.5MB].

## APPENDIX H

### TGA CURVE OF THE AS-SYNTHEZIZED BNNTs

Figure H.1 is the TGA curve of the as-synthesized BNNTs from room temperature to 600 °C.

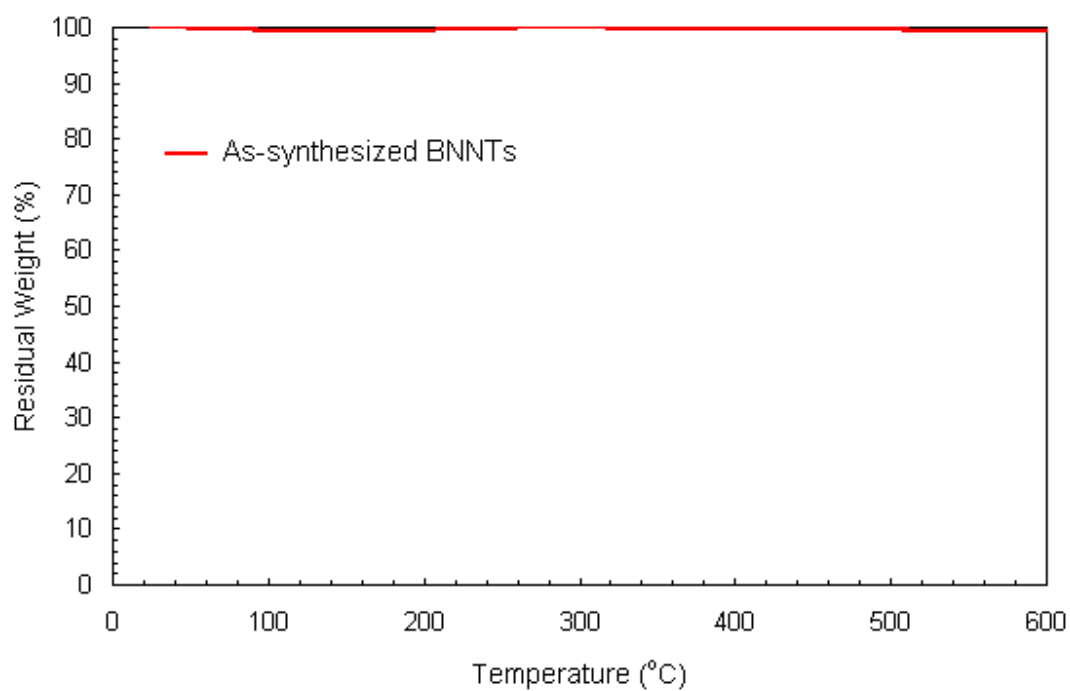


**Figure H.1** TGA curve of the as-synthesized BNNTs.

# APPENDIX I

## TMA CURVES OF SECOND AND THIRD GROUP COMPOSITES

Thermal mechanical analysis (TMA) curves of second and third group composites are given in Figures I.1 – I.12

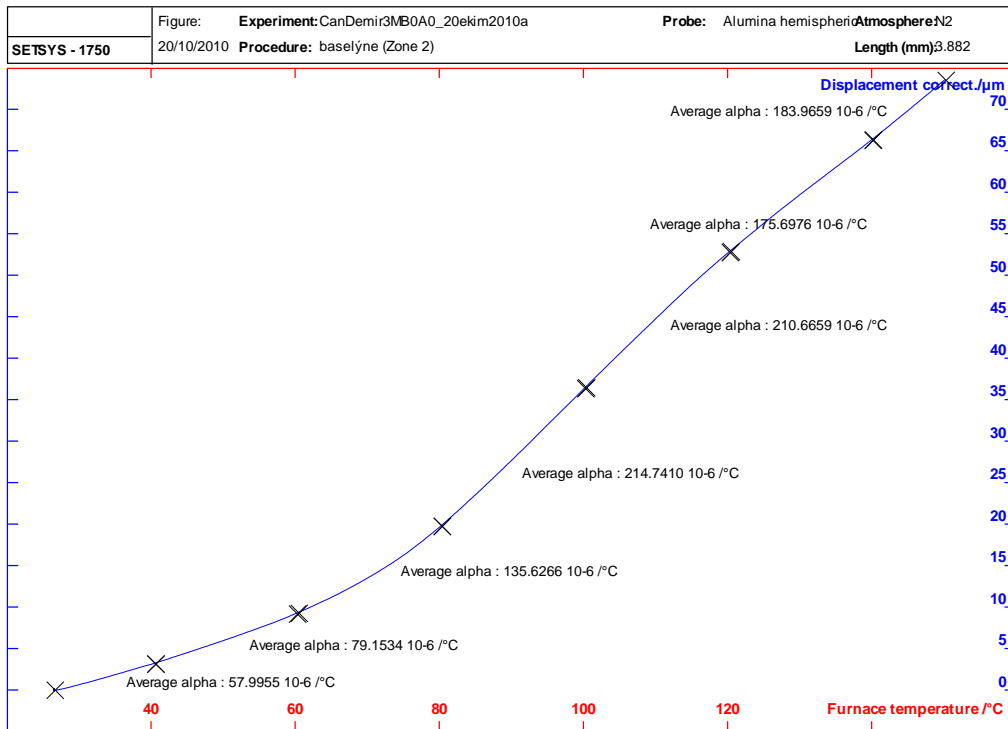


Figure I.1 TMA curve of [PP2] (1<sup>st</sup> analysis).

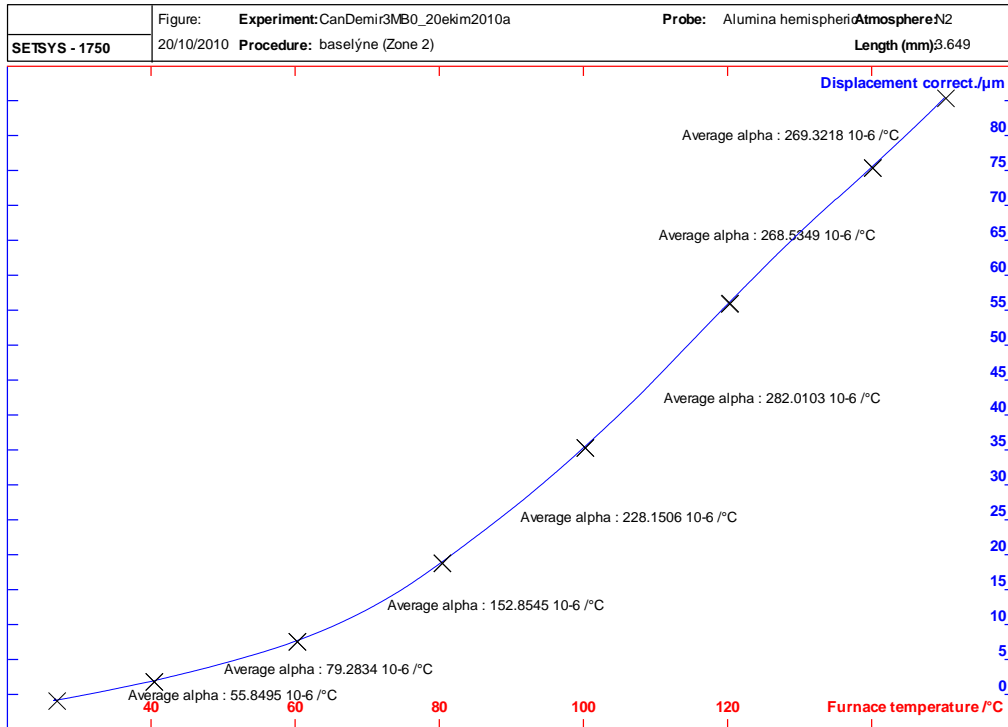


Figure I.2 TMA curve of [PP2] (2<sup>nd</sup> analysis).

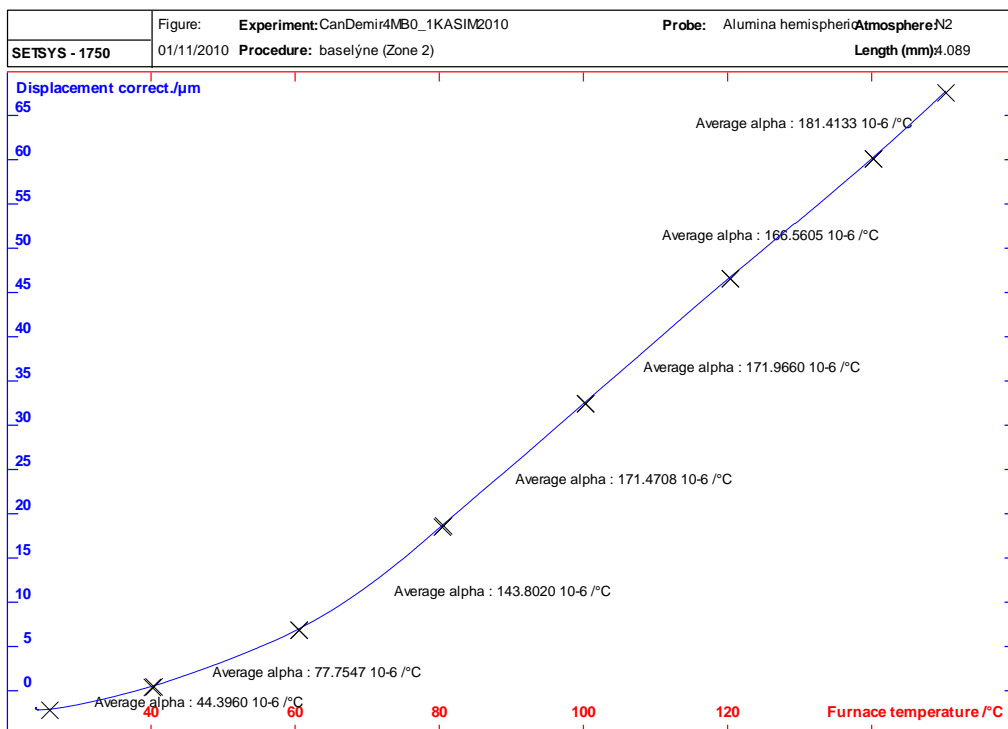


Figure I.3 TMA curve of [PP2] (3<sup>rd</sup> analysis).

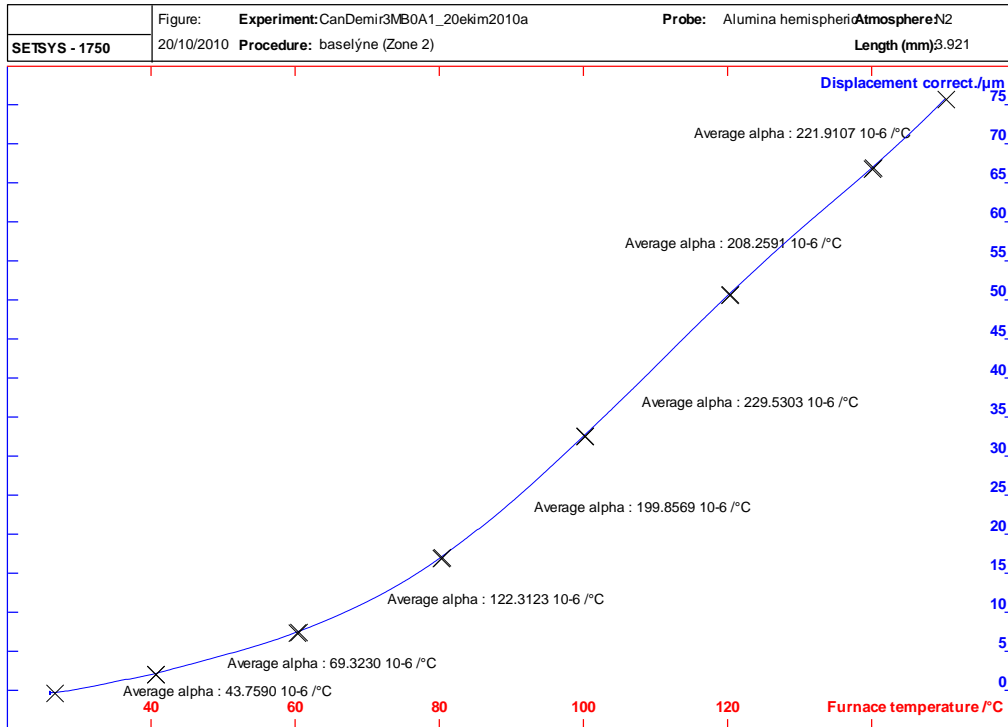


Figure I.4 TMA curve of [PP2+1A].

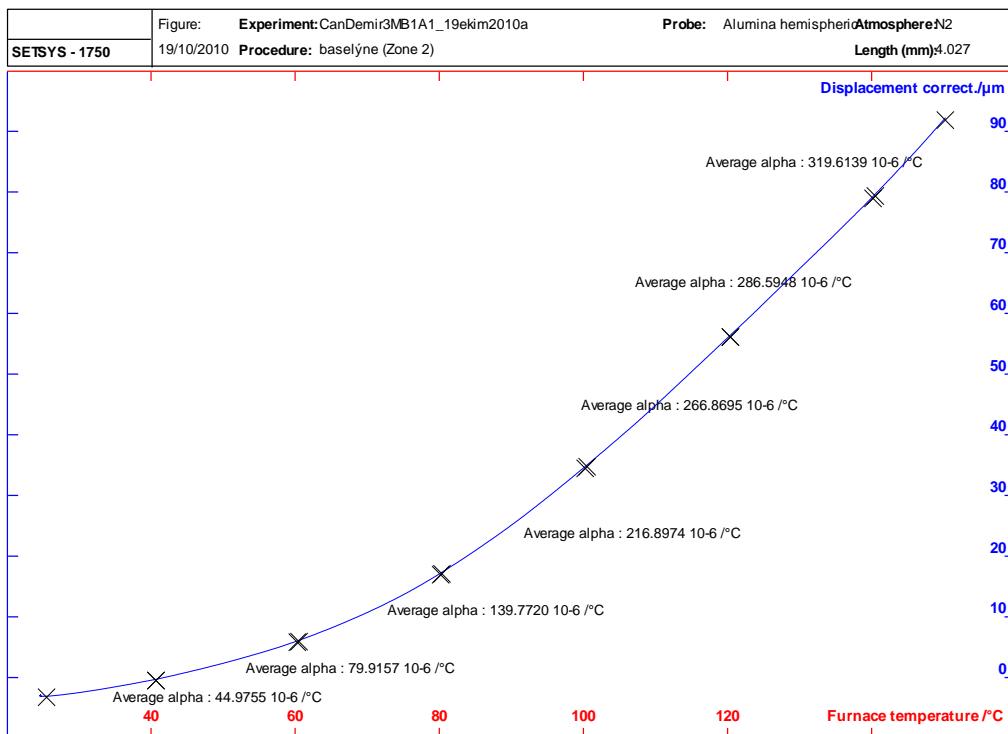


Figure I.5 TMA curve of [PP2+1A+1B].

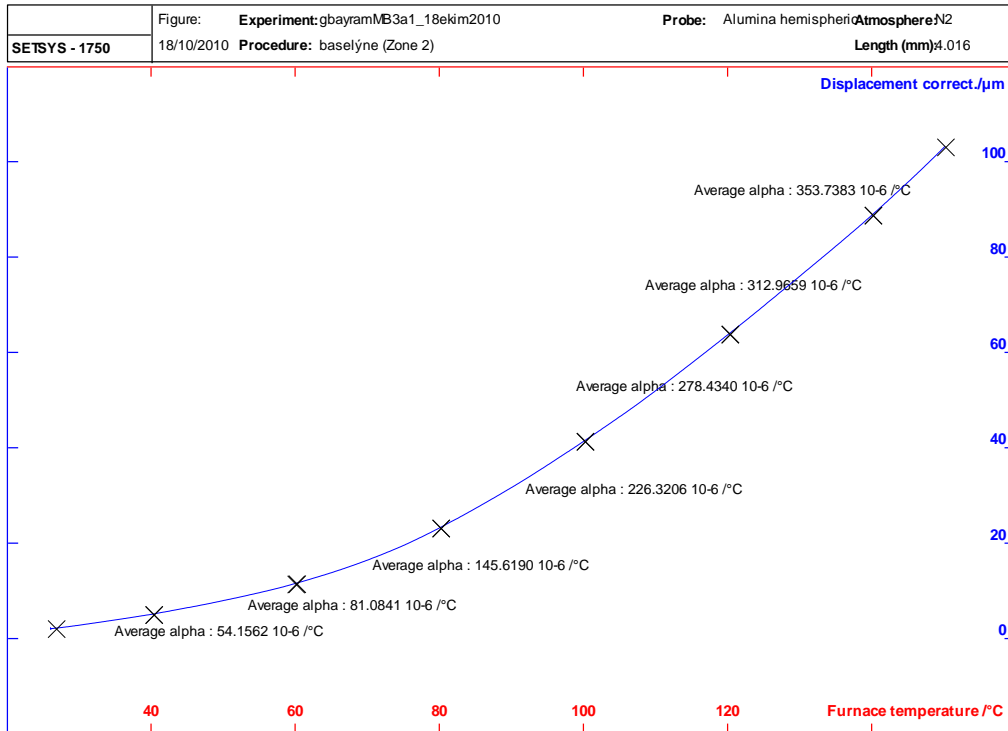


Figure I.6 TMA curve of [PP2+1A+3B].

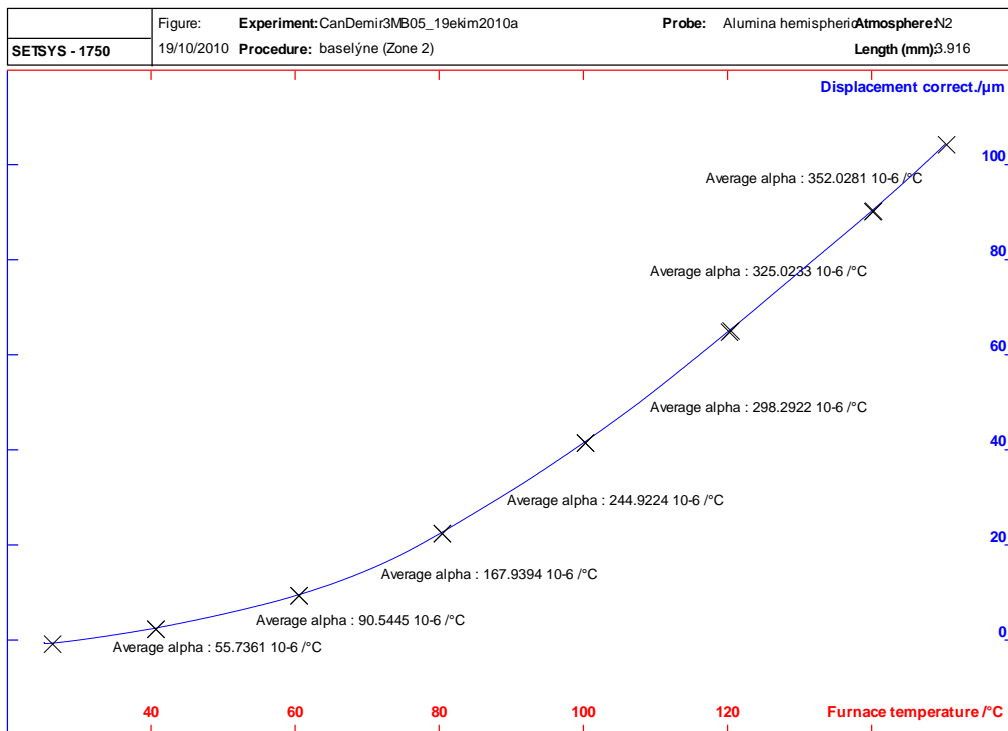


Figure I.7 TMA curve of [PP2+0.5B].

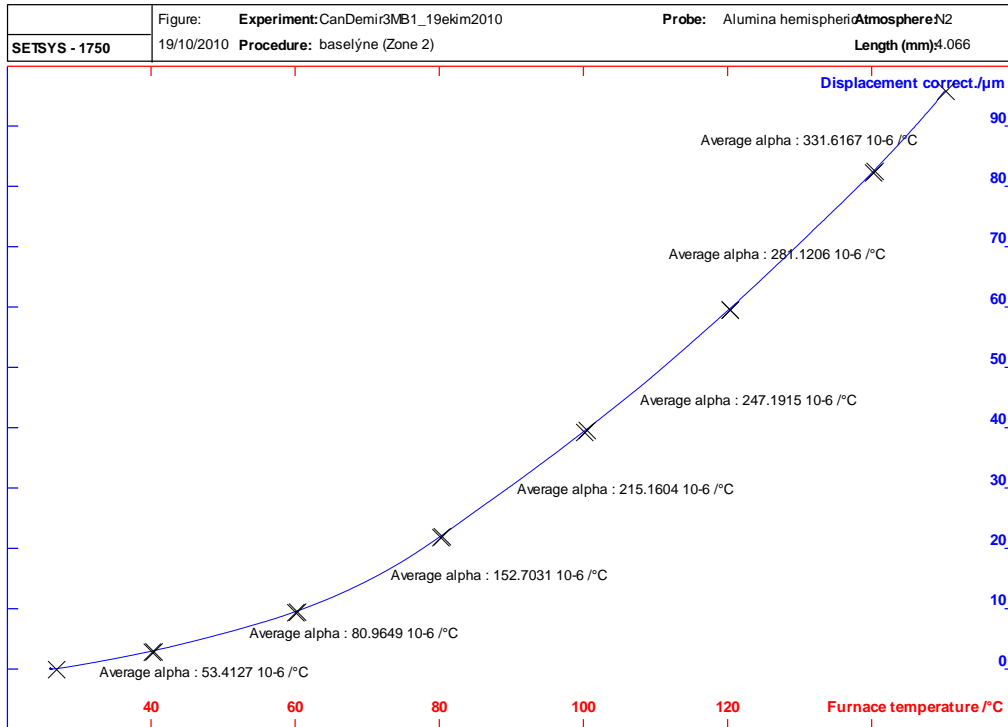


Figure I.8 TMA curve of [PP2+1B].

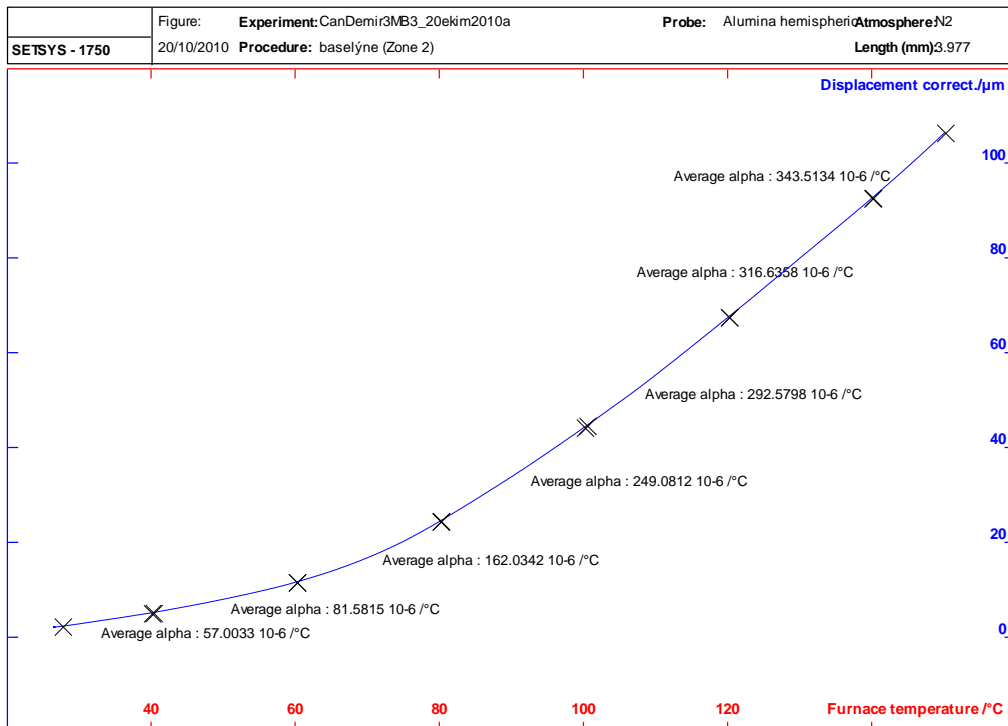


Figure I.9 TMA curve of [PP2+3B].

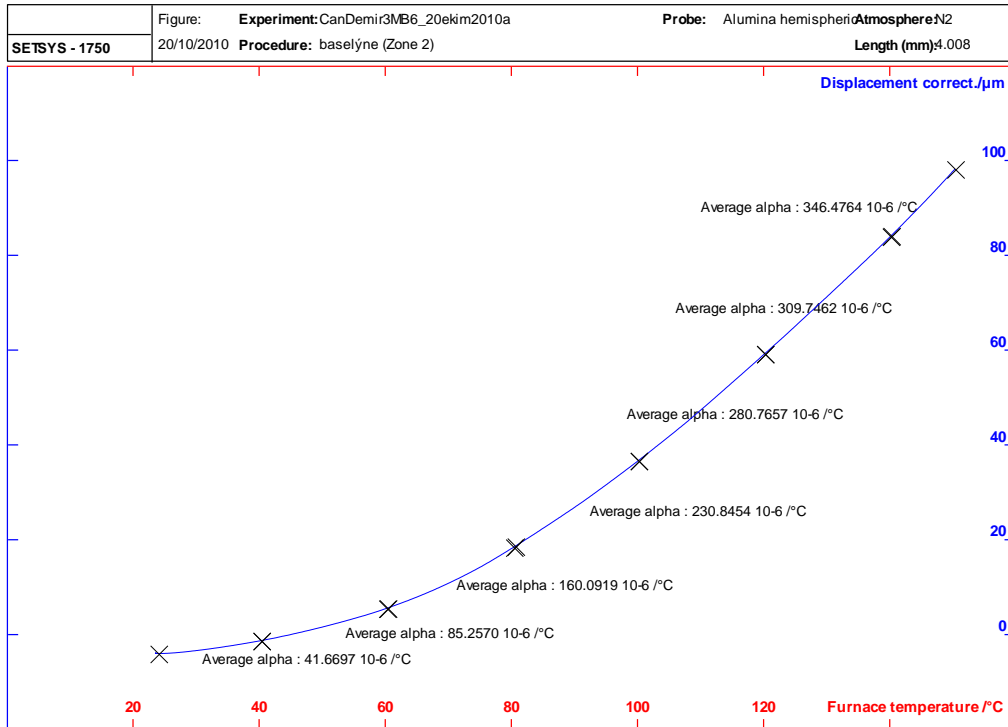


Figure I.10 TMA curve of [PP2+6B].

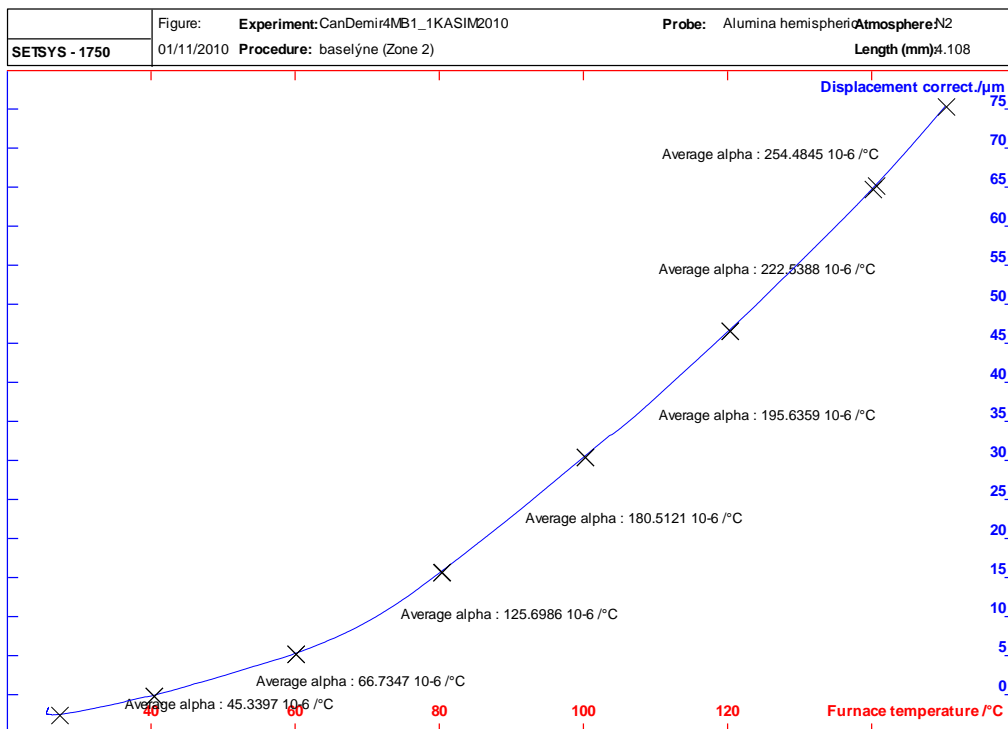


Figure I.11 TMA curve of [PP2+0.5PB].



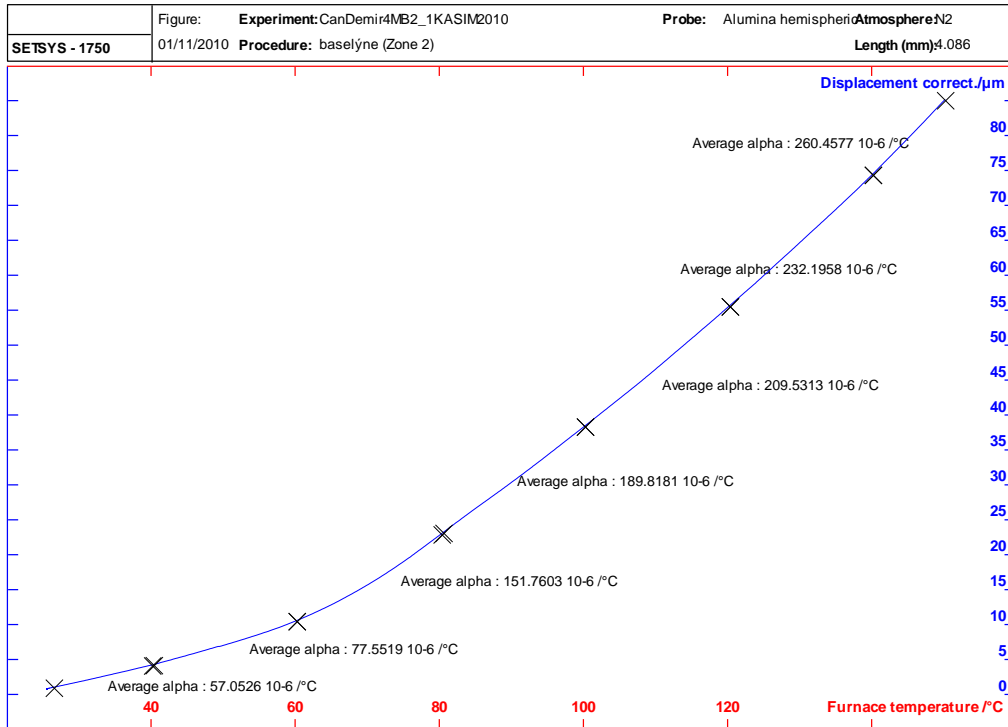


Figure I.12 TMA curve of [PP2+0.5MB].